AN INVESTIGATION INTO THE EFFECT OF LONGITUDINAL MICRO-STRIATIONS AND THEIR PROFILES, ON THE DRAG OF FLAT PLATES

KAMALLUDDIEN PARKER

Thesis presented for partial fulfilment for the degree of

MASTER OF SCIENCE

In the Department of Mechanical Engineering

UNIVERSITY OF CAPE TOWN

September 1997

I, Kamalluddien Parker, submit this thesis in part fulfilment of the requirements for the degree of Masters of Science in Mechanical Engineering. I claim that this is my original work and has not been submitted in this or any other form for a degree at any other university.

ACKNOWLEDGEMENTS

Thanks are due to the staff of the workshop in the mechanical engineering department who assisted me with the experimental preparations. Special thanks are extended to Prof. A. T. Sayers for supervising me on this MSc. Project. Thanks are also extended to Treknet Fishing company for supplying a specimen Bronze Whaler shark, *Carcharhinus limbatus* for this project. It is further necessary to thank Dane Gerneke of the E. M. Unit for assisting with the electron microscopy.

SYNOPSIS

This report describes an investigation into the use of streamwise-machined grooves as a means of reducing the drag force experienced by a flat plate. V-grooves of specific dimensions are machined onto the surface of a smooth plate, in a streamwise direction. The effect of these surface modifications on the drag force of a smooth plate is examined.

The use of surface modifications as a means of reducing viscous drag on a body has potential aerodynamic and hydrodynamic applications. The idea that a longitudinally grooved surface ("riblets") could reduce the turbulent skin friction developed in part from the concept that the scales of fast-swimming sharks may have a surface structure that improves boundary-layer performance. Previously conducted experiments show that v-grooves parallel to the airflow reduce drag by 4 to 7 percent. Reduced aerodynamic drag in aircraft for example, translates into reduced engine power required to overcome the drag and ultimately to lower fuel consumption. The initial part of this thesis, which dealt with the assimilation of information regarding previous riblet research, indicated that riblets with a v-groove or triangular geometry had shown the greatest potential for use as a drag reducing mechanism.

The experimental part of this thesis explores two possible riblet geometries. The performance of a symmetric and unsymmetrical v-groove pattern is investigated. Previous research indicated that counter-rotating vortices formed within the valleys of riblets. These vortices were responsible for the suppression of the streamwise vortices that prevail in the viscous sublayer of a turbulent boundary layer. The streamwise vortices produce a local upwash of slow fluid away from the surface. This is equivalent to the occurrence of low speed streaks. The velocity profile in a low speed streak is highly unstable and this causes the high fluctuation activity (bursts) in the layer adjacent to the viscous sublayer. Thus, the streamwise vortices should be hampered in order to decrease turbulent mixing and hence decrease the turbulent shear stress. This can be achieved by small longitudinal riblets which impede the cross flow of the streamwise vortices. One underlying factor that was apparent during investigation of previous studies was that it is not possible to define cause and effect.

More specifically, the observed turbulence modifications may be the cause of the drag reduction or they may result as a consequence thereof. However, preliminary experimental results indicate that the drag reduction may not be so much from a direct interaction with the turbulence, but from the low velocities (and hence low shear stress) in the bottom of the grooves. This further suggests the existence of a quiescent viscous-like flow within the riblets, a theory that was later verified from flow visualisation research done elsewhere.

The initial phase of this dissertation was to gather information regarding research that had been conducted on the effect of riblets. Since research of this nature has not been conducted locally, information was gathered primarily from overseas research papers. The next phase was to interpret and assimilate the information and hypotheses that the previous studies had postulated, and then to decide on the type of experimentation that would be conducted in order to satisfy the objectives of this thesis. In order to incorporate an aspect of riblet technology from the study of shark scales or dermal denticles, it was decided to look briefly at the physical characteristics of shark scales. For this purpose fresh shark skin specimens belonging to a fast swimming species, *Carcharhinus limbatus* were viewed under an electron microscope and the subsequent observations served as a first hand verification of documented details.

It was decided to test the drag reducing effect of two riblet geometries with a smooth plate used as a reference. The turbulent boundary layer characteristics of the three test surfaces were analysed in a wind tunnel. Using a hypodermic probe the velocity profiles along the test surfaces were measured. The subsequent boundary layer results are presented. The final experimental phase involved direct measurement of the drag force on the test surfaces. These results are also presented. Based on the findings of these results, appropriate conclusions have been made.

Analysis of the turbulent boundary layer of the three test surfaces have shown that at any particular distance along the plate and at any particular height close to the surface of the plate, the velocity for the riblet surfaces are less than the smooth plate value. This amounts to a reduction in shear stress for the riblet surfaces. Furthermore, of the riblets surfaces, the surface with the smaller symmetric riblet appears to produce the greatest drag reduction. Using established flat plate theory and equations the flow

within the viscous sublayer of the three surfaces was modelled. By plotting the universal velocity profile in law of the wall units, it was possible to see how well the experimental results fell within the turbulent flow regime. Direct drag measurements verified that the drag force on the riblet surfaces were less than the smooth plate value. Theoretical and experimental results for the smooth plate agreed within acceptable deviation from each other. A maximum drag reduction of 6.83% was recorded for the riblet with $h/s = 1$, at a Reynolds number based on plate length of 117 101. Results have also indicated that the effects of the riblets were to increase the laminar sublayer thickness and local Reynolds number while reducing the boundary layer thickness. This agrees with a hypothesis that riblets hamper momentum and turbulent energy exchange from regions of high velocity to regions of low velocity. Results have shown a dependency of the amount of drag reduction, on the flow Reynolds number and the riblet dimensions.

Based on the findings of this thesis it is concluded that there exists a v-groove-like pattern on the scales of the fast swimming shark. Machining these v-grooves on the surface of smooth plates reduces the wall shear stress on the surface. A significant amount of drag reduction can be achieved based on the dimensions of the riblet and the Reynolds number of the fluid. It is recommended that the effect of riblets as discussed by this thesis be verified through laser Doppler and hot-wire anemometry. It would also be of interest to see the flow behaviour using flow visualisation techniques such as hydrogen bubble and dye injection methods. It is further recommended that the effect of riblets should be studied on more realistic surfaces such as airfoils and yacht hulls.

TABLE OF CONTENTS

NOMENCLATURE

b	test plate width (mm)
C_D	dimensionless coefficient of drag
C_f	dimensionless coefficient of skin friction
D	Total drag force (N)
h	riblet height (mm)
h^+	dimensionless riblet height in law of the wall co-ordinates (= $(hu_\infty/\nu)\sqrt{C_f/2}$)
l	test plate length (mm)
P	Total pressure (Pa)
R	universal gas constant (= 8.31 J/mole·K)
Re_x	dimensionless Reynolds number at any x
Re_L	dimensionless Reynolds number based on test plate total length
s	riblet spacing (mm)
s^+	dimensionless riblet spacing in law of the wall co-ordinates (=$(su_\infty/\nu)\sqrt{C_f/2}$)
S	span area (= b x l) (m^2)
T	temperature (K)
u_∞	freestream velocity (m/s)
v_x	velocity at a point along the flow (m/s)
x	spanwise distance moved by the traverse, measured from the plate leading edge (mm)
y	vertical distance moved by the traverse, measured from test plate surface (mm)
z	chordwise distance moved by the traverse (mm)

Greek

δ	boundary layer thickness (mm)
δ_L	Laminar sublayer thickness (mm)
μ	dynamic viscosity (Pa.s)
ν	kinematic viscosity (m^2/s)
ρ	fluid density (kg/m^3)
τ	shear stress (Pa)

Subscripts

W	wall

LIST OF ILLUSTRATIONS

Tables:

1. INTRODUCTION

The importance of energy conservation has been a driving force behind the initiation of research into methods that will reduce the turbulent skin friction drag on transport aircraft fuselages. Fuselage skin-friction reductions as small as 10 percent provide the potential for a 500 million dollar per year fuel saving for the airlines. In the past several years significant efforts have been made to develop passive techniques which effect a net reduction in surface shear stress due to boundary layer turbulence. One technique that has demonstrated net surface drag reduction and has the potential for practical aerodynamic and hydrodynamic applications is the use of streamwise triangular v-groove or riblet surface modifications. Surface modifications seem to be the most attractive of the passive devices investigated so far, simply because they require little or no maintenance and are relatively easy to install.

The present study combines a turbulent boundary layer analysis with a direct drag measurement analysis. The drag reducing effect of two different v-groove geometry riblets machined on the surface of a smooth flat plate is investigated. One ribbed surface is machined with an unsymmetrical v-groove with the rib height to rib spacing ratio, h/s of 0.22 and another surface is machined with a symmetric v-groove with $h/s = 1$. A smooth plate of the same area is used as the reference plate for the analysis. The plates are suspended at zero angle of attack in a wind tunnel while the flow over the surfaces is turbulent.

The main objective of this project is to investigate the turbulent drag reducing potential of micro-groove surface modifications, called 'riblets.' The v-groove riblet was chosen since it has shown the greatest potential for drag reduction and is the easiest to manufacture. Any turbulent boundary layer comparison between the three test surfaces would include a comparison of the shear stress, coefficient of friction, boundary layer thickness and laminar sublayer thickness of the smooth plate and the grooved plates.

The report begins by examining literature on previous studies of riblets as a drag reducing mechanism. The discussion also focuses on the different theoretical models

developed by other researchers in explanation of the drag reducing capability of riblets. It is believed that the effect of v–groove riblets is to modify and effectively reduce the momentum and turbulent energy exchange properties caused by streamwise vortices developing near the surface beneath a turbulent layer, with a consequent reduction in the wall shear stress. The latter part of the literature survey section of this report discusses one of the sources of riblet research, namely the study of sharkskin. While it is beyond the scope of this report to study in detail the physics, hydrodynamics and structure of placoid scales, the report will attempt to show the connection between dermal denticles (shark scales) and riblets, as well as their mutual ability to reduce the drag force on the body they cover. Only the scales of fast sharks are considered. Of late, research has undoubtedly shown that on the pectoral fins of a number of fast shark species, scales with v-shaped central ridges are found. These scale structures are investigated more closely by studying past reports and also by the use of electron microscopy on the skin of a fresh shark specimen that was prepared for the purpose of this report.

The next step is to prepare a theoretical basis for this study. As there is no boundary layer equations that describe the flow over a ribbed surface, the theoretical analysis is restricted to the smooth surface only. Using the one-seventh power law as the basis for the study of turbulent flow over a smooth plate, the shear stress, coefficient of friction, local drag, boundary layer thickness, laminar sublayer thickness and total drag are calculated. These boundary layer parameters are then measured experimentally in a wind tunnel and the results are compared. The final experimental stage of this report concerns the direct drag measurement of the three test surfaces. For this, the test surfaces were aligned with the wind tunnel roof and with the use of strain gauges the drag force acting on the test surface was measured. Based on the results of the preceding chapters, conclusions are drawn about the effect of riblets on the turbulent boundary layer structure and recommendations are made.

2. LITERATURE REVIEW ON RIBLETS AS A DRAG REDUCING TECHNIQUE

Discussion of the literature survey for this report is two-fold. Chapter 2 will discuss the concept of riblets and how this has been researched as a means of reducing drag on a body immersed in a fluid. Chapter 3 will discuss one of the possible origins of the concept of riblets as a means to reduce drag, namely, from studies of sharkskin.

TURBULENT BOUNDARY LAYER DRAG REDUCTION USING RIBLETS

The viscous drag of turbulent boundary layers is a significant factor contributing to the fuel costs of airlines. Several studies have indicated that micro-surface geometry variations, which change the near-wall structure of the flow, have been effective in reducing drag.

In the past several years, significant efforts have been made to develop passive techniques that result in net reductions in surface shear stress due to boundary-layer turbulence. One technique that demonstrated net surface drag reduction and has the potential for practical aerodynamic and hydrodynamic applications is the use of streamwise micro-grooves or riblet surface modifications. Extensive wind tunnel investigations at NASA Langley[1-3] have shown that, when these riblets have a v-shape geometry and are reduced in size to less than 30 viscous length in height and span, surface drag reductions of up to 8% can be achieved.[2] A typical v-shaped riblet is shown in Figure 2.1. However, despite this apparent success of the riblets in reducing surface drag, it is still unclear how this type of surface affects the fluid interaction with the surface. The purpose of this chapter is to report on the research done elsewhere, thus far and discuss the explanations other researchers give for the drag reducing mechanism of riblets.

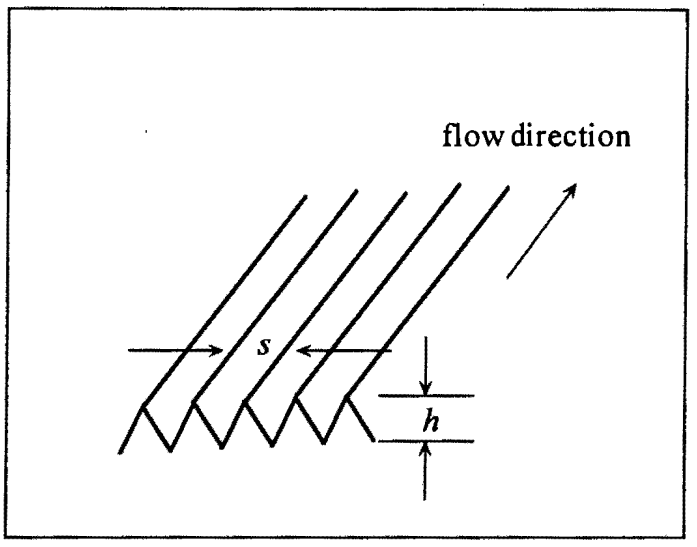

Figure 2.1 Riblet groove geometry ($h = s$)

Liu, Kline and Johnstone[4] have examined the turbulent bursting rate from a surface with rectangular fins having heights h^+ ($= h\sqrt{\tau_\omega \rho/\mu}$) of 45-111 and spacing s^+ ($= s\sqrt{\tau_\omega \rho/\mu}$) of 190-373 in terms of law of the wall co-ordinates, where τ_w is the wall shear stress, h the riblet height, s the riblet spacing, μ the dynamic viscosity, and ρ the density. For particular fin heights and fin spacings they found a 20-25% reduction in the turbulent bursting rate, which result in a 3-4% net drag reduction. Kennedy, Hsu and Lin[5] have examined rectangular fins with $h^+ = 70\text{-}150$ and $s^+ = 500\text{-}1100$; they found the drag for the finned surface was 10-50% higher than the smooth surface value. Walsh and Weinstein[6] examined the drag characteristics of longitudinally ribbed surfaces having a wide variety of fin shapes that included rectangular grooves, v-grooves, razor-blade grooves, semicircular grooves and transverse curvature. Some of these geometries are shown in Figure 2.2. The data obtained for the rectangular and v- grooved surfaces extended into the range of h^+ and s^+ less than 100. This range was of particular interest since the birth region of the turbulent burst is in the area of $y^+ = 30$ and the transverse spacing of the bursts is 100 in terms of law of the wall co-ordinates. Walsh et al[6] found a possible 2-4% drag reduction for a symmetric v-groove riblet but suggested that further experiments were necessary to verify the limited data at that time.

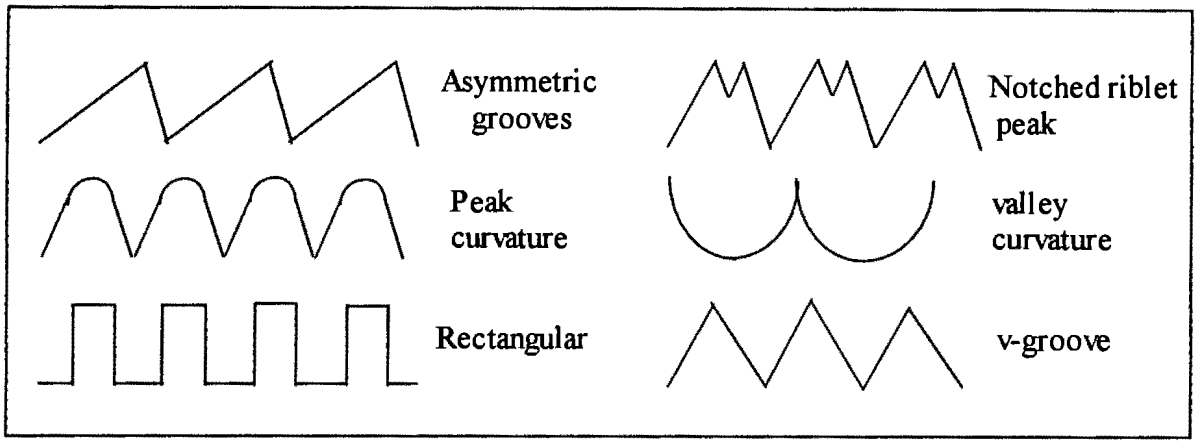

Figure 2.2 Riblet geometries that have been investigated (from Ref. 6,7)

Subsequent experiments by Walsh[7] suggested that symmetric v-groove riblets of $h^+ < 25$ and $s^+ < 200$ give reductions in drag. The amount of drag reduction increases as h^+ and s^+ decrease; maximum drag reduction obtained was 7%. The results obtained with a highly accurate drag balance indicated that v-groove riblet surfaces could produce consistent net drag reductions as large as 8 percent. Momentum balances were used to confirm the direct drag measurements. Conditionally sampled data indicated that the burst frequency for the riblet surface was approximately the same as that of a smooth flat plate but the turbulence intensity was reduced.

Walsh[8] also investigated other riblet geometries such as rounded-apex v-groove riblets, convex-concave curvature and unsymmetrical and non-periodic v-groove riblets. Rounding the apex was found to slightly decrease the drag reduction effectiveness of the significant increase in drag, but the amount of increase significantly reduces by increasing free stream velocity. The unsymmetrical and non-periodic v-groove riblets seemed to provide drag reduction approximately equal to those found for the symmetric v-groove riblets for the same h^+ and s^+.

The investigation by Walsh[7] was later repeated by Balint et al[9] in an effort to optimise the application of riblets. Riblet surfaces were tested in boundary layers that had different upstream histories and at higher Reynolds numbers than what had previously been reported. The drag reduction for the riblet was found to be dependant on the height and spacing of the riblets in law of the wall variables regardless of freestream Reynolds number or upstream boundary layer history. Microphotographs of the actual

rib geometries indicated that attempts to modify the basic v-groove riblet geometry to improve the drag reduction effectiveness reduced the effectiveness of the riblets. To further increase drag-reduction performance, Balint et al[9] used riblets in combination with another drag reduction concept, the large eddy break-up devices. In addition, Balint et al[9] investigated the yaw sensitivity of riblets and found that riblet drag reduction remained insensitive to yaw angles up to 15°.

Galagher and Thomas[10] quantified the turbulent boundary layer characteristics over streamwise grooves (on the order of 15 wall units in height and spacing), in a water channel using hot film anemometry. The turbulent structure of both the smooth and the riblet surface was investigated using traditional cross correlation and triple correlation. A 30% reduction in the measured bursting frequency was found for the riblet surface. Local skin friction reductions were found towards the end of the riblet model, however the total drag for both surfaces was the same. Flow visualisation using multicoloured dye and hydrogen bubble techniques showed a quiescent slow moving viscous-like flow in the grooves of the riblet plate. All the measurements indicated a subtle change in the near wall flow, with the outer flow in the boundary layer remaining the same.

Galagher and Thomas[10] found that the momentum thickness increases on the riblet surface and then tend towards a lower value than the flat plate. Flow visualisation showed that dye collected in the valleys of the riblet, forming a viscous-like pool. While the study by Galagher and Thomas[10] showed a modification in the near wall flow due to the presence of the riblets, this effect was localised as the outer wall flow remained unchanged. The difficulty that exists in the interpretation of their findings was that it was not possible to define cause and effects. For example, the observed turbulence modifications may have been the cause of the drag reductions or they may have arisen as a consequence thereof. However, the flow visualisation suggested that the observed drag reductions occur not so much from a direct interaction with the turbulence, but from the low velocities (and hence low wall shear stress) in the bottom of the grooves. If this is so, then the drag reductions are more of a characteristic of the flow of a viscous fluid over the riblet geometry and the perceived turbulence changes are simply a passive response of the flow to the different boundary condition.

Hooshmand et al[11] also studied turbulent boundary layer characteristics over streamwise grooves. Of the geometries tested, the most promising was the symmetric v-groove with dimensions of 15 viscous height and lengths. Net drag reductions of 8% were recorded when compared to a flat plate. Hooshmand et al[11] found as much as 50% difference in bursting frequency between the riblet surface and the flat surface. In 1991, with the use of riblets as a means of reducing drag showing immense promise, the use thereof was tested on airfoils. Caram and Ahmed[12] made measurements in the near and intermediate wake regions of a NACA 0012 airfoil with three different riblet sizes at a freestream Reynolds number of 2.5×10^5. The riblets were a symmetric v-groove type of heights 0.0229, 0.076, 0.152 mm, corresponding to h^+ of 1.5, 5, and 10 respectively.

Wake velocity profiles and turbulence parameters were measured with a temperature compensated hot film x-probe. Riblet effectiveness was indicated by a marked decrease in turbulence levels in the wake. Integration of the wake mean velocity profiles indicated a net reduction in drag of up to 13.3%, which was possibly caused by the combined effect of decreased turbulent shear stress and lower momentum exchange near the surface due to a viscosity-dominated region in the riblet valley. The riblet surface of height 0.152 mm showed the greatest drag reduction. In another study, Viswanath and Mukund[13] conducted experiments to assess the viscous drag reductions using riblets on a supercritical airfoil at transonic speeds. Symmetric v-groove riblets of height 0.018 and 0.033 mm were tested. The airfoil angle of attack was varied between –0.5 to 1 degree. Results showed skin friction reductions in the range of 6-12%. Riblets with a height of 0.018 mm showed the greatest drag reduction. Their results suggested increased effectiveness of riblets in adverse pressure gradients. These results were consistent with the observations of Nieuwstadt et al[14] at low speeds, wherein adverse pressure gradients were imposed on a flat plate turbulent boundary layer and the drag reduction was appreciably greater compared with the performance of riblets in a zero pressure gradient.

Bacher and Smith[15] in their study of turbulent boundary layer modifications by surface riblets, used triangular riblets 1.6 mm deep by 1.6 mm wide. The test plate was 0.15 x 1.21 m and the peaks of the riblets were flush with the wind tunnel floor. Using dye visualisation and Hydrogen bubble visualisation they were able to observe

the behaviour of the fluid over the riblet surface. Visualisation studies confirmed that the flow within the riblets is slow and quiescent, in addition, they show the existence of low speed streak structures as shown in Figure 2.3. Furthermore, Figure 2.3 shows the comparative dye slot visualisation and it appears that fluid was drawn from the grooves.

Figure 2.3 Plan view photographs showing comparative dye slot visualisation (from Ref 17)

The increased streak spacing and apparent increase in flow uniformity above the riblet surface, in comparison to the flat plate, implied that there are fewer regions of instability and that those regions may behave more weakly in implementing exchange of momentum between the near wall and the outer region of turbulent boundary layers. This suggestion appears to be borne out by the companion anemometry results presented by Bacher and Smith[16]

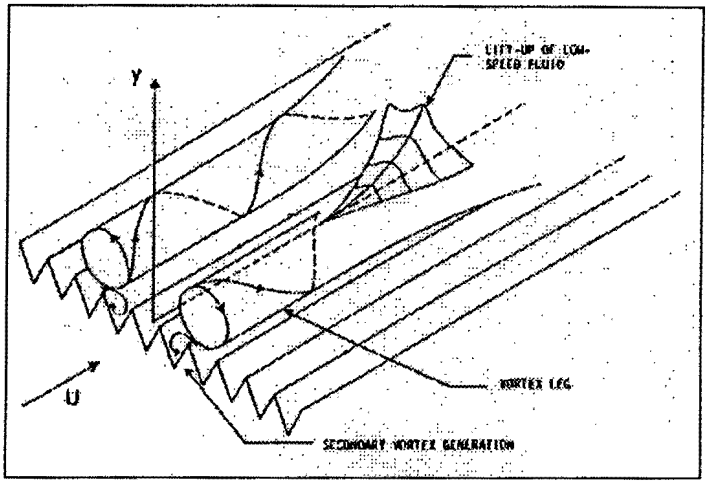

Figure 2.4 Perspective schematic showing the hypothesised interaction of counter-rotating streamwise vortices in the wall region of a turbulent boundary layer with a riblet surface (from Ref. 15).

As discussed in detail in Refs. 15 and 16, it is suggested that the effect of the riblets is to modify and effectively reduce the momentum exchange properties caused by the streamwise vortices developing near the surface beneath a turbulent layer, with a consequent reduction in the surface shear stress. It is thought that an important action of the sharp-peaked riblets is to limit spanwise concentration of low-speed fluid. It is suggested that this is accompanied by a mechanism which relies on secondary vortex generation.[16] A schematic drawing in Figure 2.4 illustrates the hypothesised interaction of the riblets with a pair of counter-rotating streamwise vortices.

Note the generation of secondary vortices at the riblet peaks serves two functions; weakening of the streamwise vortices, and inhibiting the spanwise concentration of low-speed fluid into streak formation (i.e., increasing streak spacing) should decrease the number of 'burst' sites, which will inhibit turbulent momentum exchange in the boundary layer. This process enables the riblet surface to retard the development of the turbulent boundary layer and thus reduce the surface drag.

In another study, Park and Wallace[17] made detailed measurements with a miniature single-sensor hot-wire probe of the streamwise velocity field within a riblet groove of dimensionless size $h^+ = 14$ and $s^+ = 28$ (based on the riblet surface average friction

velocity). For all the single-sensor measurements, the freestream velocity was 1.29 m/s corresponding to a momentum thickness Reynolds number of 1.2×10^3. The riblet surface, which had the same projected area as the smooth surface, was constructed with low thermal conductivity fibreglass with symmetric grooves of triangular cross section as recommended by Ref. 6. The dimensions of the riblets were 5 mm high and 10 mm span between peaks, with the wall inclined at 45° to the horizontal. Park and Wallace[17] found that the wall shear stress, when integrated over the riblet surface, yields about 4% reduction compared with the smooth surface. This was ascribed largely to the greatly diminished wall shear stress near the bottom of the riblet valley. Four-sensor hot-wire probe measurements revealed that riblets significantly reduce the vertical flux of the streamwise momentum within the riblet valley.

The comparatively large riblet sizes investigated by Park and Wallace[17] made it possible to study the behaviour of the fluid along, below and above the peaks of the riblets. It was found that the mean velocity is greatly retarded, along lines parallel to a riblet sidewall, as the riblet valley is approached. The mean shear stress, τ_w, at about one-quarter of the riblet sidewall below the peak is about the same as that on a smooth surface with the same freestream velocity. Thus, about three-quarters of the riblet sidewall experiences a mean shear stress less than the smooth surface value, resulting in a net drag reduction. The turbulence intensity is greatly diminished along lines parallel to the riblet sidewall with distance into the valley. Deep within the riblet groove the flow is in an almost laminar state. High momentum fluids from layers above the riblet rarely penetrate into the lower half of the riblet groove.

Suzuki and Kasagi[18] investigated the structure of a turbulent flowfield along a riblet surface with the aid of three-dimensional particle tracking velocimetry. The statistics of all three velocity components were measured and compared with those above a smooth wall. Riblets had a triangular cross section with height 2.2 mm and spacing 3.5 mm. Under a drag-reducing condition, all of the turbulent velocity fluctuations and the Reynolds shear stress were decreased near the riblet surface, although the flow characteristics in most of the flow field were quite similar to those above the smooth wall. It was also found that the redistribution mechanism of the turbulent kinetic energy, from the streamwise component to the spanwise component was

was considerably suppressed in the region above the riblet valley. On the other hand, under a neutral drag condition, a cross-stream secondary flow was apparent near the ribs. This fluid motion should enhance the turbulent momentum transport and deteriorate the drag-reducing effect of the riblet.

The parametric studies by Walsh[7] and Balint et al[9] of various riblet geometries established the symmetrical v-groove riblet as a practical means for turbulent viscous drag reduction. In an effort to improve riblet performance, Lazos and Wilkinson[19] initiated an experimental project and extended the riblet database to additional, untested geometries. One of the achievements of that program was the identification of thin element, rectangular geometry with a maximum drag reduction equal to the symmetric v-groove (8%)[6,7] and the drag reduction at larger riblet spacing. Several rectangular riblets were investigated by Lazos and Wilkinson[19] and their study concluded that thin element riblets such as shown in Figure 2.5, are as effective in reducing drag as symmetric v-grooves, but exhibit a larger range of allowable spacing. The thin element geometry shows qualitatively an influence of independent variation of riblet height and spacing on overall drag reducing performance.

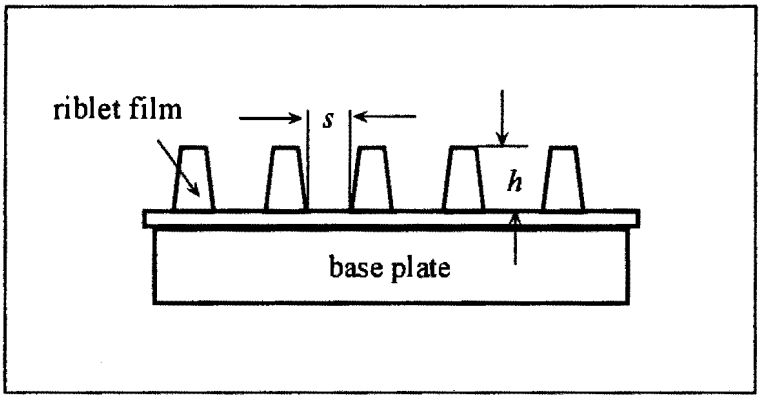

Figure 2.5 Thin element riblet arrays

A number of investigations discussed thus far, have made comparative measurements and computations of the total drag and of the mean and fluctuating velocity fields above riblet and smooth flat-plate surfaces, in attempts to document and explain the drag reducing effect of riblets. Walsh [6,7] reported up to 8% drag reduction for triangular riblets, a result later confirmed by Bechert et al.[20] Wallace and Balint[21]

compared the streamwise turbulence intensity profiles from various experiments for smooth and riblet surfaces, accounting for the effect on the profiles of Reynolds number variation as documented for smooth surfaces by Purtell et al.[22] With the exceptions of data of Bacher and Smith, [15] riblets appear to significantly reduce the turbulence intensity over most of the boundary layer, a result that has been confirmed by detailed measurements of Choi et al.[23] However, none of the measurements compared were able to approach close to the riblet surface.

Vukoslavcevic et al [24] made an attempt to reveal in detail the flow behaviour within the valleys of v-groove riblets. Vukoslavcevic et al[24] concluded that the local wall shear stress varies greatly in the spanwise direction, from about 85% greater than the smooth plate value at the riblet peak for flow with the same free stream velocity, to vanishingly small at the riblet valley. The turbulence intensities of the streamwise velocity fluctuations all indicate that the turbulence nearly vanishes below the midlevel of the grooves. Occasionally, relatively large positive streamwise fluctuations occur in the region between the midlevel and peak of the grooves due to the penetration of the higher velocity fluid from above.

However, unlike the vertical momentum transport over the smooth surface, this high momentum fluid rarely gets close to the riblet surface except near the peaks. Thus, the wall shear stress is lower than the flat-plate value over much of the span. When the resulting spanwise average shear stress is sufficiently lower than that of the smooth plate, more than compensating for the increased wetted surface area of the riblets, net drag reduction occurs.

In a similar manner, Bacher and Smith[15] used a combined visualization-anemometry study of the turbulent drag reducing mechanisms of triangular micro-grooved surface modifications. Streamwise, triangular riblets were machined on a 0.15 m by 1.21 m perspex plate with a 5:1 elliptic leading edge. A three-dimensional flow trip was used to initiate the turbulent boundary layer. The test surface was machined with triangular grooves (v-grooves) corresponding to $h^+ = s^+ = 15$. Visualisation of flow in the water was accomplished through the use of conventional food dye injection through slots and also using hydrogen bubble. Visualisation studies indicated that the familiar low-speed streak structure forms above the riblet surface, but that spanwise streak spacing

is increased by 40% over the flat plate flows. Fluid within the riblets was observed to move very slowly, with lateral transport of fluid becoming negligible near the riblet surface. Bacher and Smith[15] maintained that profiles of mean velocity and turbulence statistics indicated that the overall character of the turbulent flow over the riblet surface is similar to that over a flat plate. A momentum balance indicated that the surface drag for the riblet surface was approximately 25% lower than a flat plate flow, with more momentum retained in the logarithmic region above the grooved plate than above the flat plate.

In the most recent studies, direct numerical simulations by Karnadiakis et al[25] and Moin et al [26] have shown a 6% drag reduction with v-groove riblets. From examination of the instantaneous flow fields, a drag reduction mechanism is proposed: riblets with small spacings reduce viscous drag by restricting the location of the streamwise vortices above the wetted surface such that only a limited area of the riblets is exposed to the downwash of high-speed fluid that the vortices induce. Other areas of fluid dynamics where riblets are being investigated are in pipe flow. Anderson et al[27] investigated the effect of riblets with $h^+ = 12$, in fully developed turbulent pipe flow. He has reported a maximum drag reduction of between 5% and 7%. In a related study by Lancy et al, [28] the effects of surface riblets on the reduction of wall pressure fluctuations in turbulent boundary layers was investigated. Using triangular riblets, it was found that the wall noise was reduced approximately 2.8 dB by the riblets.

While studies of riblets have been presented, these have focused primarily on investigations into the effectiveness of different riblet geometries or the possible direct application of riblets. In some instances the conclusions of these works are sufficiently contradictory to warrant a more detailed investigation. Of the references that have been previously cited, some assert that the reduction of turbulent drag is due to the formation of counter-rotating vortices within the riblet valleys that do not reduce the turbulent shear stress, but is believed to reduce drag by preventing flow separation. On the other hand, it is felt that longitudinal vortices caused by flow over the riblets and low speed streaks in the viscous sublayer, lead to local instabilities of the flow. These bursts are in turn responsible for the chaotic motion above the viscous sublayer and subsequent drag reduction.

From all the research literature that was discussed previously, it appears that the v-groove riblet geometry offers the most potential in as far as turbulent drag reduction is concerned. Furthermore, there exists a suitable range for the riblet height, h^+ and riblet spacing, s^+ within which studies have shown that optimal drag reduction can occur. However, there is still some uncertainty as to the exact degree of drag relief that these riblets can offer. Therefore, it is the purpose of this study to investigate the v-groove riblet with two known geometries but to extend the direct drag analysis with a study of the boundary layer characteristics of the riblet and smooth surfaces.

All the measurements to date have shown only subtle changes in the turbulence structure itself. The principal conclusion would appear to be that flows within the riblet valleys are more greatly dominated by viscosity than the smooth plate flow at equivalent locations relative to the surface. In effect, it seems that the riblets shield the surface from much of the turbulent momentum transport resulting in smaller velocity gradients at the bounding surface.

Furthermore, the idea of the shear stress reduction mechanism by riblets is this: There are small streamwise vortices in the viscous sublayer of a turbulent boundary layer. The streamwise vortices produce a local upwash of slow fluid away from the surface. This is equivalent to the occurrence of low speed streaks. Whereas the main part of a turbulent boundary layer exhibits chaotic fluid motion, the viscous sublayer shows quite a regular streak pattern.[4] The velocity profile in a low speed streak is highly unstable and this causes the high fluctuation activity (bursts) in the layer adjacent to the viscous sublayer. Thus, the streamwise vortices should be hampered in order to decrease turbulent mixing and hence decrease the turbulent shear stress. This can be achieved by small longitudinal riblets that impede the cross flow of the streamwise vortices. The riblets should have a finer lateral spacing than the spacing of the streamwise vortices.

If one is to reduce turbulence in a boundary layer, then one must limit three-dimensionality of the flow; failing this, if the strength of three-dimensional vorticity in the near-wall can be reduced, then communication between the near-wall region and the outer region should also be reduced.[15] It is now generally accepted that some[8,

[15, 29] form of counter-rotating streamwise vortices play a role, if not the key role in this communication process, promoting and controlling the momentum exchange to and from the surface. It is suggested that the effect of the riblets is to modify and effectively reduce the momentum exchange properties of these streamwise vortices, with a consequent reduction in surface shear stress.

The preceding suggestion is a conceptual extension of 1) recent numerical studies of viscous-inviscid interactions between vortex structures and solid boundaries[17] and 2) several experimental studies of fully turbulent or transition-type flows.[10, 21] These studies indicate that streamwise vortices are capable of both concentrating low speed fluid in the spanwise sense and of triggering an outward eruption of low momentum fluid. It is suggested that this is accomplished by a feedback mechanism which relies on secondary vortex generation. As shown in Figure 2.6, the riblet peaks are speculated to accelerate and accentuate the development of cross-stream secondary vorticity, which could potentially yield discrete vortices within the riblet grooves themselves where they would rapidly dissipate. The resultant weakening of the parent vortices would thus inhibit their ability to concentrate low momentum fluid, thus inhibiting the momentum exchange process.

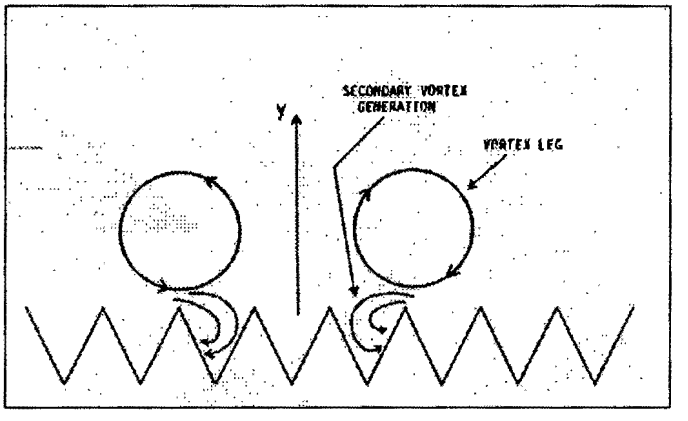

Figure 2.6 Schematic of streamwise vortex interaction with riblet surface via viscous effects (from ref. 15)

It is suggested that in order to reduce drag by surface modifications, the surface geometry must be chosen to maximise its effect on the streamwise vortex structures. Specifically, one should inhibit both spanwise concentration of fluid as well as outward eruptions of fluid from the wall region. Streamwise riblets with sharp peaks

will inhibit spanwise concentrations of low speed fluid by the secondary vortex generation mechanism discussed above. Low-speed streaks still form, as was observed in Ref. 15, but the number of streaks per unit span will be lower. In addition, the difference in velocity between the low-speed and the high-speed regions appears to be smaller above the riblet surface than above the flat plate. This suggests that the shear layer instability, which leads to streak breakdown and bursting, may not be as intense, and thus the ejection of low-momentum fluid into the outer region should not be as strong as above the flat plate. Weaker ejection should retard development of the boundary layer, yielding smaller momentum deficits in the outer region of the flow, as was observed in Ref. 15.

A schematic drawing illustrating a proposed interaction of the grooved surface with a pair of counter-rotating streamwise vortices is shown in Figure 2.7. Note that the generation of secondary vortices at the riblet peaks serves two functions: 1) weakening of the streamwise vortices that spawn the secondary vortices and 2) the retention of low speed fluid within the grooves. This process enables the riblet surface to retard the development of the turbulent boundary layer and thus reduce drag in comparison to a flat surface.

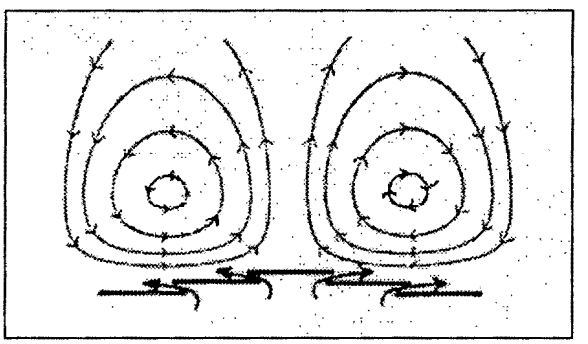

Figure 2.7 Perspective schematic showing the hypotesized interaction of counter-rotating streamwise vortices (from Ref. 15)

In summary, the survey of previous studies on the drag reduction of riblets has shown beyond question, that streamwise-aligned riblets can reduce viscous for a limited range of heights and spacing of the riblet. The v-grooved riblet has shown the greatest potential for drag reduction with a maximum of 8% recorded. This is

probably due to a displacement of most of the vertical momentum transport away from the surface, which is also reflected in a reduction of the free stream turbulence intensity. This is accompanied by a reduction in the near wall shear stress and a decrease in the drag force acting on the surface. The increase in the wetted surface area, through the introduction of riblets on the surface, appears to not increase the drag on the surface but appears to have an effect on the amount of drag reduction that occurs. In other words, the amount of drag reduction that has been measured, appears to be related to the riblet height and spacing.

3. DRAG REDUCTION MECHANISM DERIVED FROM SHARK SKIN

One approach that has led to the development of riblet surfaces has come from the studies of shark scales or dermal denticles. At the outset of this report it should be stressed that it is not within the scope of this report to discuss in detail, all the functional aspects of placoid scales (dermal denticles), but to show the existence of a relationship between the placoid scales and hydrodynamics, namely its function in drag reduction. In order to accomplish this, the following section is dedicated to discussing the results of experiments that have previously been conducted. The interested reader is requested to consult the references that are cited, for a more detailed explanation of other functions of placoid scales.

Section 3.1 discusses past research on the use of sharkskin as a drag reducing mechanism. The latter part of this chapter will discuss briefly, the physical and hydrodynamic aspects of shark scales with specific reference to microscopic analysis of an actual shark specimen that was studied for the purpose of this report. This section will make references to recorded information and compare these to the studied specimen.

3.1 ON THE DRAG REDUCTION OF SHARK SKIN

Interest in the drag characteristics of sharks is found as early as 1970 in the work of Johnson[30], who measured drag levels on a dead shark towed through the water. The drag levels for the shark were 8-10 times higher than the estimated drag of a dolphin. At the time, Johnson concluded that the high drag levels of the brown shark were due to the rough sandpaper-like skin surface. Bechert et al[31] have since speculated that the high drag levels measured by Johnson[30] may actually have been due to improper fin position on the dead shark or that the shark may not have been towed at zero angle of attack. A typical shark scale is shown in figure 3.1. The specimen in question is from a fast swimming shark, *Carcharhinus falciformis* or commonly referred to as a silky shark. 'A' represents the crown width; 'B', crown length; 'C', primary inter-keel

distance; 'D', primary keel height; 1°, 2°, 3° are the primary, secondary, and tertiary keels.

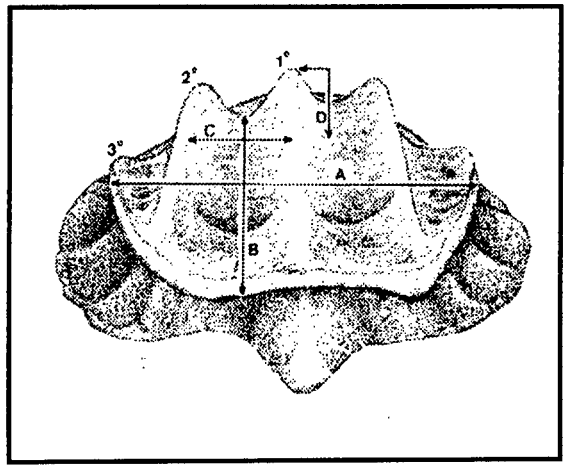

Figure 3.1 Drawing of a shark scale, *Carcharhinus falciformis* (from Ref. 35)

More detailed studies of the scale structure of sharks have been reported by Reif[32, 33] who determined that all shark scales could be divided into the following four functional categories:

1) abrasion protection
2) parasite protection
3) drag reduction
4) luminescence capability

The thrust of this report will be in the drag reduction aspect of placoid scales. The shark scales in the drag reduction category were of particular interest as Reif[32] found that the fast-swimming sharks had scales with finely spaced ridges, which were basically aligned with the local flow angle, whereas slow sharks did not have this scale structure. Reif[32] speculated that the ridges on the scales reduced the drag of fast swimming sharks by stabilizing either the laminar or turbulent boundary layer. Reif and Dinkelacker[34] and the Virginia Institute of Marine Sciences (VIMS) have conducted further work relating the dimensions of the ridges on the shark scales to the near-wall structure of the turbulent boundary layer. The VIMS research was initiated in 1980 under grant to NASA Langely Research Center and is reported by Raschi and Musick[35] and Raschi and Elsom.[36] Reif and Dinkelacker[34] and Raschi and Musick[35]

all report that the ribs on the fast swimming sharks' scales have sharp peak with rounded valleys.

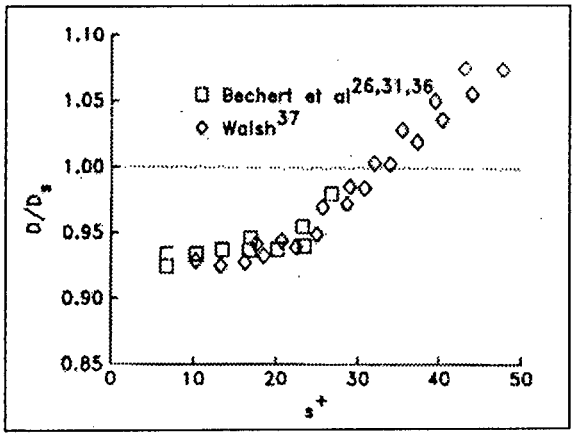

Figure 3.2 Drag reduction performance of sharklike riblets (from Ref. 35)

Figure 3.2 presents the data obtained by Walsh[8] and Bechert et al[31] for a streamwise riblet with the cross section similar to the shark scale with sharp peaks and rounded valleys. The sharklike riblet gave drag reductions of 7-8%. It should be pointed out that the riblets tested in Refs. 31 and 8 were continuous in the streamwise direction, whereas the shark riblets are discontinuous. Figure 3.3 shows a typical scale arrangement on a dusky shark, *(Carcharinus obscurus)*. This denticle pattern was taken from just behind the pectoral fin region of the shark. Notice the array of hand-like scales with ridges on the crown of the scales. It is felt that these ridge patterns on scale crowns are to redirect, or canalize, water flow.[37]

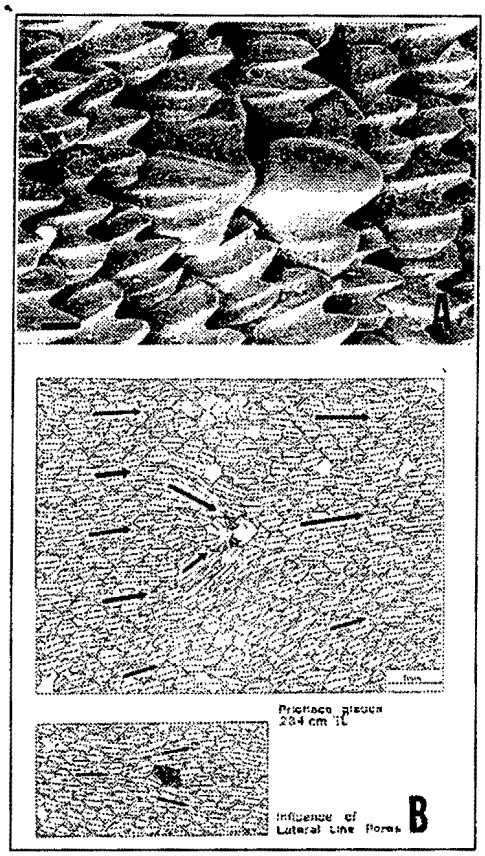

Figure 3.3 Modified denticles around the pectoral fin region of *Carcharhinus obscurus* (from ref. 35)

In Figure 3.3 in the second picture from above, we see the arrows point towards a hole in the scale pattern that is connected to the lateral line organ. Realigned ridges on the scales appear to channel the water flow toward the corresponding pit opening. This serves as a pressure sensing organ. Raschi et al[35, 36] examined the scale structure of 15 species of galeoid sharks in detail. He was able to find a relationship between the shark ridge height and the body length of the shark. He determined the shear stress as a function of the swimming speed of the shark. Raschi et al[35, 36] found that for cruise speeds, the ribs are small and appear as a smooth surface to the boundary layer.

Waid[38] correlated the ridge dimensions for a blue shark (*Prionance glauca*) and found results similar to those of Raschi et al.[35, 36] As figure 3.1 indicates, fine ridges in the streamwise direction are found on the scales of fast sharks. On the surface of the pectoral fins of a number of sharks Bechert[31] found scales with v-shaped central ridges. These are considered to be longitudinal vortex generators that enhances mixing and keep the flow attached to the surface. Raschi and Musick[35] explain that all

fast off-shore sharks have scales with fine ridges (spacing (35 – 105 μ), whereas reef sharks have a similar scale structure but slightly wider ridge spacing. In contrast to that, slow sharks have completely different and largely varying scale patterns, which may be interpreted as devices for protection against abrasion, parasites and predators.[33] The burst speeds of fast offshore sharks are in the range of 10-15 m/s.[31] The cruise speed is estimated at 2-5 m/s. The Reynolds number that Bechert et al[20] used in his analysis was based on a shark body length of 2-3 m and was calculated in the order of 10^6- 10^7. Thus, it is reasonable to assume turbulent flow on most parts of the surface of a fast shark.

Separation control by enhanced mixing of the turbulent boundary layer is useful in regions of strong positive pressure gradients where separation is likely to occur.[31] The pectoral and caudal fins of sharks have airfoil profiles and operate, roughly speaking, similar to the blades of a turbomachine. Of the species of fast shark that Rashi and Musik[35] investigated, several had scales with v-shaped central ridges. Such structures produce enhanced mixing by the generation of streamwise vortices with an upwash of fluid downstream of the v-shaped wedge.

Bechert, Reif and Hoppe[39] conducted what is widely recognized as an extensive and ground breaking study on the drag reduction of the shark skin. It was the first study to attempt to closely map the shark skin and then test it. They considered only the scales of fast sharks. These are very small (size: 0.2-0.5 mm) and have very fine longitudinal ridges on the crown. Figure 3.1 clearly shows this physical feature. The analysis led to the consideration of several interaction mechanisms between the viscous sublayer and the shark skin surface.[39] The artificial surface used by Bechert et al[39], was tested in a turbulent boundary layer and a 7% drag reduction was found. This led to a fluid dynamic explanation that shark scales were longitudinal vortex generators. This was consistent with some previous experimental results[39].

On the surface of the pectoral fins of a number of shark species, scales with v-shaped central ridges were found. These are considered to be vortex generators that enhance mixing and keep the flow attached on the surface. It was found that the angle of attack of the scales of fast sharks could be altered. It was assumed that, with the mechanical

tension of the skin of live sharks being present, there was an elastic anchoring of the scales. The actual angle of attack would then be established by the local flow shear stress. Following this model, high angles of attack would occur under conditions close to flow separation. On the other hand, it was shown experimentally that mixing is enhanced rapidly with increasing angle of attack of the scales. Therefore, it was assumed that these scales, with a variable angle of attack, prevent separation by stress-dependant anchoring.[39]

With the absence of complete shark scale data at the time, Bechert, Reif and Hoppe[39] postulated on other novel interaction mechanisms, which explained most of the geometrical features of shark scales. A hypothetical streak cancellation mechanism was considered. It was concluded from various experimental and theoretical considerations, that the low speed streaks of the viscous sublayer occur in the regions of low instantaneous local pressure on the surface. This instantaneous low pressure is utilized to eject fluid through the slits between the scales, in the downstream direction in order to compensate the low speed streaks. A close inspection of the geometry of the shark scales reveals that indeed the rounded leading edges and the very sharp trailing edges of the scales, as well as the cavities underneath the surface can be explained with this mechanism.[39]

3.2 THE HYDRODYNAMIC ASPECTS OF SHARK SCALES

There are four galeoid families that are believed to be fast, active swimming sharks; namely, *Sphinodae, Carcharhinidae, Isuridae and Alopiidae*. Reif and Dinklacker[34] have conducted a preliminary study on the physical aspects of the scales of these species. Typical ridge heights and spacing in a fast shark is less than 30 μm and 100 μm respectively. The ridge pattern on fast sharks (eg. *Carcharhinus obscurus*) differ considerably in appearance from those of slow sharks (eg. *Echinorhinus brucus*). Furthermore, on any shark, the ridge structure on each scale varies depending on the strategic position of the scale on the body of the shark. Figure 3.4 shows the variation of the scale shapes and ridge arrangements of a Galapagos shark

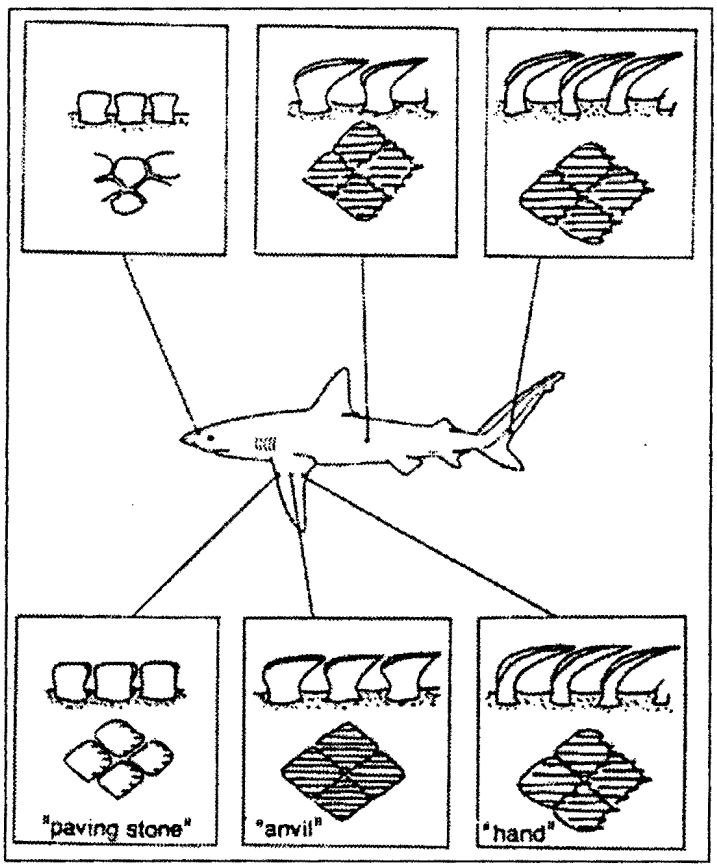

Figure 3.4 Galapagos Shark: *Carcharhinus Galapogensis*, 2.55m length, scale shapes on various locations of the body. (From Ref. 31)

In addition to the specific ridge patterns, hydrodynamic scales can alter their angle of attack through skin tensioning at higher swimming speeds. This may be to generate increased turbulence at higher swimming speeds, preventing flow seperation.[34] Another characteristic of shark skin is that Aster sharks exhibit greatly increased scale densities but at significantly reduced scale weights.[36] In order to see these variations of shark scales first hand, it was decided to acquire fresh sharkskin specimens and to view them under an electron microscope.

A Bronze whaler, *Carcharhinus limbatus*, that had caught itself in treknets off Faure on the Cape coast, was used for this purpose. The shark was skinned at specific points on its body. The skin was de-fleshed, cleaned, frozen and then cut into portions suitable for use. The specimens were then ultrasonically cleaned in distilled water whereupon a fixative was applied in order to remove small amounts of fat that would cause rotting. The normal procedure for preparing a specimen for electron microscopy was followed, but to avoid shrinkage and surface deformation, that

normally accompanies drying of the skin, the specimen was submerged overnight in a special aldehyde solution. Once ready, the twelve specimens representing the scale formations on twelve different parts of the shark's body were viewed under an electron microscope and photographed. Electron microscopy was chosen over other viewing techniques since it allowed clear and distinctive photography at the required magnification. The images that follow clearly indicate the ridge formations and the different scale geometries on the sharkskin, depending on the body position the specimen was taken from.

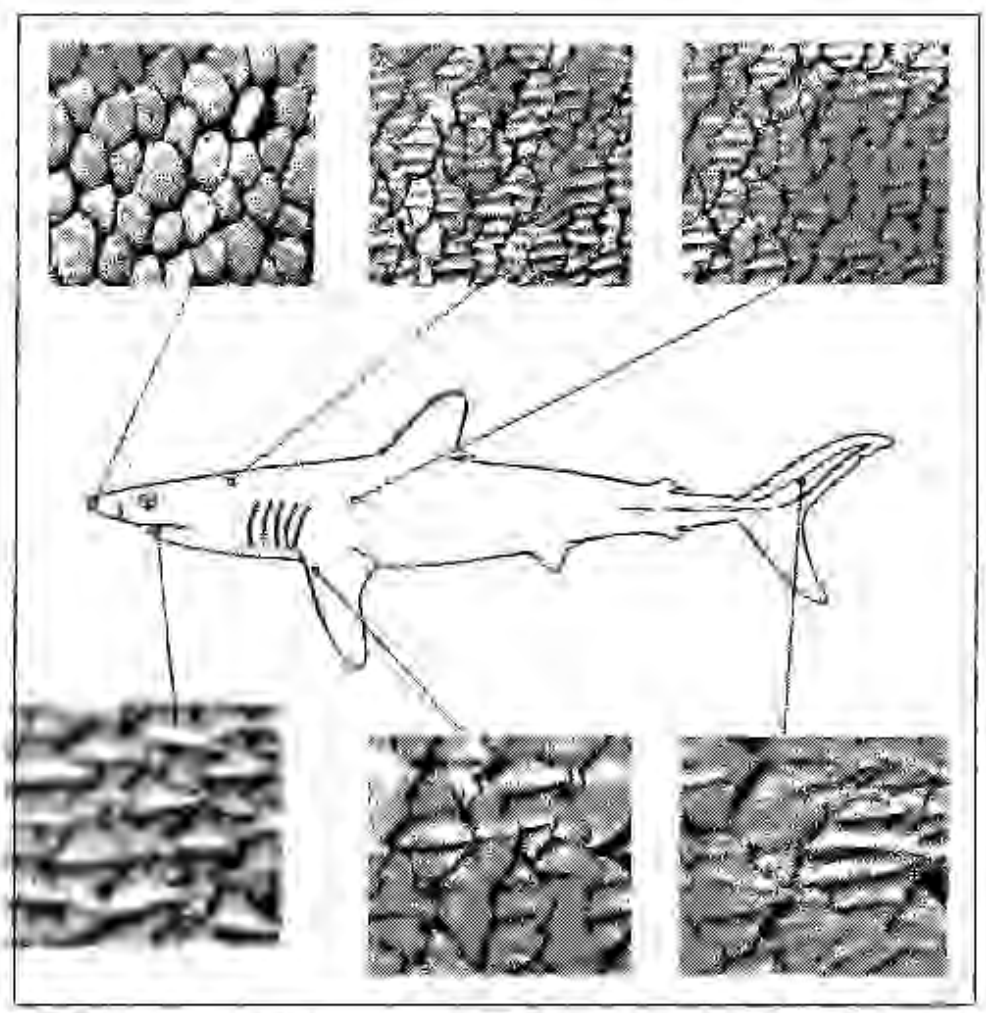

Figure 3.5 Comparative SEM micrographs of dermal denticles from a Bronze whaler, *Carcharhinus limbatus*, 1.5 m at different locations on the body.

The scanning electron micrographs in figure 3.5 were not unlike those expected. They confirm the micrographs in Raschi and Musick[35] and Bechert et al[31] regarding the scale shapes and ridge patterns on fast-swimming sharks, in this case from the *Carcharhinidae* family. From figure 3.5 it can be seen at the snout (rostrum) of the

shark, the scales look like well-adjusted paving stones with a very smooth surface. In this location laminar flow and varying flow directions, due to varying stagnation point locations can be assumed.[31]

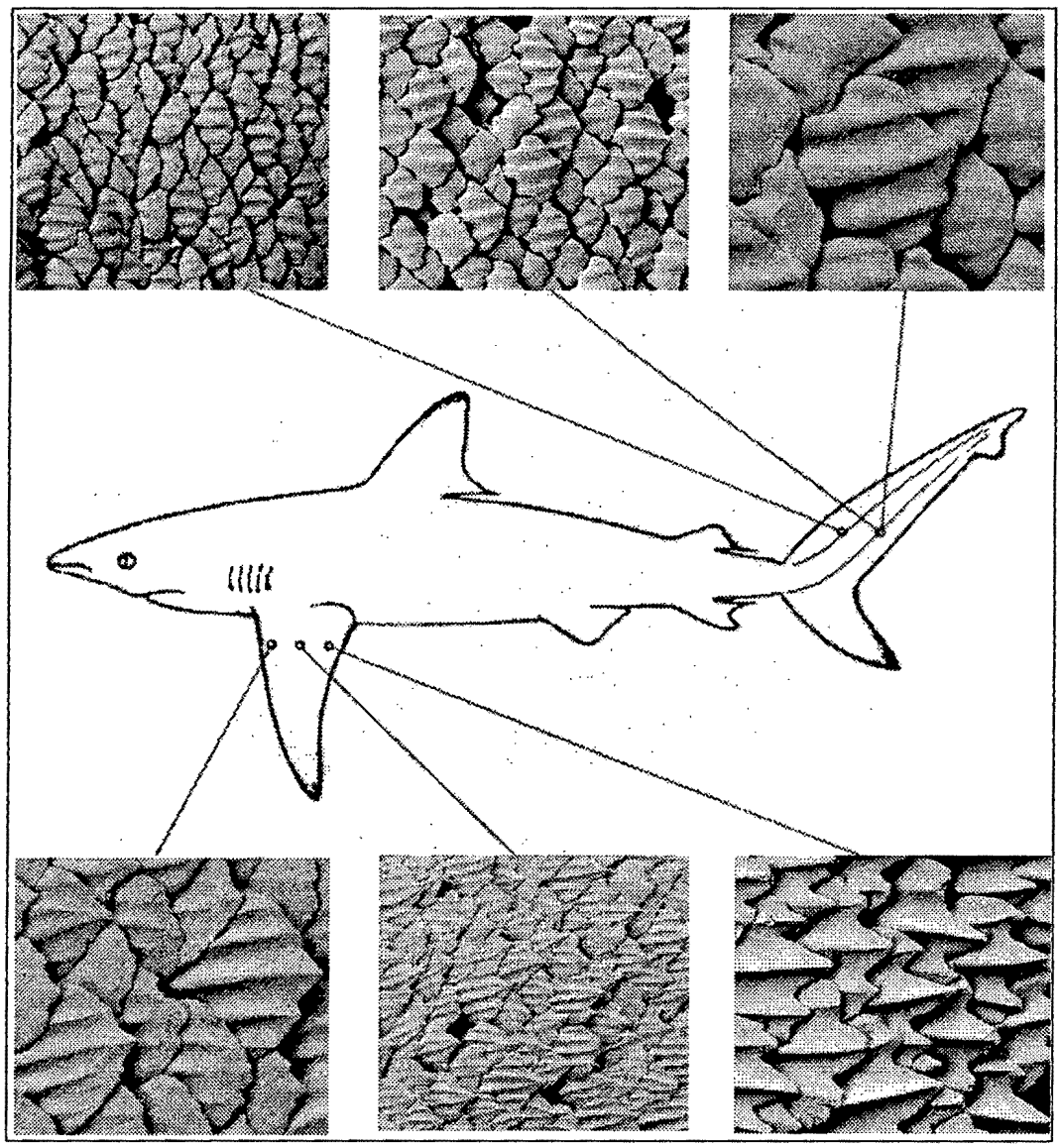

Figure 3.6 Comparative SEM micrographs of dermal denticles from a Bronze whaler, *Carcharhinus limbatus*, 1.5 m at the pectoral and tail fin regions of the body.

In the middle of the body and the fins we recognise an anvil-like structure of the scales, with ridges in the downstream direction. It appears as if the direction of the ridges follow the local flow direction. The arrays of overlapping ridges appear to form channels. On the pectoral fins we see scales with v-shaped ridges. It appears that the ridge formations are more extreme on the rear part of the shark. The scales appear to

have a smooth surface on the front part of the shark and then gradually as one looks along the shark, the ridge definition and depth become more extreme.

On the rear part of the body and the fins, the scales look like little hands and these are less rigidly anchored in the skin than the anvil-like scales. On some species, like the Hammerhead and Mako shark, the body is almost completely covered with very small scales.[35] It appears that the density of the grooves, per scale, is greater for the scale at the leading edge of the fins than on the trailing edge. Like other fast sharks, the dimensions of the scales lie between 0.2 and 0.5 mm. The lateral spacing of the ridges on the crown of the scales is between 0.035 and 0.1 mm.[31] The scales can carry between 3 and 7 ridges, depending on the scale size. Notice how on some scales the ridges can form channels as they overlap other scales. Bechert and Hoppe[31] manufactured an artificial fin similar in shape to the one shown at the trailing edge of the pectoral fin. It was found that in this region, high adverse pressure gradients in the boundary layer are to be expected. Enhanced mixing of these particular scales was likely to keep the flow attached here in order to improve the performance of the fins.[31] Further studies of the scale structure of this species and others are discussed in detail by Raschi and Tabit[37] and Raschi and Musik.[35] It is left to the interested reader to consult these references for further information.

In summary, it is clear that the distinct physical structure of placoid scales could complement the swimming performance of the shark. The next step is to reproduce the skin structure onto a lifting surface, such as a flat plate, and to investigate the effect of these surface modifications on the lift and drag forces on the flat plate.

4. TURBULENT BOUNDARY LAYER THEORY OVER A FLAT PLATE

The literature survey has shown that riblets could reduce drag in a turbulent boundary layer. It is necessary to model the theoretical boundary layer characteristics of the test surfaces so that a comparison can be made with the corresponding experimental values. However, no theoretical boundary layer theory and equations exist for ribbed surfaces and since it is beyond the scope of this dissertation to attempt to model the flow over the ribbed surfaces, the theoretical analysis will be restricted to analysing turbulent boundary layer theory over a flat plate.

While there have been attempts in the past, to create a mathematical model that would describe turbulent flow over ribbed surfaces[17], these have been widely received, by other researchers, with suspicion. The underlying procedure that had been adopted, simplified riblets in two-dimensions and used conformal mapping techniques to solve complex transformation. However, this analysis will not consider these models and rather concentrate on the flat plate analysis. Furthermore, the detailed derivations of the boundary layer equations that will be used are omitted as these can be found in any fluid mechanics textbook. The equations that will be used have been validated by other authors and are recognised and accepted equations in fluid dynamics. The interested reader is requested to refer to any one of Bowden et al[40], Hollman, [41] Schlichting[42], Anderson[43] and Janna[44] for detailed turbulent boundary layer derivations from first principals.

There is no simple methodology for turbulent flow but the Navier-Stokes equations apply. None of the velocities in the equations vanish. Solving them, if possible yields instantaneous values of velocity and pressure. In turbulent flow, velocity and pressure fluctuate wildly about mean values.

Continuity: $\nabla \cdot V = 0$ (4.1)

Equation of motion:

$$\frac{\partial V}{\partial t} + (V \cdot \nabla)V = -\frac{\nabla p}{\rho} - \nabla g + \nu \nabla^2 V + \nabla \cdot \rho V V' \qquad (4.2)$$

Where the terms V are the velocity vectors and $V'V'$ are the turbulent velocity fluctuations. For turbulent flow, a region exists near the wall where the flow is not random. A change in the flow exists near the wall where the velocity is zero. In this region near the wall, a laminar sublayer forms, within which Newton's law of viscosity describes the flow. Between the two is a buffer zone, within which both laminar and turbulent effects are considered to be important. With the absence of an exact solution to describe the behaviour of turbulent flow, experimental results are used. It has been found that a seventh-root velocity profile correlates well with turbulent boundary layer date over a wide range of Reynolds numbers: [44]

$$\frac{v_x}{u_\infty} = \left(\frac{y}{\delta}\right)^{1/7} \tag{4.3}$$

where v_x is the velocity at any height y above a surface, u_∞ is the free stream velocity and δ is the boundary layer thickness. At the wall or surface, $y = 0$, and the gradient becomes infinite. Because this is physically impossible, the laminar sublayer along the wall is assumed to have a linear profile that becomes tangent to the seventh-root profile at the edge of the buffer layer, where $y = \delta$. The wall shear stress is obtained from experimental results. Hollman[39] recommends for $Re_x < 10^7$, Eq. (4.4)

$$\tau_w = 0.029 \rho u_\infty^2 \left(\frac{\nu}{u_\infty x}\right)^{1/5} \tag{4.4}$$

where ρ is the fluid density, ν is the kinematic viscosity and x is the position along the plate measured from the leading edge. The local skin friction coefficient, C_f is

$$C_f = \frac{\tau_w}{\frac{1}{2}\rho u_\infty^2} \tag{4.5}$$

The total drag force on the plate is determined by integrating the wall shear stress over the surface area of the plate of length l. This equation is determined by Janna[44] to be

$$D = b\int_0^l \tau dx = \frac{0.0358 \rho u_\infty^2 bl}{(\mathrm{Re}_L)^{1/5}} \tag{4.6}$$

where Re_L is the Reynolds number over the whole plate.

At any particular point along the plate the Reynolds number is given by

$$\mathrm{Re}_x = \frac{\rho v_x x}{\mu} \tag{4.7}$$

The corresponding coefficient of drag is then

$$C_D = \frac{0.074}{(\mathrm{Re}_L)^{1/5}} \tag{4.8}$$

Janna[44] recommends, from experimental results, that the boundary layer thickness, δ, is calculated from,

$$\delta = \frac{0.368x}{(\mathrm{Re}_x)^{1/5}} \tag{4.9}$$

For the viscous sublayer, the equation from Schlichting[42] is used to determine the laminar sublayer thickness, δ_L

$$\delta_L = \frac{8\nu}{\sqrt{\tau/\rho}} \tag{4.10}$$

Using a test plate with dimensions of 300 by 520 mm and an air free stream velocity of 3 m/s, it was now possible to determine what the theoretical boundary layer characteristics of a flat plate in turbulent flow would be. A low free stream velocity was chosen in order that a sufficiently thick boundary layer could be found. The estimated free stream velocity of 3 m/s was later adjusted to match the actual velocity of 3.6 m/s. This velocity was used in the theoretical calculations. With all the equations at hand, the shear stress, τ_w, coefficient of friction C_f and Reynolds number were calculated at different x positions along the test surface. The total drag and coefficient of drag on the test surface was also calculated. The results are shown in Table 4.1. The results are calculated at x = 110, 200, 300, 380, 490 and 590 mm. These are the x stations at which the experimental boundary layer will be tested.

x (mm)	τ (Pa)	C_f	Re
110	0.0607	0.007712	26661
200	0.0538	0.006843	48475
300	0.0496	0.006310	72712
380	0.0473	0.006018	92102
490	0.0450	0.005720	118764
590	0.0434	0.005511	143001

Table 4.1 Theoretical boundary layer characteristics over a smooth flat plate

The corresponding boundary layer thickness and laminar sublayer thickness values are shown in Table 4.2. The total drag force on the test section calculated with Equation (4.6) is 0.008 N. Using Equation (4.8) the corresponding dimensionless coefficient of drag, C_D for the smooth plate was calculated to be 0.00715.

x (mm)	δ (mm)	δ_L (mm)
110	5.27	0.53
200	8.51	0.56
300	11.77	0.59
380	14.22	0.60
490	17.42	0.62
590	20.21	0.63

Table 4.2 Theoretical boundary layer and laminar sublayer thickness

5. EXPERIMENTAL APPARATUS AND TESTING PROCEDURE

Two sets of experiments were required. First the riblet surface and flat plate surfaces were placed in a test section where the boundary layer study could be conducted. Upon completion of the boundary layer analysis, the test surfaces were mounted in a direct drag balance in which the drag force on the surfaces could be measured directly.

Both experiments were conducted in the wind tunnels in the Duncan McMillan Laboratory at the University of Cape Town. The two experimental approaches used to fulfil these requirements will be discussed separately in this chapter. Two v–groove riblet surfaces were studied and a smooth flat plate was tested as the reference surface. The riblet geometries that have been used were tested before and have shown net drag reductions of 7% to 8%.[7] The dimensions of the riblets were chosen such that $h^+ = s^+ < 30$ in law of the wall units.[7,8] Figure 5.1 shows the height h and spacing s of the symmetric and unsymmetrical v-groove models that were tested. The test surfaces were machined on 10 mm perspex boards.

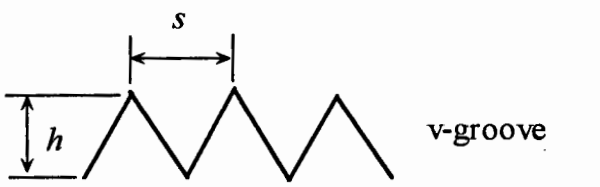

Model	h (mm)	s (mm)	h/s
#1	0.254	1.143	0.22
#2	0.51	0.51	1

Figure 5.1 V-groove riblets

5.1 BOUNDARY LAYER MEASUREMENTS

The experiment was conducted at a free stream velocity of 3.6 m/s. The test surfaces dimensions were 720 mm by 526 mm so that the sides fitted exactly against the wind tunnel test section walls, preventing any possible edge flow effects. Figure 5.2 shows one of the test surfaces. A low speed closed jet wind tunnel was used. This tunnel has an 880 mm long test section with a cross section 530 mm high and 530 mm wide. The test surface was suspended, 210 mm above the test section floor, at zero degree angle of incidence to the free stream. Figure 5.3 shows a sketch of the experimental setup.

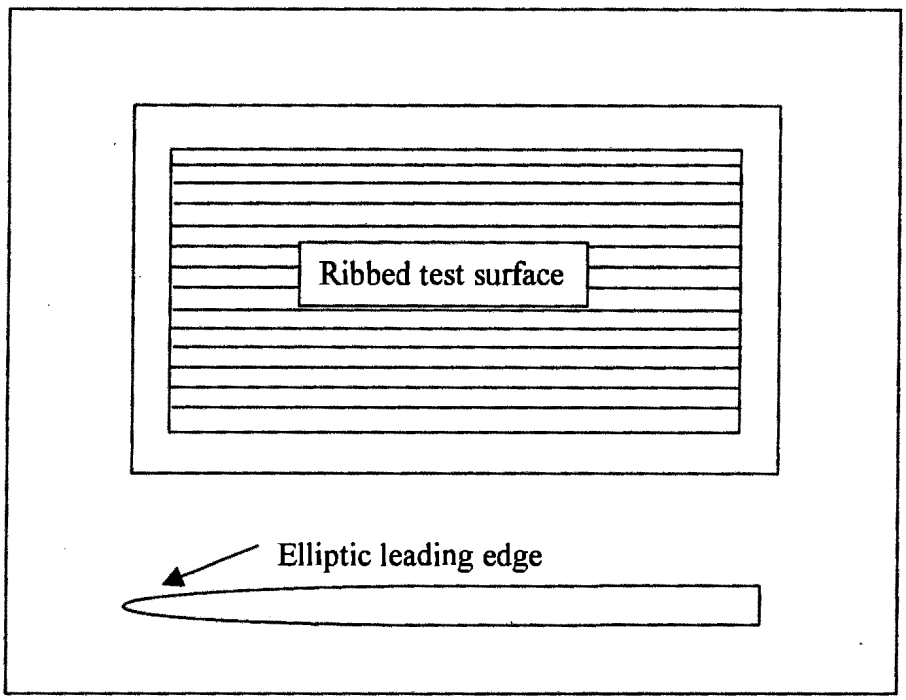

Figure 5.2 Test surface

At this point it must be stated that the following assumption was made: **Static pressure in the wind tunnel is constant, the static pressure thus exerts no resultant forces on the control surfaces of the flat plate and the only external forces in the x direction (i.e. along the plate) acting on the fluid inside the control surface is the drag force.**

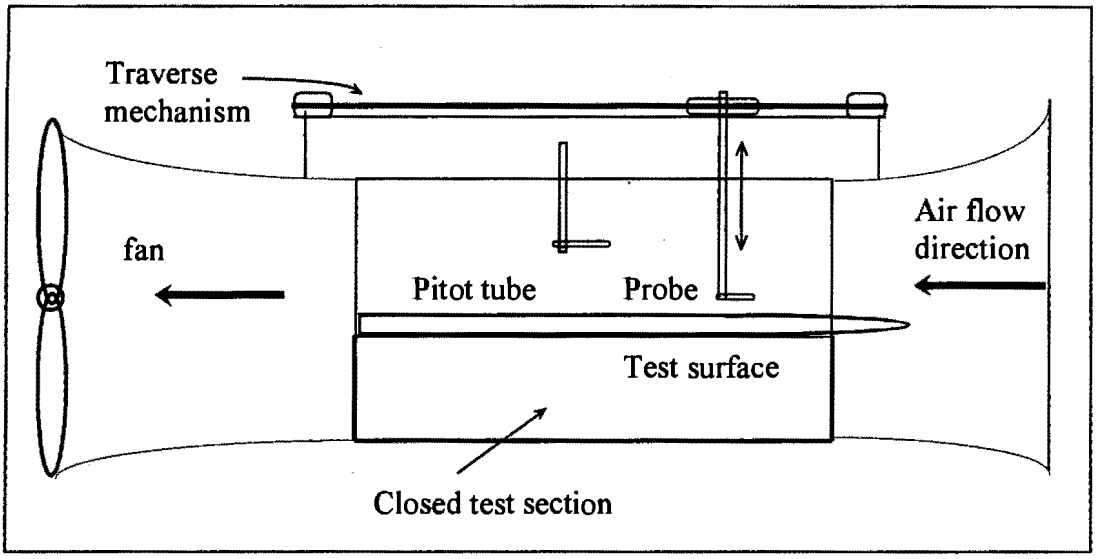

Figure 5.3 Experimental setup for Boundary Layer measurements

A flattened hypodermic needle was used as the pitot probe. The tip had outside dimensions of 0.58 x 0.98 mm. The pitot probe was mounted on a traverse mechanism described in Ref. 45. The spanwise position of the probe was on the tunnel centerline. The pitot probe was first calibrated against a known pitot static tube and the resulting calibration curve is presented in Appendix F. To measure the boundary layer experimentally on the test surfaces, the velocity profiles had to be determined along each plate from the leading edge. The velocity profiles were measured at different x distances from the plate leading edge, where the flow is turbulent. As noted earlier, a turbulent boundary layer was required. It was therefore necessary to trip the boundary layer to achieve turbulent flow. This was accomplished by sticking 40 grit course sandpaper onto the leading edge of each test plate. The leading edge of the test surfaces was elliptical with a leading edge radius of 3 mm. Appendix A shows the engineering drawings of the test surfaces

One method of determining whether or not the boundary layer has time to become fully developed is to examine the similarity of the velocity profile. Two streamwise velocity profiles for the tripped boundary layer are shown in Figure 5.4. One profile was taken close to the leading edge and the other was taken close to the trailing edge of the smooth test plate. Note that the u in the abscissa of Figure 5.4 is the same as the free stream velocity, u_∞.

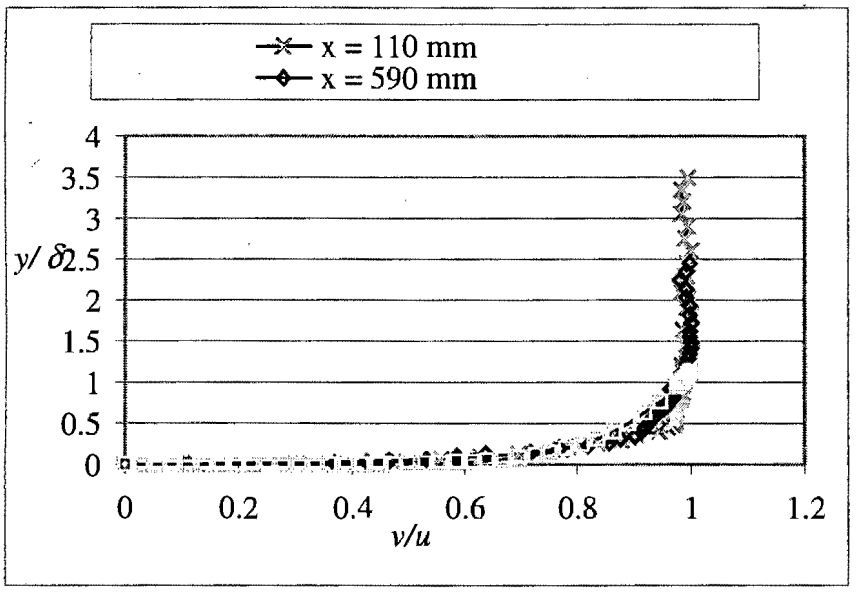

Figure 5.4 Similarity of velocity profiles for smooth plate

At each x distance from the leading edge, the pitot probe was traversed in the y direction. The traverse could move vertically down in 0.1 mm increments. At each y, the difference between the total and static pressure was measured with a micro-manometer. Due to the low pressures that were being encountered and the minute pressure differences that had to be measured, a digital micro-manometer, which was able to measure a pressure difference of 0.01 Pa was used. The $y = 0$ position was taken as the position where the probe just made contact with the test surface. In the case of the riblet surface, this was the peak of the ribs. The probe was traversed until the pressure difference was zero and the velocity at that point, v_x, was equal to the free stream velocity, u_∞. The smooth plate and the riblet models were surveyed at the following distances from the leading edge of the test plate: 110, 200, 300, 380, 490 and 590 mm.

5.2 DIRECT DRAG MEASUREMENTS

Direct drag measurement were performed in a re-circulating open jet wind tunnel. The open jet test section measures 870 mm x 580 mm with corner fillets at the throat and a working length of 1.6 m. The direct drag measurements were made for free stream velocities between 1 and 12 m/s. Previous experiments of a similar nature indicated

very small changes in the measured drag forces.[7] A sensitive measuring device was thus required. The existing drag measuring device in the wind tunnel is a three component balance. Based on measured drag values of previous studies[7], it was anticipated that this device would not be sensitive enough for this experiment. The differences in the drag forces as measured by Walsh[7] were of the order of 0.0001 N whereas the existing device could measure only differences up to 0.02 N. Consequently, another method had to be devised to measure the small drag forces.

The procedure used to measure the direct drag was to suspend the test surface from 4 spring steel hacksaw blades, approximately 1mm thick. The test surface was aligned with the roof of the wind tunnel so that flow was restricted to the area being tested. In the case of the riblet surfaces, the riblet peaks were aligned with the wind tunnel roof. Strain gauges were mounted at the most suitable cantilever position (which would register the greatest bending moment) along the spring steel blades. The three test surfaces were cut to the same dimensions of 300 by 500 mm. In the case of the riblet surfaces, the entire surface was covered with riblets. When the test plates experienced a drag force, it caused the steel blades to deflect, as well as the strain gauges on them. A strain gauge amplifier then amplified this deflection. The result was a deflection value for the steel blade due to the drag force. The strain was measured in micro-strains, $\mu\varepsilon$.

The measured strain was related to a force by initial calibration of the strain gauges. Initially, the strain gauges were calibrated by applying a known force to the steel blades and reading the resultant strain on a digital readout. In this manner a calibration curve was drawn showing micro-strain versus force applied. The calibration curve is presented in Appendix F. A sketch of the experimental setup is shown in Figure 5.5 as well as in Appendix A.

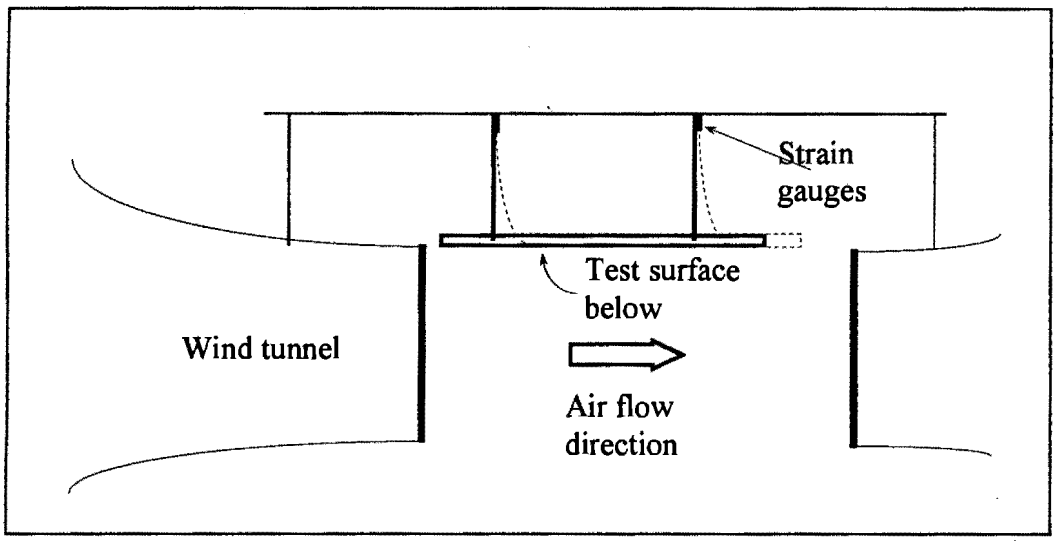

Figure 5.5 Experimental setup for direct drag measurements

Behind the test surface a flat wooden board was mounted level with the test surface so that flow continuity could be maintained over the trailing edge of the test surface. A series of 2 runs were used to establish the mean drag curve for each of the test surfaces. Between each run the model was removed from the tunnel and rotated 180 degrees. Due to the sensitivity of the setup, the strain gauges were re-calibrated before each run. With careful alignment of the model leading and trailing edge, the individual drag measurements were repeatable to within 5%.

6. EXPERIMENTAL RESULTS

A basic part of any drag reduction study is a comparison of the proposed drag reduction surfaces with a reference surface, in this case a flat plate. This chapter examines the boundary layer and direct drag measurements for the three test surfaces. Comparisons are then made between riblet model data and reference flat plate results. At this point it is important to mention that the data that is directly recorded from the experiments are pressure differences, ΔP. These pressure differences are then converted to velocities by applying the Bernolli equation to the static and stagnation holes of the Pitot-static tube.[44] The flow velocity is therefore given by,

$$v = \sqrt{2\Delta P / \rho} \qquad (6.1)$$

6.1 EXPERIMENTAL BOUNDARY LAYER MEASUREMENTS

The velocity, v_x was taken at a particular height, y, above the plate, at different stations, x along the plate from the leading edge. A complete list of the recorded data points is attached in Appendix B. The data has been arranged in order of incrementing distances of x along the plate, for all three plates. In order that the experimental results can be delivered systematically, the universal velocity profiles will be shown and will be broken down into the graphs for the flat plate followed by the graphs for the two ribbed plates.

6.1.1 LAW OF THE WALL PLOTS

One method of checking whether the flow along the plate is turbulent is to plot the universal velocity profile, also known as the 'law of the wall'. The equations of these graphs generally match very well with experimental data. The idea is to plot our experimental data on the log curve and check how well it matches the universal velocity profile. The law of the wall is applied from the surface of the plate, where the laminar sublayer exists, to where the flow is fully turbulent.

The universal velocity profile is reported by Holman[41] as,

Laminar sublayer: $0 < y^+ < 5$ $\quad u^+ = y^+$

Buffer layer: $5 < y^+ < 30$ $\quad u^+ = 5.0 \ln y^+ - 3.05$ (6.2)

Turbulent layer: $30 < y^+ < 400$ $\quad u^+ = 2.5 \ln y^+ + 5.5$

Where $u^+ = \dfrac{u}{\sqrt{\tau_w/\rho}}$ and $y^+ = \dfrac{\sqrt{\tau_w/\rho}\, y}{\nu}$

Consequently, Figure (6.1) to (6.3) represent the experimental velocity data obtained for the three test surfaces, plotted against the universal velocity profile. The graphs are presented as u^+ versus y^+. The velocity profiles for all the x stations along the plate are shown in the figures that follow. Once plotted, one is able to observe whether or not the experimental data was taken from the turbulent flow regime.

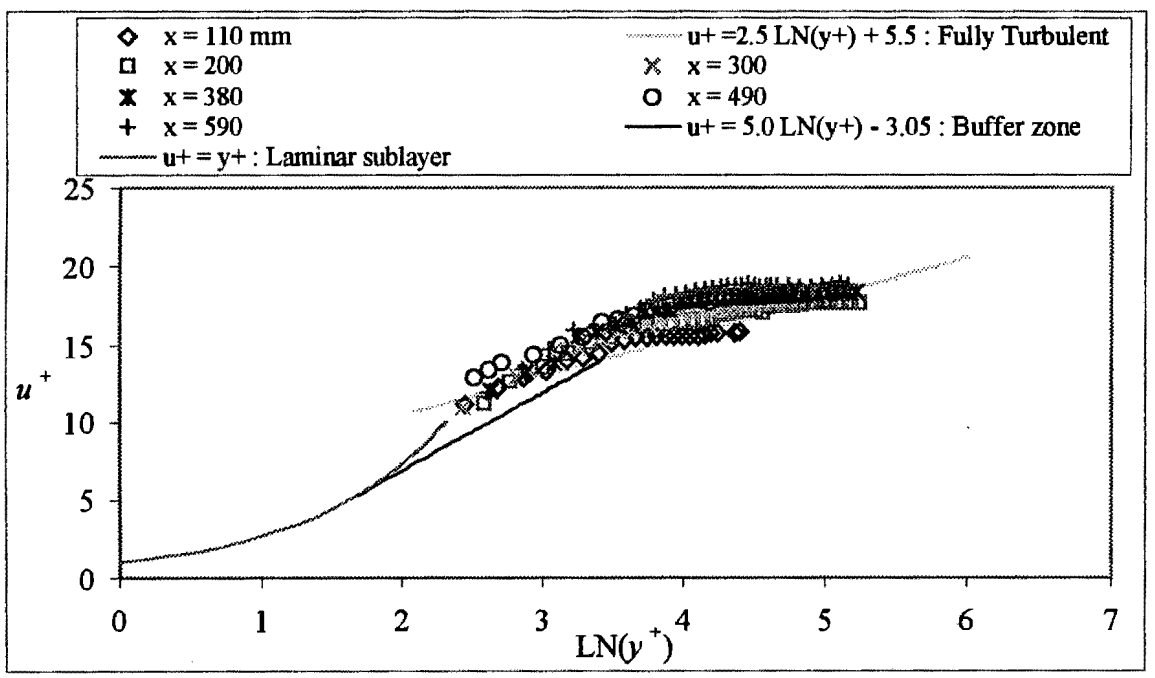

Figure 6.1 Velocity profiles in universal law of the wall co-ordinates for a smooth plate.

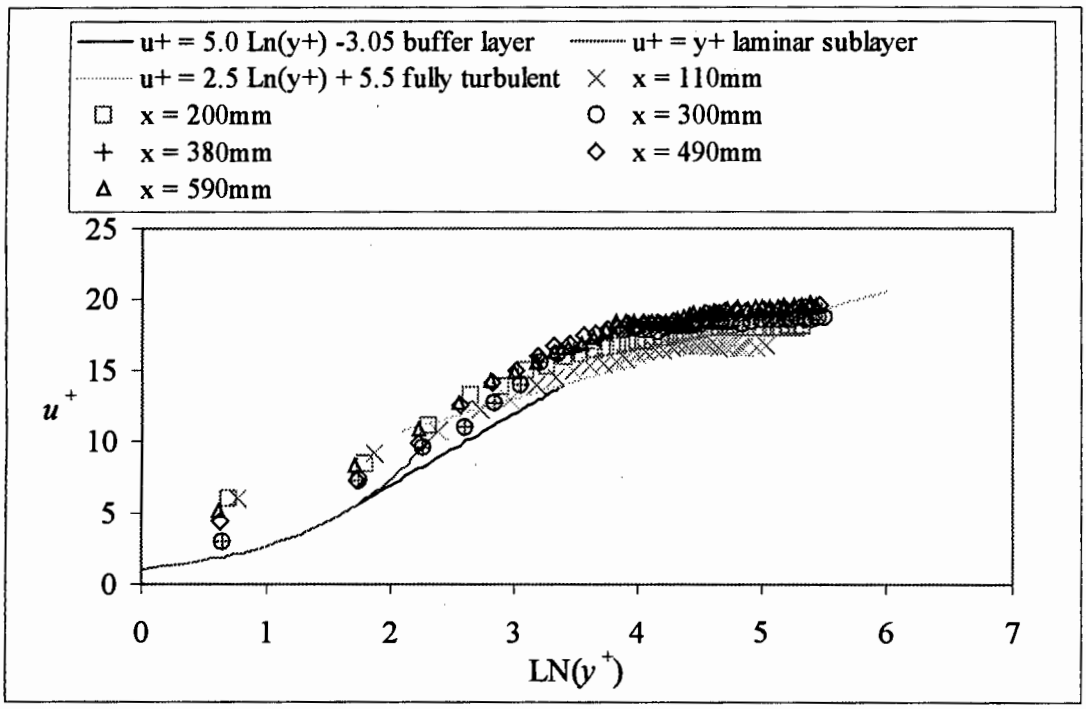

Figure 6.2 Velocity profiles in universal law of the wall co-ordinates for ribbed plate #1.

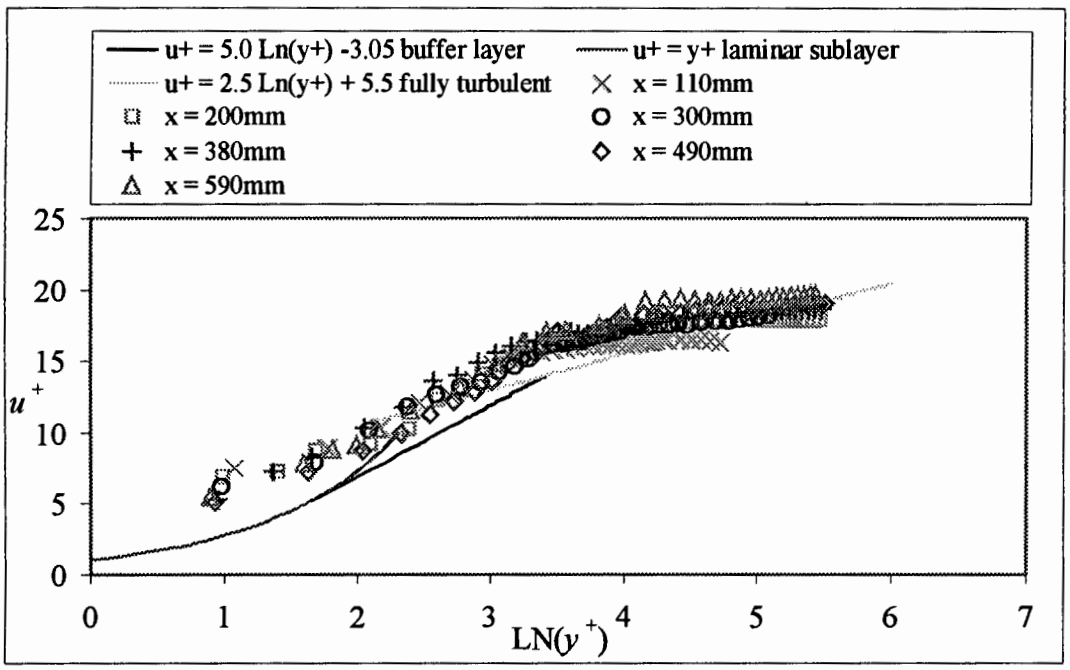

Figure 6.3 Velocity profiles in universal law of the wall co-ordinates for ribbed plate #2.

6.1.2 VELOCITY PROFILES

At any particular x position along the test plates, the data points were used to plot the velocity profile at that point. The velocity profiles were then plotted in the dimensionless form, by plotting v_x/u_∞ versus y/δ. The free stream velocity, u_∞ was maintained at 3.6 m/s. The experimental boundary layer thickness, δ, was calculated at the edge of the boundary layer, where $v_x = 0.99u_\infty$. In order to check the validity of the experimental data, the experimental curves were plotted against the theoretical seventh-power curve in Equation 4.3. In order to avoid confusion, only the velocity profiles at x = 110 mm and x = 590 mm will be presented here, for each of the test surfaces. The rest of the intermediary x position velocity profiles are presented in the Appendix C. Note that the zero point is included in the graphs since it is understood that the velocity reaches zero at the surface of the plate, i.e. at $y = 0$.[46] Note that the u in Figure 6.4 and 6.5 is in fact u_∞.

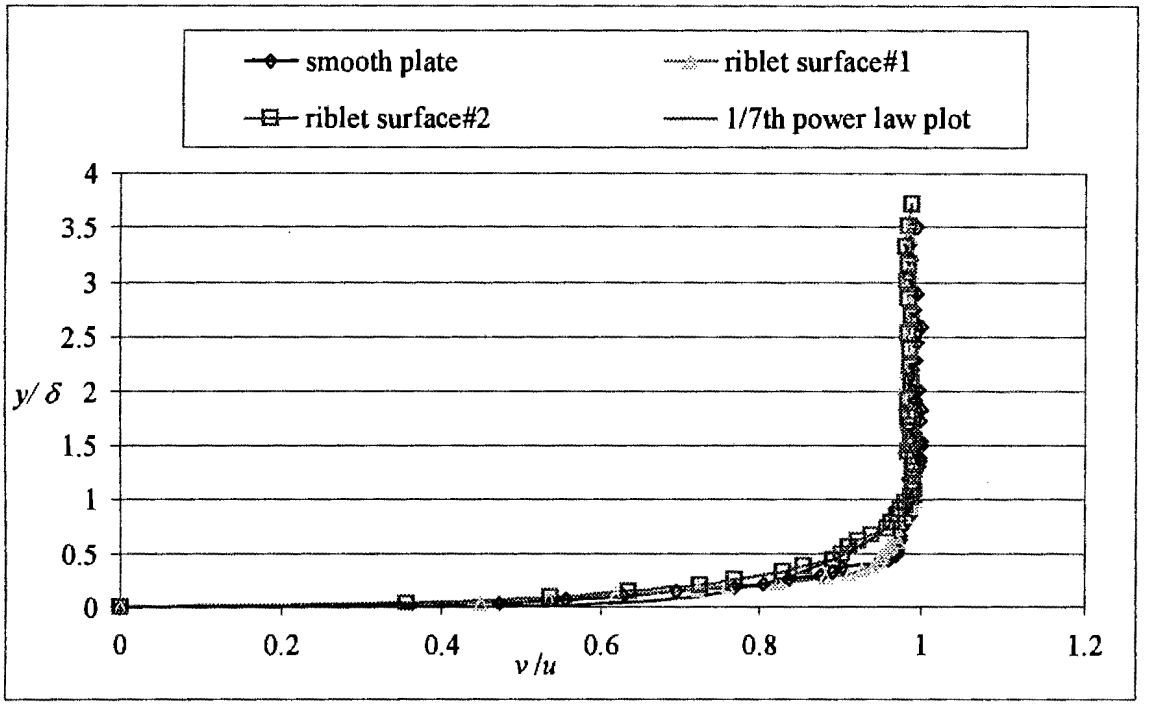

Figure 6.4 Turbulent boundary layer velocity profiles at x = 110 mm

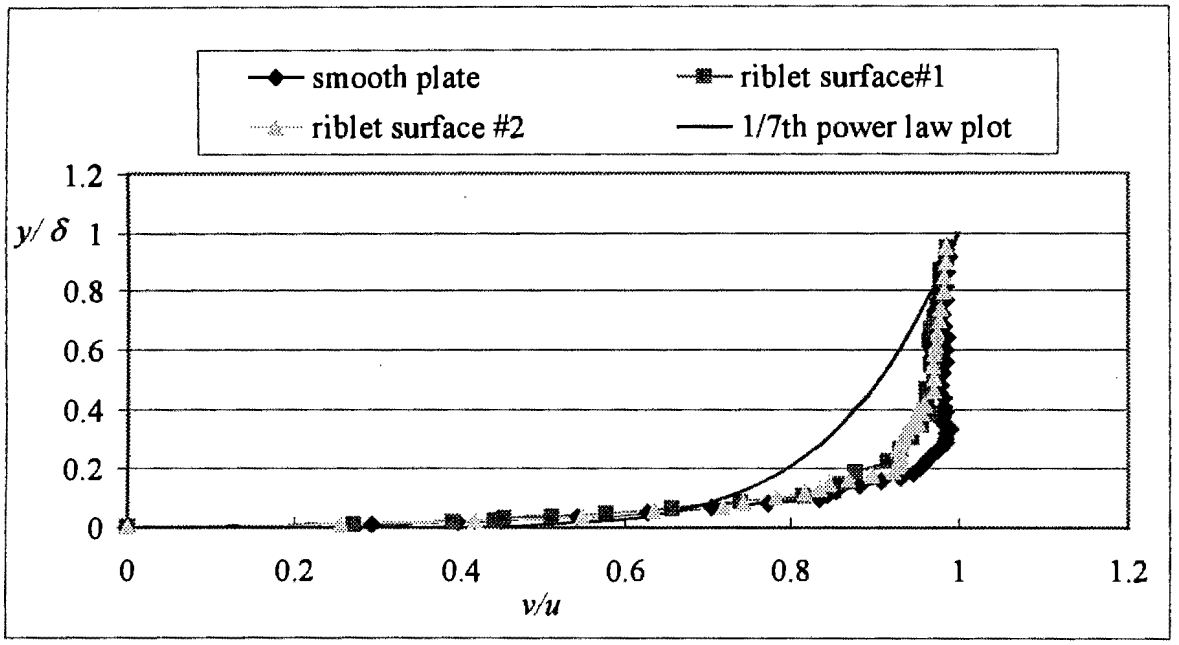

Figure 6.5 Turbulent boundary layer velocity profiles at $x = 590$ mm

6.1.3 WALL SHEAR STRESS

In order to calculate the wall shear stress, the laminar sublayer region of the boundary layer is investigated. It is here where Newtonian viscosity laws apply and the wall shear stress, τ_w can be calculated from the shear stress equation for laminar flow.[46] namely,

$$\tau_w = \mu \frac{dv_x}{dy} \tag{6.3}$$

In order to calculate τ_w from Equation (6.3), the slope of the velocity profile that lies within the laminar sublayer is required. Having calculated the theoretical sublayer thickness already from Equation (4.10), it is possible to estimate the height y, above the test surface, at which the flow is in the buffer zone.[46] Therefore, using only the fairly linear part of the velocity curve and a least squares fit of the data, it was possible to find the slope of the velocity profile in the laminar sublayer. Using the universal velocity profiles one is able to see which data points lie within the laminar sublayer region. For the graphs that follow the velocity profiles of the three test surfaces, at $x = 110$ mm and $x = 590$ mm are plotted. A best-fit linear approximation to each profile is also displayed on the same axes. The equation defining each best-fit line is also shown on the axes. The rest of the x position velocity profiles are found in

Appendix D. R^2 represents how well the best-fit equation represents the data points. The graphs are presented as v_x vs. y. Notice that the zero point has been included. The slope of best-fit line for the velocity profile can now be found directly from the equation of the best-fit lines. The smooth plate results are presented first and the ribbed plates follow.

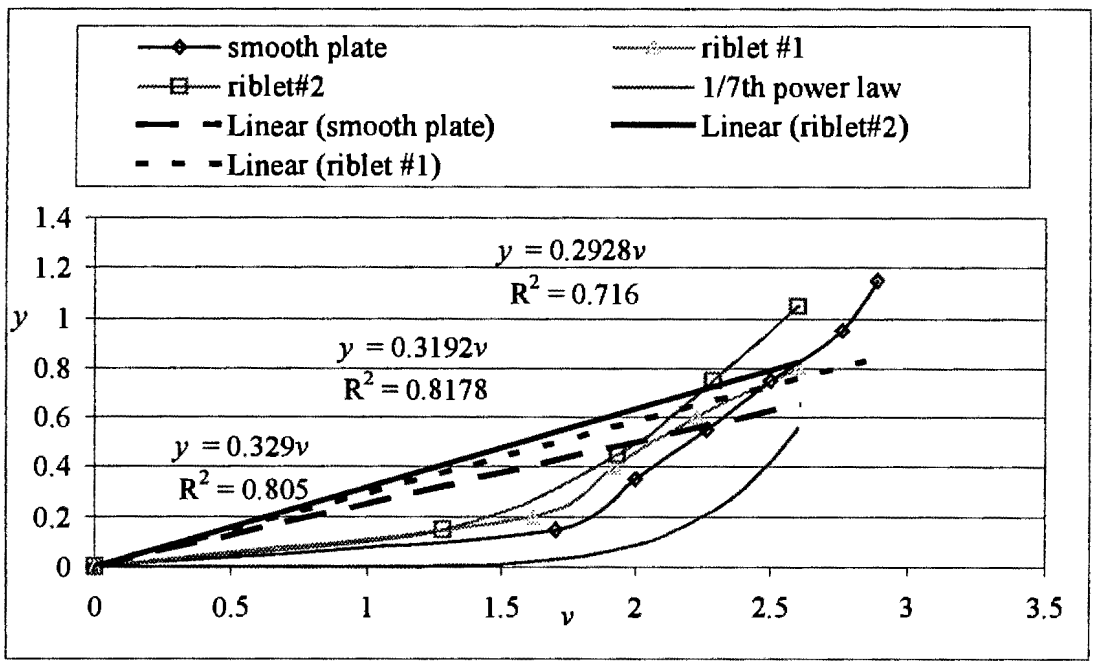

Figure 6.6 Velocity profile in the laminar sublayer region, at $x = 100$ mm

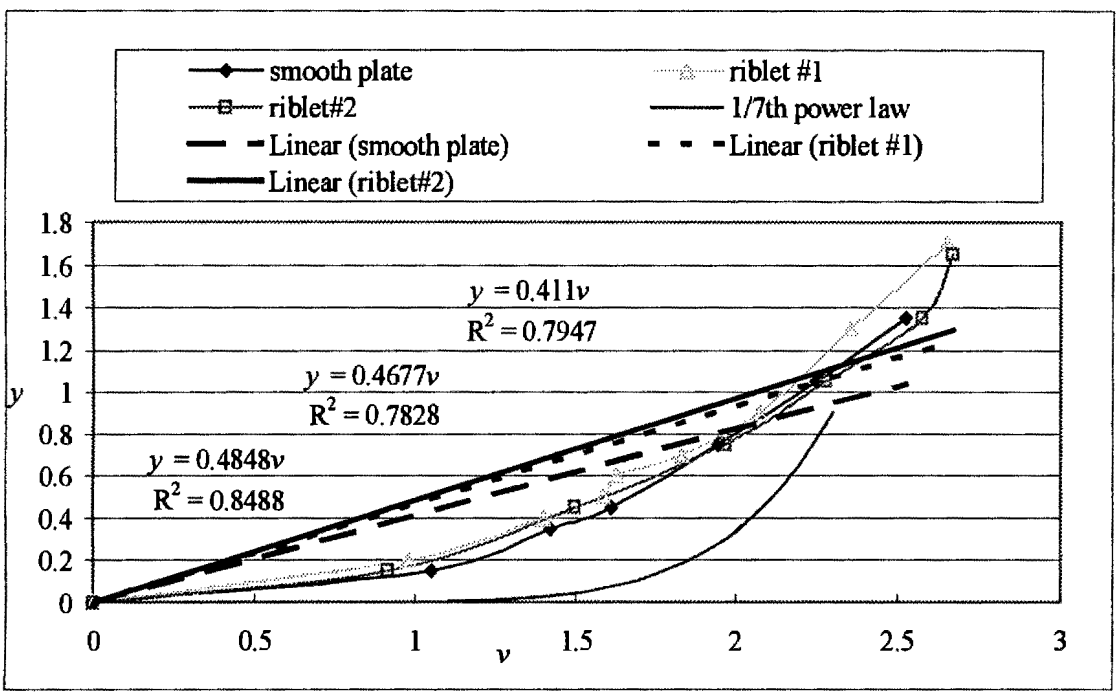

Figure 6.7 Velocity profile in the laminar sublayer region, at $x = 590$ mm.

With the wall shear stress calculated for all three test surfaces and at all x positions using Equation (6.3), the coefficient of friction, C_f can be calculated from Equation (4.5). The experimental boundary layer thickness, δ, is determined at $v_x = 0.99u_\infty$. The experimental Reynolds number is determined by using the experimental boundary layer thickness and solving for Re in Equation (4.9). The experimental laminar sublayer thickness is determined by using Equation (4.10) but substituting the experimental shear stress for τ_w.

The total drag is calculated by integrating the experimental shear stress over the entire test surface. This amounts to using Equation (4.6) to calculate the total drag and Equation (4.8) to calculate the coefficient of drag, C_D. However, these two equations apply to the smooth plate only and since no equations are available to calculate the total drag on the riblet surfaces, this part is left out for these surfaces. Table 6.1 shows the experimental results of the boundary layer analysis on the flat plate. Table 6.2 and 6.3 show the corresponding results for riblet surface #1 and #2 respectively.

x (mm)	τ (Pa)	C_f	Re
110	0.06182	0.00786	25991
200	0.05440	0.00692	88035
300	0.05097	0.00648	76422
380	0.04609	0.00586	74050
490	0.04464	0.00567	121261
590	0.04404	0.00560	141701

Table 6.1 Experimental boundary layer results on a smooth plate

The total drag force for the smooth plate, calculated from the experimental velocity profiles, was found to be 0.00797 N. The corresponding coefficient of drag is 0.00712.

x (mm)	τ (Pa)	C_f	Re
110	0.05670	0.00721	28045
200	0.05200	0.00661	91009
300	0.04963	0.00631	85177
380	0.04342	0.00552	80611
490	0.04171	0.00530	134269
590	0.03870	0.00492	154609

Table 6.2 Experimental boundary layer results on riblet surface #1

x (mm)	τ (Pa)	C_f	Re
110	0.05502	0.00699	31503
200	0.04985	0.00634	97326
300	0.04899	0.00623	91009
380	0.04139	0.00526	84882
490	0.03995	0.00508	146770
590	0.03733	0.00475	160570

Table 6.3 Experimental boundary layer results on riblet surface #2

From the table of results, it is possible to plot the coefficient of friction, C_f, distribution for the test surfaces in Figure 6.8. C_f is plotted against the traverse distance, x from the leading edge.

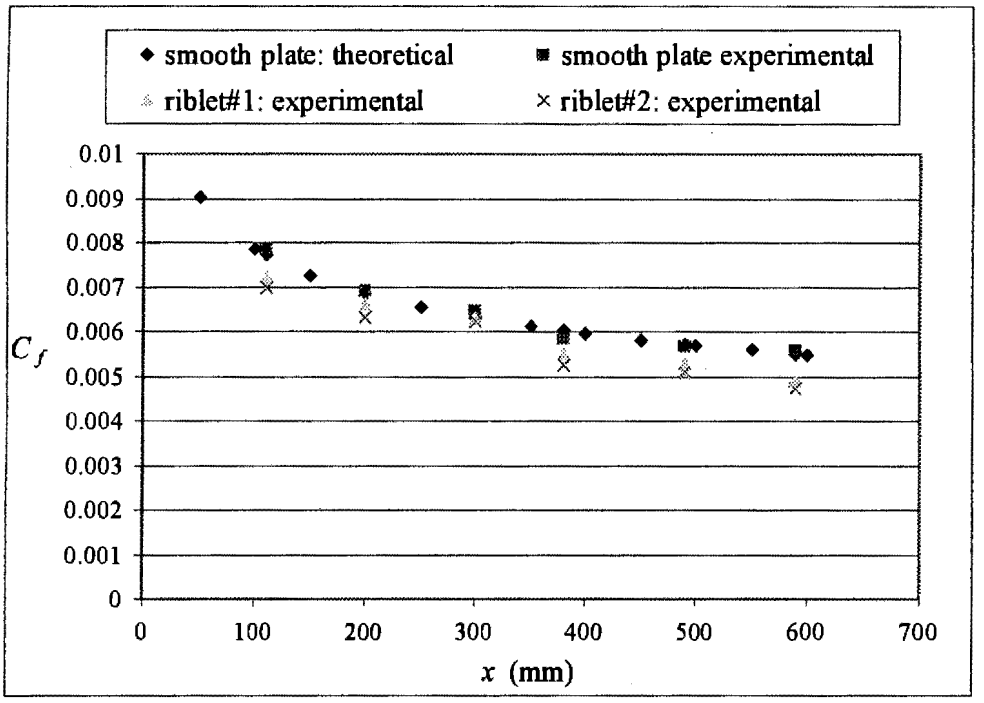

Figure 6.8 Coefficient of friction distribution

It is also possible to plot the laminar sublayer thickness distribution from the leading edge of the plates. Table 6.4 shows the boundary layer and laminar sublayer thickness values of the three test surfaces, calculated from the experimental velocity profiles.

	Smooth plate		Riblet plate #1		Riblet plate #2	
x (mm)	δ (mm)	δ_L (mm)	δ (mm)	δ_L (mm)	δ (mm)	δ_L (mm)
110	5.30	0.527	5.22	0.550	5.100	0.558
200	7.55	0.561	7.50	0.574	7.400	0.586
300	11.65	0.580	11.40	0.588	11.250	0.592
380	14.85	0.610	14.60	0.628	14.450	0.643
490	17.35	0.620	17.00	0.641	16.700	0.655
590	20.25	0.624	19.90	0.665	19.750	0.678

Table 6.4 Experimental δ and δ_L for the three test surfaces

Figure 6.9 shows this distribution of δ for the three test surfaces graphically. The analysis could not be complete without looking at the viscous sublayer growth along the plate. Figure 6.10 shows δ_L, the laminar sublayer thickness development from the leading edge of the plate. Since the properties of the smooth plate were also calculated theoretically, the theoretical δ and δ_L is also included in Figure 6.9 and 6.10.

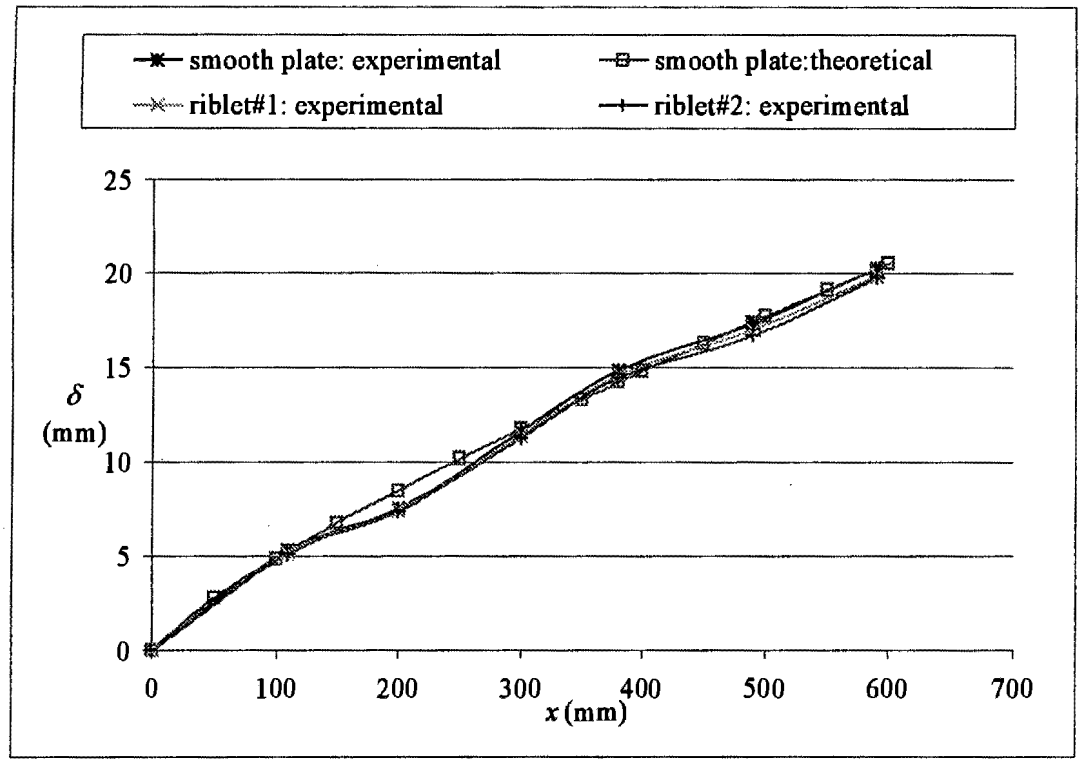

Figure 6.9 Boundary Layer thickness

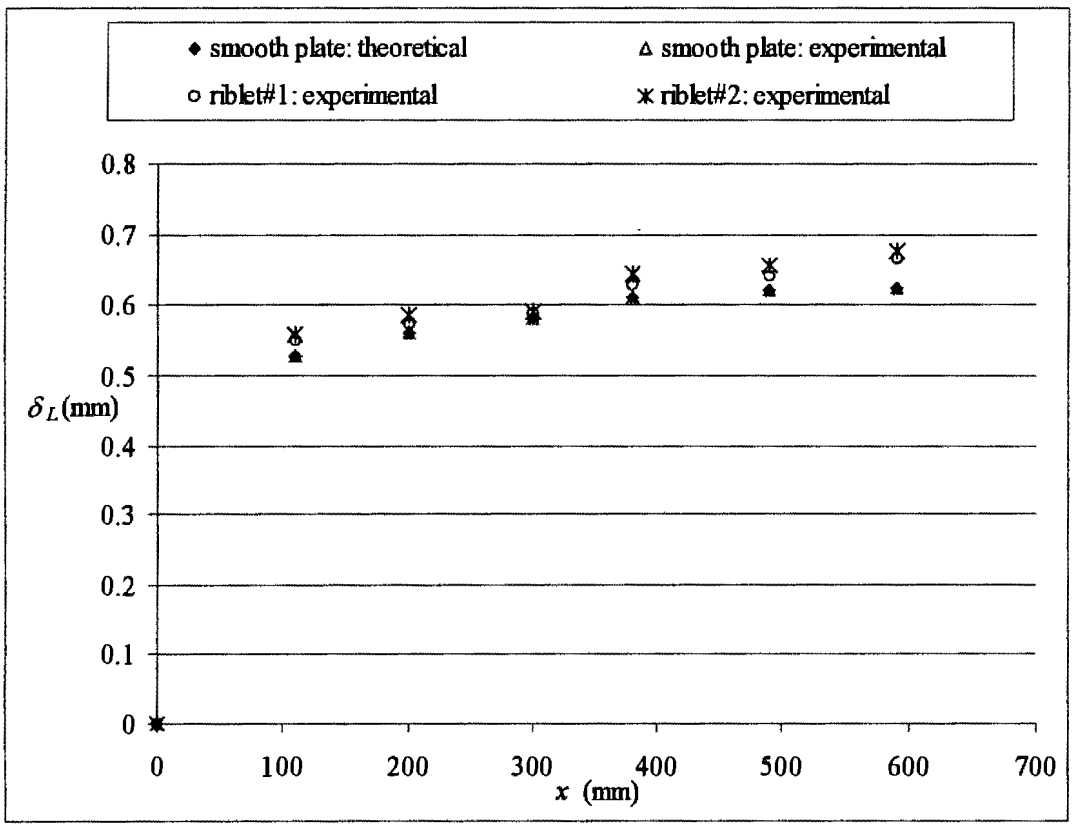

Figure 6.10 Laminar sublayer thickness distribution along the test surfaces

distribution along the test surfaces

6.2 DIRECT DRAG MEASUREMENTS

As discussed in section 5.2, the drag force for each test surface was measured twice. The plates were turned through 180° after each measurement. Before each test the strain gauges were re-calibrated. Measurements were repeatable to within 5% of each other. The calibration curves relating the strain of the strain gauges to the force applied is attached in Appendix F. The direct drag data, relating the free stream velocity to the resultant drag force on the surface of each test plate is attached in Appendix E. Note that the information in the appendices shows the two drag curves for each surface. The mean drag curve was established by a least squares fit of the data. For the purpose of conformity, the dimensionless coefficient of drag, C_D has been calculated for each drag force recorded. C_D has been calculated using Equation (6.3). The free stream velocity has been expressed as a Reynolds number, Re with the test surface length used as the characteristic length over which flow occurs. Re was calculated using Equation (4.7) with $x = l$.

$$C_D = \frac{D}{\frac{1}{2}\rho u_\infty^2 S} \tag{6.3}$$

where S is the span area, $S = b \times l$. The coefficient of drag versus Reynolds number curve for the three test surfaces is depicted in Figure 6.11. This represents the total drag force on the surface of the plates. C_D for the three surfaces has been plotted on the same set of axes so that they may be compared to each other. The total drag as measured directly from the smooth plate was 0.00868, expressed as C_D. The corresponding C_D for riblet plate #1 was 0.008357 and 0.00809 for riblet plate #2. The experimental drag data with which Figure 6.11 has been plotted appears in Appendix E.

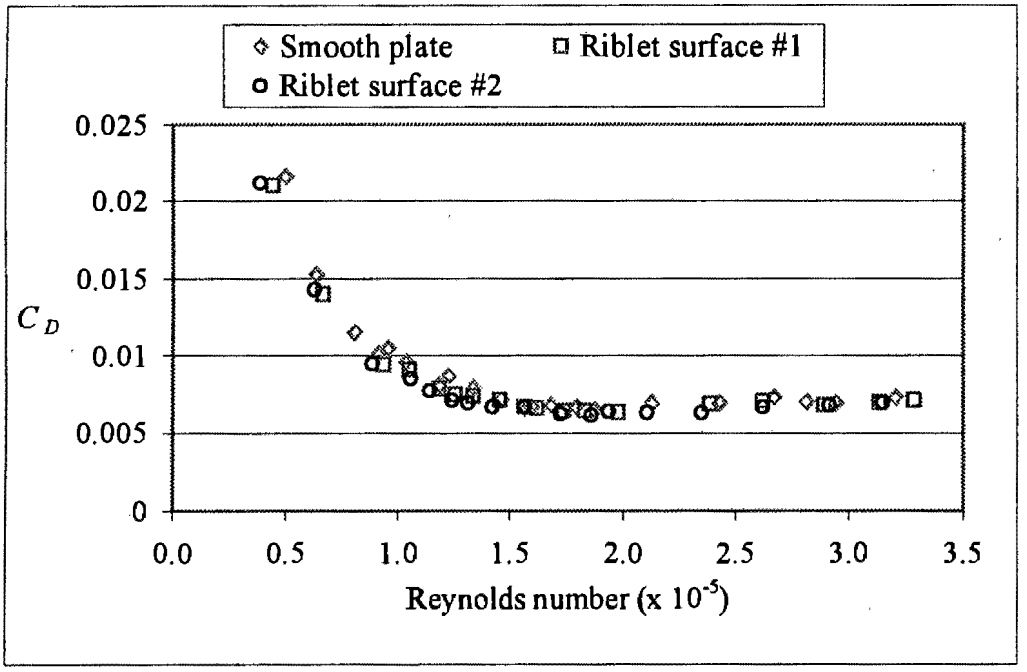

Figure 6.11 Comparative direct drag data for v-groove riblets models #1 and #2

7. DISCUSSION OF RESULTS

One method of determining whether the boundary layer is turbulent is by looking at the velocity profiles of the smooth plate close to the leading edge and close to the trailing edge. Figure 5.4 confirmed the presence of a turbulent boundary layer by the similarity of the velocity profiles. Further investigations of the universal velocity profiles in law of the wall plots indicated that the test was within the turbulent flow regime.

In Figure 6.1 the velocity data expressed in law of the wall co-ordinates of Equation (6.2), shows that the data lay within the turbulent flow regime and fell reasonably well along the fully turbulent line. Approximately 5% of the data fell in the buffer zone. The velocity profiles exhibited an overall upward shift as the probe moved further from the leading edge. The general profile of each velocity profile remained essentially the same indicating that the slope of the profiles did not change. The shift of the profiles indicates a change in the y intercept of the profiles in all the figures. These characteristics were also evident for the universal log-law (law of the wall) plots of the other two test surfaces.

However, unlike for the smooth surface, the graphs showed a greater degree of scatter. As a result approximately 7% of the data fell within the laminar and buffer zone. If one looks at the profiles of the three surfaces in Figures 6.1 to 6.3, it is evident that for any particular profile (at a particular x), the profiles of the ribbed surfaces lie above the smooth plate profiles. The profiles of Riblet surface #2 appear to have shifted by the greatest margin. This relates to the y intercepts of the riblet profiles being greater than that of the smooth plate. The upward shift can be seen as an adjustment of the turbulence energy production and the momentum transport from regions of high velocity to regions of low velocity. Finally, Figures 6.1 to 6.3 have shown that the experiments were being conducted within the proper region, namely the fully turbulent zone.

The velocity profiles at $x = 110$ mm in Figure 6.4 and at $x = 590$ mm in Figure 6.5 show a sudden increase in y/δ close to $v/u_\infty = 1$. This is in contrast to the $1/7^{th}$ power

law plot, which shows a gradual increase in y/δ with increasing v/u_∞. Besides this feature, the experimental velocity profiles closely resembles the $1/7^{th}$ law plot. This applies to velocity profiles for all x. While this was the case, it appears that, as the measurements where taken further from the leading edge, the velocity profile deviated relatively more from the $1/7^{th}$ law plot. This behaviour was most prominent at the point of inflection on the velocity profiles. Walsh[7] and Bechert et al[31] report that the effect of riblets on the velocity profile appears as a shift of the smooth plate values. An upward shift is associated with decreased values of friction velocity or skin friction, and a downward shift indicates skin-friction increases. In the case of Figure 6.4 and 6.5 the velocity profiles of the ribbed surfaces appear to have shifted upwards from the profile of the smooth plate. The velocity profile of riblet surface #2 appears to have shifted upwards by the largest margin.

Although these shifts appear to be very small, this trend is evident for the profiles at all x-stations along the plates. It appears that this effect is most evident at x = 110 mm. Furthermore, for profiles taken in the central region of the test plates, it appears that this effect is least visible. At x = 200, 300 and 380 the shift of the profiles is so small that the curves appear to overlap each other. These observations indicate that riblets are most effective over the front 200 mm of the test plates.

Walsh[7] comments that unless measurements are made close to the wall, the effects of riblets on the velocity profile will appear to be small. In a study completed previously, a momentum thickness variation in terms of R_θ, Reynolds number based on momentum thickness and R_x, Reynolds number based on the distance from the leading edge, the data showed the greatest reduction in θ, momentum thickness occurring in the region close to the leading edge. This discovery was supported by subsequent turbulent fluctuation profiles for the ribbed and smooth surfaces. The average skin friction over this region was lower than regions further away from the leading edge. This indicated that in the region close to the leading edge, the riblets were confining the turbulent bursts.[10] The experimental boundary layer for this study has been taken at $v = 0.99u_\infty$. Table 7.1 shows the boundary layer thickness as calculated using Equation (4.9) as well as the laminar sublayer thickness from Equation (4.10). These are for the smooth plate.

Theoretical δ (mm)	Experimental δ (mm)	% difference	Theoretical δ_L (mm)	Experimental δ_L (mm)	% difference
5.273	5.3	0.51%	0.532	0.527	-0.95%
8.507	7.55	-12.67%	0.564	0.561	-0.54%
11.767	11.65	-1.00%	0.588	0.580	-1.34%
14.216	14.85	4.27%	0.602	0.610	1.33%
17.422	17.35	-0.42%	0.617	0.620	0.40%
20.213	20.25	0.18%	0.629	0.624	-0.79%
	average =	*-1.52%*		*average =*	*-0.32%*
	std.Deviation	5.77%		*std.Deviation*	0.99%

Table 7.1 Theoretical and Experimental boundary layer thickness and viscous sublayer thickness for a smooth plate.

For both δ and δ_L the theoretical and experimental values show good correlation with average differences of 1.52% and 0.32% for δ and δ_L respectively. The slight decrease in δ and δ_L of the experimental values is due to the change in the local flow Reynolds numbers, as Table 4.1 and 6.1 indicates. Table 7.2 compares the δ characteristics of the three surfaces and Table 7.3 shows the corresponding δ_L values. From Table 7.2 it appears that δ for the smooth surface is thicker than for the ribbed surfaces. The boundary layer thickness for riblet surface #1 was on average 1.62% less than for the smooth plate.

Riblet surface #2 (with the small riblets) showed the greatest reduction in δ with a 3.02% thinner boundary layer thickness than the smooth plate value. If one looks at the values in the tables above, the reduction of δ for the ribbed surfaces is evident at all x-stations. This reduction of δ indicates that the local Reynolds number is higher over the grooved surfaces. If one uses the theoretical smooth plate equations in Chapter 4 as a basis for argument then the reduced experimental δ taken at $v = 0.99u_\infty$ shows, from Equation (4.9) that δ is inversely proportional to the $1/5^{th}$ root of the Reynolds number. From Equation (4.10), δ_L is inversely proportional to τ_w and thus an increase in δ_L would indicate a decrease in the wall shear stress, C_f and drag force. Another way of analysing the situation is by realising that an increased Reynolds number on the ribbed surfaces would reduce the coefficient of friction on the surfaces.

Experimental δ smooth plate (mm)	Experimental δ riblet plate #1 (mm)	% difference	Experimental δ riblet plate #2 (mm)	% difference
5.3	5.22	1.51%	5.1	3.77%
7.55	7.5	0.66%	7.4	1.99%
11.65	11.4	2.15%	11.25	3.43%
14.85	14.6	1.68%	14.45	2.69%
17.35	17	2.02%	16.7	3.75%
20.25	19.9	1.73%	19.75	2.47%
	average =	*1.62%*	*average =*	*3.02%*
	std. Deviation	0.53%	*std. Deviation*	0.74%

Table 7.2 Comparison of boundary layer thickness over v-groove riblets with smooth plate values

From Table 7.3 the δ_L appears to have increased over the ribbed surfaces. δ_L for riblet surface #1 averages 3.39% greater than for the smooth surface. Riblet surface #2 averages 5.08% greater than the smooth surface. Thus, the laminar sublayer thickness of the ribbed surfaces is greater than δ_L for the smooth surface. This is evident at all x-stations along the test plates. This behaviour of δ and δ_L, shown graphically in Figure 6.9 and 6.10 respectively, reinforces the findings from the velocity profiles, which indicate a change in the turbulent structure of the ribbed surfaces.

Ultimately a reduction of the overall boundary layer thickness and an increase in the viscous sublayer thickness indicates a reduction in the momentum exchange between regions of low velocity and high velocity fluid. A reduction in the net exchange of momentum and energy would result in a reduction of the force created in the direction of the flow, namely a reduction in the wall shear stress. This is evident in the reduced values of the coefficient of friction which were calculated from the slopes of the velocity profiles.

Experimental δ_L smooth plate (mm)	Experimental δ_L riblet plate #1 (mm)	% difference	Experimental δ_L riblet plate #2 (mm)	% difference
0.527	0.550	4.22%	0.558	5.66%
0.561	0.574	2.24%	0.586	4.28%
0.580	0.588	1.32%	0.592	1.97%
0.610	0.628	2.95%	0.643	5.24%
0.620	0.641	3.34%	0.655	5.40%
0.624	0.665	6.26%	0.678	7.93%
	average =	*3.39%*	*average =*	*5.08%*
	std. Deviation	1.72%	*std. Deviation*	1.94%

Table 7.3 Comparison of Laminar sublayer thickness over v-groove riblets

The experimental wall shear stress was calculated from Equation (6.3), using dv_x/dy, the slope of the velocity profiles. From Figure 6.6 and 6.7 it can be seen that the slopes of the velocity profiles of the ribbed surfaces are less than that of the smooth surface. Note that the slopes of the lines shown in the figures are dy/dv_x, the inverse of the velocity slope required in Equation (6.3). The slopes describe a best-fit linear approximation of the data points that fell within the laminar sublayer region of the velocity profile. The velocity slope for riblet surface #2 is the least for the three surfaces. This tendency is exhibited by all the profiles at all other x-stations. A reduction in the velocity slope results in a reduced wall shear stress. From the behaviour of the velocity slopes of the three test surfaces, one can deduce that the wall shear stresses on the ribbed surfaces are less than the smooth surface.

The wall shear stress can be shown in terms of a friction coefficient, C_f, using Equation (4.5). Table 7.4 shows a comparison of the theoretical and experimental C_f for the smooth plate. As shown, the experimental C_f was on average 0.61% greater than the theoretical value predicted using a wall shear stress calculated from Equation (4.4). Thus, the experimental and theoretical values compared closely with each other.

Theoretical smooth plate C_f	Experimental smooth plate C_f	% difference
0.00771	0.007859	1.87%
0.00684	0.006916	1.07%
0.00631	0.006480	2.63%
0.00602	0.005860	-2.71%
0.00572	0.005675	-0.80%
0.00551	0.005599	1.56%
	average =	*0.61%*
	std. Deviation	1.99%

Table 7.4 Theoretical and experimental coefficient of friction on a smooth plate

A study of Table 7.5 which compares the C_f of the three test surfaces indicate that C_f for the ribbed surfaces were less than the smooth surface values. The graphical representation of Table 7.5 is in Figure 6.8. C_f of riblet plate #1 was reduced by 6.64% from the smooth plate value. C_f for riblet surface #2 was reduced by a greater amount of 9.87%. This was expected since the wall shear stress of the ribbed surface was lower than the smooth surface value.

Experimental smooth plate C_f	Experimental riblet plate #1 C_f	% difference	Experimental riblet plate #2 C_f	% difference
0.007859	0.007209	8.27%	0.006994	11.00%
0.006916	0.006610	4.42%	0.006337	8.37%
0.006480	0.006310	2.63%	0.006228	3.90%
0.005860	0.005520	5.80%	0.005262	10.20%
0.005675	0.005302	6.57%	0.005079	10.51%
0.005599	0.004920	12.12%	0.004746	15.22%
	average =	*6.64%*	*average =*	*9.87%*
	std. Deviation	3.30%	*std. Deviation*	3.70%

Table 7.5 Coefficient of friction on v-groove surfaces

Figure 6.8 shows that the ribbed surfaces experience lower surface drag forces than the smooth surface. The observed reduction in the drag force corresponds with the original observation of the velocity profiles. These results are reinforced by the change in the values of δ and δ_L on the test surfaces and the higher Reynolds numbers

on the ribbed surfaces. From the experimental boundary layer analysis it appears that the ribbed surfaces experience reduced wall shear stresses than the smooth plate but that the surface with the smaller riblets exhibits the greatest degree of shear stress reduction.

The next step is to analyse and discuss the results from measuring the drag on the test surfaces directly. This would indicate the actual drag force on the test surfaces. To this end Figure 6.12 shows the variation of the coefficient of drag, calculated with Equation (6.3), with Reynolds number. The curves in Figure 6.11 are very close to each other indicating only small changes in C_D. However, there does exist a distinct difference in the drag values of the three surfaces at any particular Reynolds number. The data points appear to form a hyperbolic relation between C_D and Re. The drag curves for the two ribbed surfaces appear to have shifted downward from the smooth plate curve indicating reduced drag. The surfaces have been examined up to a Reynolds number of 350 000. It can be seen that for Re < 100 000, the reduction in C_D for the ribbed surfaces appear to be greater. The least amount of drag reduction appears in the range 150 000 < Re < 200 000.

In general, it appears that riblet surface #2 has experienced the greatest drag reduction. There are however scattered regions where it appears that no drag reduction has occurred for riblet surface #1 and also instances where the ribbed surfaces have experienced the same amount of drag reduction. By applying a 3rd order best-fit polynomial trendline to the data it was possible to determine the average drag reduction for the ribbed surfaces. A figure showing these trendlines is attached in Appendix E. The equations describing the data for the three surfaces are:

Smooth plate: $C_D = -3\text{x}10^{-18} Re^3 + 2\text{x}10^{-12} Re^2 - 4\text{x}10^{-07} Re + 0.0366$
Riblet plate #1: $C_D = -3\text{x}10^{-18} Re^3 + 2\text{x}10^{-12} Re^2 - 4\text{x}10^{-07} Re + 0.0339$
Riblet plate #2: $C_D = -3\text{x}10^{-18} Re^3 + 2\text{x}10^{-12} Re^2 - 4\text{x}10^{-07} Re + 0.0331$

On average, riblet surface #1 showed a 3.96% reduction in total drag force and riblet surface #2 showed an 11.59% reduction in the total drag force. These values have been calculated by finding the average difference in C_D for the ribbed surfaces and the reference smooth surface. The C_D for the three surfaces were calculated at different Re

over the range $0 < Re < 350\,000$ and using the equations of the best fit trendlines. It is felt that these values should not be used as an absolute reflection of the magnitude of drag reduction by the riblets since the drag reduction appears to vary depending on the flow Reynolds number. Furthermore, as indicated previously, there appears within the tested *Re* flow region, smaller regions where the drag reducing behaviour varies. While Figure 6.11 shows definitively that v-groove riblets do reduce drag, the average values that have been quoted must not be used generally since the amount of drag reduction appears to be dependant on Reynolds number.

It is felt that comparing the drag force measured directly from the surfaces, to the drag force calculated from the velocity profiles of the boundary layer would be more precise. In order to do this, it is necessary to look at the drag at a particular freestream velocity and Reynolds number. As discussed in chapter 5 the boundary layer analysis was conducted at a freestream velocity of 3.6 m/s. This corresponds to a Reynolds number of 117 101 based on the length of the test surfaces. At this Reynolds number the total drag force measured directly is found from Figure 6.11. It is possible to compare the theoretical and experimental drag force on the smooth plate using the boundary layer equations. There are no boundary layer equations defined for a ribbed surface. It is also possible to compare the experimental drag, calculated from the boundary layer, to the drag measured directly from the surface. Table 7.6 shows a comparison of the different drag values for the smooth surface.

Comparing the drag force calculated from boundary layer equations, it appears that the experimental values compared favourably with the theoretical values calculated from Equation (4.8). The difference in the two values was 0.42%. It was found that the drag measured directly was 17.98% greater than the drag force calculated from the experimental boundary layer. The large drag increase is attributed to inadequacies in the drag-measuring set-up and will be discussed in the next chapter.

Theoretical smooth plate total drag	Experimental smooth plate b/layer total drag	% difference	Experimental smooth plate b/layer total drag	Experimental smooth plate total direct drag	% difference
0.00715	0.00712	0.42%	0.00712	0.008681117	17.98

Table 7.6 Theoretical and Experimental smooth plate drag force

In Table 7.7 the total drag measured directly on the three surfaces, are compared. It is shown that at this specific Reynolds number, the drag force, more specifically C_D, for riblet surface #1 was reduced by 3.73% and by 6.83% for riblet surface #2. Thus, as was the case with the boundary layer analysis, the v-grooved surfaces have reduced the drag on the smooth plate. Furthermore, as before, riblet surface #2, the smaller symmetric riblet surface with $h/s = 1$ has produced the greatest drag reduction.

Experimental smooth plate total direct drag	Experimental riblet surface #1 total direct drag	% difference	Experimental riblet surface #2 total direct drag	% difference
0.008681	0.008357	3.73%	0.008088	6.83%

Table 7.7 Comparison of the total drag on v-grooved surfaces

8. DISCUSSION OF SOURCES OF DEVIATION OF RESULTS

Chapter 7 discussed the difference in results obtained for the three test surfaces. The following discussion will attempt to address some of the possible sources of deviation of the results on the smooth surface that had been calculated using the various aforementioned approaches. It has been shown that riblets give small drag reductions on the order of 3-7%; therefore, drag measurements require extreme accuracy. It is even more difficult to observe changes in drag reductions due to variations in geometry as the changes in drag may be within the scatter of the measurements.

In addition to problems with the measurement accuracy, riblet performance can be quite sensitive to the quality of the machined surface. Poor quality may result in rounding at the peaks and riblet aspect ratio varying across the machined surface. All these geometric parameters can affect the drag performance of the riblet surface and may have an unknown influence on performance comparisons of specific desired geometries. A better way to prepare the test surfaces would have been to use a riblet film machined by the 3M Company. However, on enquiry this film was not available in South Africa at the time.

Comparing the theoretical boundary layer results to the experimental results showed a small deviation from each other. Overall the experimental boundary layer results of the smooth plate compared closely with the idealised results. The theoretical δ and δ_L for the smooth plate differed from the experimental results by 1.52% and 0.32% respectively. The corresponding standard deviations of the data were calculated as 5.77% and 0.99% respectively. These results are also shown in Table 7.1. An analysis of the coefficient of friction was also made and it was found that a standard deviation of 1.99% existed between the theoretical and experimental smooth plate results. Table 7.4 shows this difference in results.

The next area of deviation of results is in the direct measurement of the total drag on the smooth surface. The difference in this value and the drag measured from the boundary layer was 17.98%. As mentioned in chapter 5.2, the drag force for each test

surface was measured twice. The plates were turned 180° after each measurement. Before each test the strain gauges were re-calibrated. Measurements were repeatable to within 5% of each other. So the actual measurements appear to be consistent. However, boundary layer measurements are specialized in that they essentially focus on the velocities of the flow regime in close proximity to the surface. The experiment is conducted in a closed test section to avoid flow discontinuities and outside effects. In contrast, the direct drag measurements are done in an open test-section wind tunnel and the test surface is exposed to outside factors. These two different experimental scenarios in itself presents an element for deviation of the results. The direct drag measurement is generally regarded as a more realistic representation of the drag force on the surfaces. However, the drag force value that was measured directly on the smooth surface and on the ribbed surfaces was in excess of the actual value for those surfaces. This is due to the presence of other objects attached to the test surfaces that were also in the freestream.

The linkages that held the test surfaces suspended along the wind tunnel roof, were 10 mm cylindrical rods. Due to the weight of the test surfaces, these were partly submerged in the free stream and thus experienced a drag force. Since these 4 rods were attached to the ribbed surface, the force on them caused the strain gauges to show a greater reading than for the plate deflection alone. While this was the case, the experimental procedure was retained because the aim of these experiments was to prove that riblets could reduce drag and the effect of the rods in the freestream did not affect this. Since all three surfaces experienced the added drag force effect of the cylinders in the freestream, it was still possible to compare the force on the three surfaces and note if any drag force changes did occur. While it is possible to determine the drag force of a 10 mm cylinder in a freestream at a particular Reynolds number, the cylinders were only partly submerged and assuming by how much, would in itself introduce another error.

9. CONCLUSIONS

Based on the findings of this thesis the following conclusions can be drawn:

1. The denticles of the shark specimen that had been studied does exhibit the v-shaped ridge structure that is believed to be one of the origins of riblet theory. Observations verify previous recorded observations of overlapping microscopic channels that form on the skin of fast shark species.
2. The riblet research conducted elsewhere reveal two points of contention on the effect of riblets. It is uncertain whether the effects of riblets on the turbulent structure are primary or secondary. There is however a consensus that the riblets induce a secondary vortex system within the groove valleys and that these vortices provide lateral resistance to the turbulent streamwise vortices, thereby reducing the skin friction component.
3. V-groove riblets can be used as a surface modification in order to reduce the drag on a smooth flat plate.
4. The theoretical and experimental analysis on the smooth plate compared favourably. A standard deviation of 1.99% was calculated for the two values of coefficient of friction.
5. The symmetric v-groove riblets with $h/s = 1$ show the greatest potential, with drag reduction of 6.83% at a Reynolds number of 117 101.
6. The unsymmetrical v-groove riblets with $h/s = 0.22$ also show drag reduction potential but to a lesser degree. Drag reduction of 3.73% was recorded at a Reynolds number of 117 101.
7. It is apparent that the drag reducing ability of riblets is dependent on the h/s ratio and the Reynolds number regime in which the flow exists.
8. It is the opinion of this report that the effects of the v-grooves is to modify and effectively reduce the momentum and energy exchange properties caused by the streamwise vortices developing near the surface beneath the turbulent layer, with a consequent reduction in shear stress levels. Riblet surfaces are characterised by a decrease in the boundary layer thickness and an increase in the laminar sublayer thickness. This coincides with an increase in the flow Reynolds number.

10. RECOMMENDATIONS

Based on the conclusions of this report, the following recommendations are made:

1. The use of hot-wire anemometry and laser Doppler anemometry should be considered and the results should be compared to those expressed in this report.
2. Flow visualisation techniques such as dye injection and hydrogen bubble methods should be employed so that the existence of laminar streaks can be more closely investigated.
3. Riblets should be applied to real bodies such as lifting surfaces and the comparative effect must be studied. Based on the fuel saving potential for an airliner, the concept of riblets as a drag reducing mechanism should be vigorously marketed to the aircraft as well as yacht building industry.

LIST OF REFERENCES:

1. Walsh M J. 'Drag Characteristics of V-groove and Transverse Curvature Riblets'. *AIAA Journal: Progress in Aeronautics and Astronautics*, vol. 72, 1980, pp. 168-184.
2. Walsh M J. 'Turbulent Boundary Layer Drag Reduction using Riblets'. *AIAA Paper 82-0169*, January 1982.
3. Walsh M J & Lindermann A M. 'Optimization and Application of Riblets for Turbulent Drag Reduction'. *AIAA Paper 84-0347*, March 1984.
4. Lui C K, Kline S J & Johnstone J P. 'Experimental study of a Turbulent Boundary Layer on Rough Walls'.*Report MD-15*, Dept. of Mechanical Engineering, Stanford University, 1966.
5. Kennedy J F, Hsu S T & Lin J T. 'Turbulent Flow past Boundaries with Small Streamwise Fins'. *Journal of the Hydraulics Division, Proceedings of the American Society of Civil Engineers*, vol. 99, April 1973.
6. Walsh M J & Weinstein L M. 'Drag and Heat Transfer on Surfaces with Small Longitudinal Fins'. *AIAA Paper 78-1161*, July 1978.
7. Walsh M J. 'Riblets as a Viscous Drag Reduction Technique'. *AIAA Journal*, vol. 21, no. 4, April 1983, pp. 485-486.
8. Walsh M J. 'Riblets: Viscous Drag Reduction in Boundary Layers'. *NASA Technical Report.* Virginia, 1990, pp. 203-261.
9. Balint J L & Wallace J M. 'Viscous Drag Reductions Using Streamwise Aligned Riblets: Survey and New Results'. Paper presented at IUTAM Symposium, Bangalore, India, January 1987.
10. Gallagher J A & Thomas A S W. 'Turbulent Boundary Layer Characteristics over Streamwise Grooves'. *AIAA Paper 84-2185*, November 1985, pp. 1-8.
11. Hooshmand D, Younis R & Wallace J M. 'An Experimental Study of Changes in the Structure of a Turbulent Boundary Layer due to Surface Geometry Changes'. *AIAA Paper 83-0230*, January 1983.
12. Caram J M & Ahmed A. 'Development of a Wake of an Airfoil with Riblets'. *AIAA Journal*, vol. 30, no.12, December 1992, pp. 2817-2818.

13. Viswanath P R & Mukund R. 'Turbulent Drag Reduction using Riblets on a Supercritical Airfoil at Transonic Speeds'. *AIAA Journal*, vol. 33, no. 5, May 1995, pp. 945-947.
14. Nieuwstadt F T M, Wolther W, Leijdens H, Prasad H K & Schwarz-van Manen A. 'The Reduction of Skin Friction by Riblets Under the Influence of an Adverse Pressure Gradient'. *Experiments in Fluids*, vol. 15, no. 1, 1993, pp. 17-26.
15. Bacher E V & Smith C R. 'Turbulent Boundary Layer Modifications by Surface Riblets'. *AIAA Journal*, vol. 24, no. 8, August 1986, pp. 1382
16. Bacher E & Smith C R. 'A Combined Visualization- Anemometry Study of Triangular Micro-grooved Surface Modifications'. *AIAA Paper 85-0548*, May 1985.
17. Park S R & Wallace J M. 'Flow Alteration and Drag Reduction by Riblets in a Turbulent Boundary Layer'. *AIAA Journal*, vol. 32, no. 1, January 1994, pp. 31-38.
18. Suzuki Y & Kasagi N. 'Turbulent Drag Reduction Mechanism over a Riblet Surface'. *AIAA Journal*, vol. 32, no. 9, September 1994, pp. 1781-1790.
19. Lazos B & Wilkinson S P. 'Turbulent Viscous Drag Reduction with Thin-element Riblets'. *AIAA Journal*, vol.26, no. 4, April 1988, pp. 496-498.
20. Bechert D, Reif W & Hoppe G. 'On the Drag Reduction of Shark Skin'. Paper presented at Euromech 181- Drag Reduction through Boundary Layer Control, Stockholm, August, 1984, pp. 1-18.
21. Wallace J M & Balint J L. 'Turbulence Management and Relaminarisation: Proceedings of the IUTAM Symposium, Bangalore, India, 1987'. *International Union of Theoretical and Applied Mechanics*. 1988, pp. 132-147.
22. Purtell L P, Klebanoff P S & Buckley F T. 'Turbulent Boundary Layer at Low Reynolds Numbers'. *Physics of Fluids*, vol. 24, no. 5, 1981, pp. 802-811.
23. Choi S K. 'Drag-reduction tests of riblets using A.R.E.'s high speed buoyancy propelled vehicle- MOBY-D'. *Journal of the Royal Aeronautical Society*, vol. 94, no. 933, March 1990, pp. 79-85.
24. Vukoslavecevic P, Wallace J M & Balint J L. 'Viscous Drag Reduction using Streamwise Aligned Riblets'. *AIAA Journal*, vol. 30, no. 4, April 1992, pp. 1119-1122.

25. Chu D C & Karnadiakis G E. 'A direct Numerical Simulation of Laminar and Turbulent Flow over Riblet Mounted Surfaces'. *Journal of Fluid Mechanics, Cambridge*, vol. 250, May 1993, pp. 1-42.
26. Moin P & Kim J. 'Tackling Turbulence with Supercomputers'. *Scientific American Journal.* January 1997.
27. Anderson G W, Rohr J J & Stanley S D. 'The Combined Drag Effects of Riblets and Polymers in Pipe Flows'. *ASME Journal of Fluid Engineering,* vol. 115, 1993, pp. 213-221.
28. Lancy T W & Reidy L W. 'Effects of Surface Riblets on the Reduction os Wall Pressure Fluctuations in Turbulent Boundary Layers'. *Journal of Acoustic Society of America*, vol. 85, no. 4, April 1989.
29. Rothenflue J A & King P I. 'Vortex Development over Flat Plate Riblets in a Transitioning Boundary Layer'. *AIAA Journal*, vol. 33, no. 8, August 1995, pp. 1525-1526
30. Johnson C S. 'Some Hydrodynamic Measurements on sharks'. Scripps Institute of Oceanography, LaJolla, CA, NUC TP-189, 1970.
31. Bechert D, Hoppe G & Reif W. 'On the Drag Reduction of Shark Skin'. *AIAA paper 8-0546,* March 1985, pp. 1044-1068.
32. Reif W E. 'Protective and the Hydrodynamic Functions of the Dermal Skeleton of Elamolranchs'. *Nues Jahrbuch fuer Geologie und Palaentologie*, vol. 157, 1978, pp. 133-141.
33. Reif W E. 'Morphogenesis and Function of the Squamation in Sharks'. *Nues Jahrbuch fuer Geologie und Palaentologie*, vol. 164, 1982, pp. 172-183.
34. Reif W E & Dinkelacker 'Hydrodynamics of the Squamation in Fast Swimming Sharks'. *Nues Jahrbuch fuer Geologie und Palaentologie*, vol. 164, 1982, pp. 184-187.
35. Raschi W & Musik J A. 'Hydrodynamic Aspects of Shark Skin'. *NASA Contractors Report No. 3963*, NASA Langely Research Centre, 1986.
36. Raschi W & Elsom J. 'Comments on the Structure and Development of the Drag Reduction Type Placoid Scale'. *Proceedings of the Second International Conference on Indo-Pacific Fishes,* edited by T. Uyeno, R Aai, T. Toniuchi, and K. Matsuua, 1986, pp. 408-424.
37. Rashi W & Tabit C. ' Functional Aspects of Placoid Scales'. *Australian Journal of Marine Research*, vol. 43, 1992, pp. 123-147.

38. Waid R L. 'Investigation of Bound Vortices'. Lockheed Missile and Space Company, Sunnyvale, CA, LMSC-0912950, September 1983.

39. Bechert D, Bartenwerfer M & Hoppe G. 'Drag Reduction Mechanisms Derived from Shark Skin'. *15th Congress of The International Council for Aeronautical Sciences*. paper 86-1.8.3. London, September 1986, pp. 1044-1068.

40. Bowden K F, Frenkiel F N & Tani I. *Boundary Layers and Turbulence*. American Institute of Physics, New York, 1967.

41. Holman J P. *Heat Transfer: 7th Edition*. Mc. Graw Hilll Co., New York, 1992.

42. Schlichting H. *Boundary Layer Theory: 7th Edition*. Mc. Graw Hill, New York, 1979.

43. Anderson J D. *Fundermentals of Aerodynamics : 2nd Edition*. Mc. Graw Hill Inc., New York, 1991.

44. Janna W S. *Introduction to Fluid Mechanics: 3rd Edition*. PWS Publishing, Boston, 1994.

45. Rindfuss C. 'Wind tunnel 3-Component Traverse'. *Undergraduate Thesis: Design Project No. 59*, University of Cape Town, 1995.

46. Sayers A T. *An Introduction to Fluid Mechanics*. Oxford University Press, Cape Town, 1992.

47. Johnson F T, Tinoco E N, Lu P R & Epton M A. 'Three-dimensional flow over wings with leading edge vortex separation'. *Journal of the American Institute of Aeronautics and Astronautics*, vol. 18, no. 4, April 1981, pp. 367-368.

48. Davis M R. 'Design of a Flat Plate Leading Edge to Avoid Flow Separations'. *AIAA Journal*, vol. 18, no. 5, May 1980, pp. 598.

49. Mueller T J & Batill S M. 'Experimental Studies of Separation on a Two-dimensional Airfoil at Low Reynolds Number'. *AIAA Journal*, vol. 20, no. 4, April 1982, pp. 457.

50. Gray D & Sheldon G F. 'Growth of Two-dimensional Wakes behind Solid and Porous strips'. *AIAA Journal*, vol. 20, no. 1, Jan. 1982, pp. 150.

51. Thomas A S W & Cornelius K C. 'Investigation of a laminar Boundary Layer Suction Slot'. *AIAA Journal*, vol. 20, no. 6, June 1982, pp. 790-796.

52. Hefner J N & Bushnell D M. ' =Turbulent Boundary Layer Relaxation with Application to Skin Friction Drag'. *AIAA Journal*, vol. 22, no. 7, July 1984. pp. 203-261.

53. Moore A R & Lowson M V. 'Drag Reduction In Rectangular Ducts using Riblets'. *Journal of the Royal Aeronautical Society*, vol. 99, no. 985, May 1995, pp. 187.

54. Pope G G. 'Aeronautical Technology- Recent Advances and Future Prospects'. *Journal of the Royal Aeronautical Society*, vol. 99, no. 983, March 1995, pp. 81.

55. Squire L C. 'Measurement of Drag using a Momentum Balance'. *Journal of the Royal Aeronautical Society*, vol. 99, no. 985, May 1995.

56. Johansen J B & Smith C R. 'The Effect of Cylindrical Surface Modifications on Turbulent Boundary Layers'. *AIAA Journal*, vol. 24, no. 7, July 1986, pp. 1080.

57. Green J E. 'The 2nd Goldstein Lecture-Modern Developments in Fluid Dynamics- an Addendum'. *Journal of the Royal Aeronautical Society*, vol. 96, no. 953, March 1992.

58. Squire L C & Young C P. 'The Interaction of a Vortex with a Boundary Layer'. *Journal of the Royal Aeronautical Society*, vol. 98, no. 978, October 1994.

59. Thomson K D. 'Some Comments on the Later Stages of Transition from Laminar to Turbulent Flow in a Flat Plate'. *Journal of the Royal Aeronautical Society*, vol. 92, no. 918, October 1988, pp. 309-314.

60. Caram J M & Ahmed A. 'The Effect of Riblets on the Turbulence in the wake of an Airfoil'. *AIAA Journal*, vol. 20, no. 11, November 1991, pp. 1769-1770.

61. Choi H, Moin P & Kim J. 'Direct Numerical Simulation of Turbulent Flow over Riblets'. *Journal of Fluid Mechanics, Cambridge*, vol. 255, October 1993, pp. 503-539.

62. Grek G R, Kozlov V & Titarenko S V. 'An Experimental Study of the Influence of Riblets on Transition'. *Journal of Fluid Mechanics, Cambridge*, vol. 315, May 1996, pp. 31-50.

63. Ojha M, Irisbarne A P & Tantirige S C. 'The Turbulent Boundary Layer over Single V-shaped Grroves'. *International Journal of Heat and Mass Transfer*, vol. 37, October 1994, pp. 2261-2271.

64. Keith W L. 'Spectral Measurements of pressure Fluctuations on a Riblet Surface'. *AIAA Journal*, vol.27, no. 12 December 1989, pp. 1822-1824.

65. Graham J B, Dewar H & Lai N C. 'Aspects of Shark Swimming Performance Determined in a Large Water Tunnel'. *Journal of Marine Biology*, vol. 151, July 1990, pp. 175-192.

ADDITIONAL BOOKS

66. Gilbert P W & Rall D P. *Sharks, Skates and Rays*. John Hopkins Press, Maryland, 1967.

67. Marshal N B. *The Life of Fishes*. Weidenfeld and Nicolson Press, London, 1965.

68. Alexander R M N. *Functional Design in Fishes*. Hutchinson and Co., London, 1967.

69. Goldstein S. *Modern Developments in Fluid Dynamics: Vol. 2*. Clarendon Press, Oxford, 1938.

70. Ferri A, Kuchemam D & Sterne L H G. *Progress in Aeronautical Sciences : Vol. 2, Boundary Layer Problems*. Pergamon Press, New York, 1962.

71. Durst F, Launder B E, Schmidt F W & Whitelaw J H. *Turbulent Shear Flows 1*. Springer-Verlag Press, New York, 1979.

APPENDIX A:

Engineering Drawings

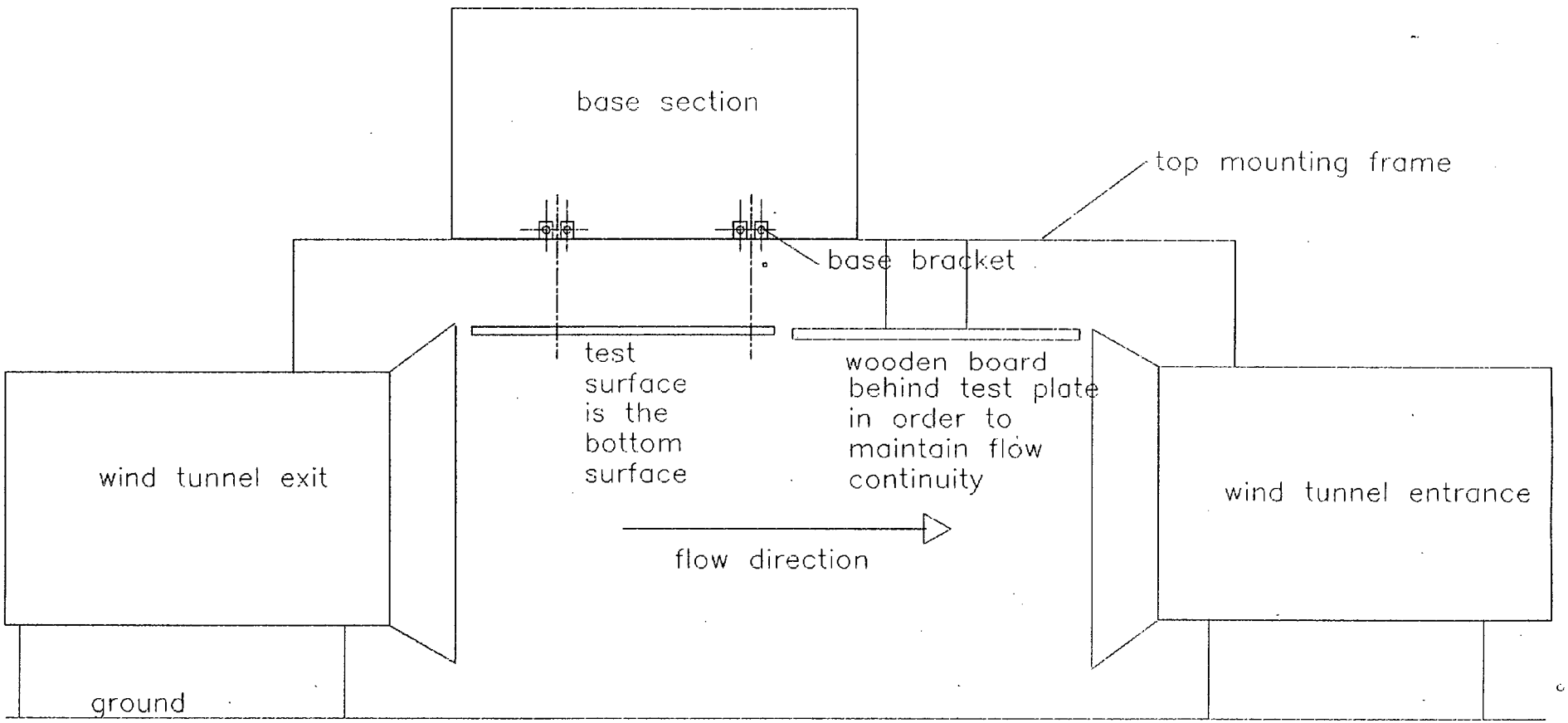

DEPARTMENT OF MECHANICAL ENGINEERING, UNIVERSITY OF CAPE TOWN		
ASSEMBLY DRAWING OF WIND TUNNEL TEST RIG		
Supervisor : Prof. A.T. Sayers	Date: 18 May 1997	Drawn by Kamalluddien Parker
Project : MSc. Mechanical Engineering	Scale ; None	Drawing No. 1 of 9

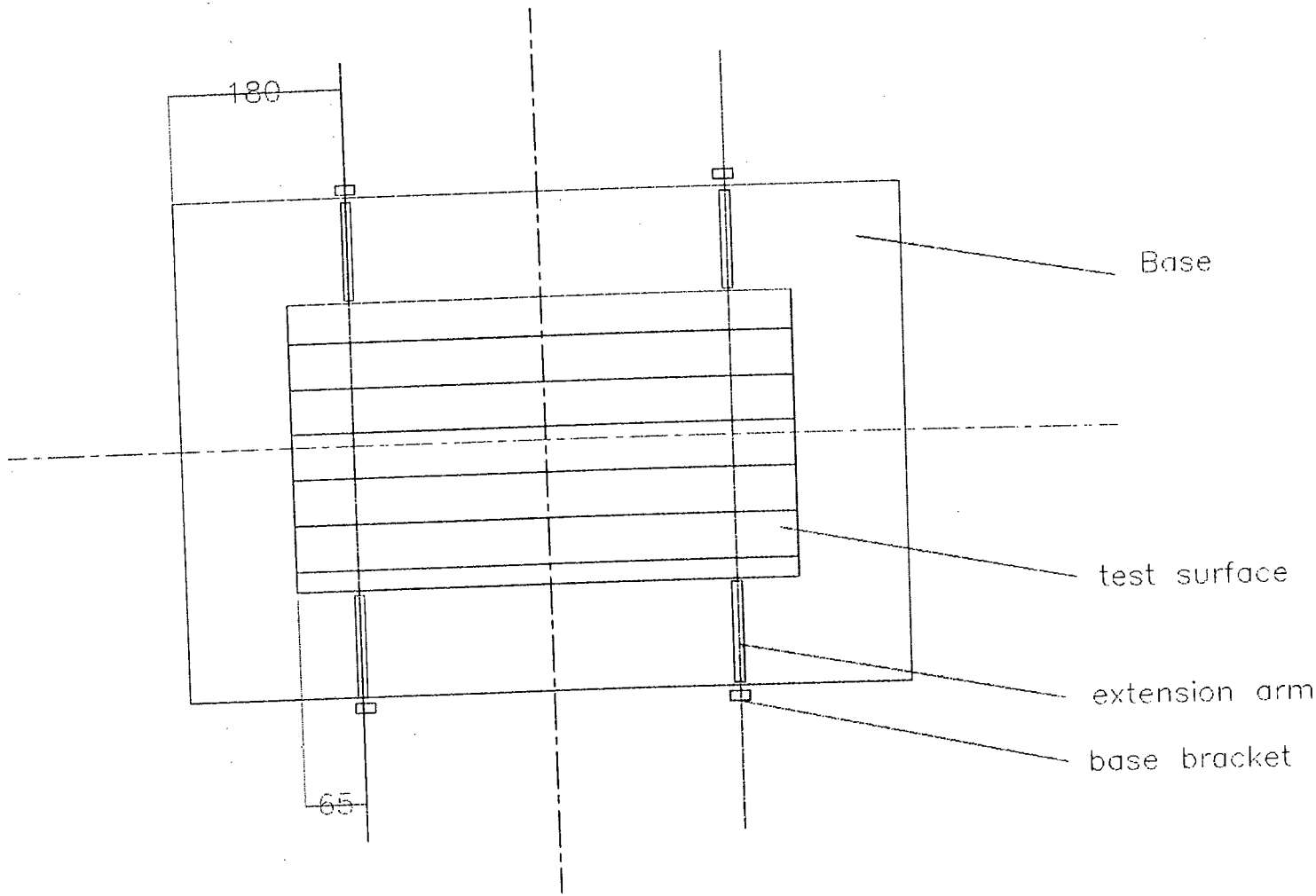

DEPARTMENT OF MECHANICAL ENGINEERING, UNIVERSITY OF CAPE TOWN

ASSEMBLY DRAWING OF TEST SURFACE AND BASE

Supervisor : Prof. A.T. Sayers	Date: 18 May 1997	Drawn by Kamalluddien Parker
Project : MSc. Mechanical Engineering	Scale ; None	Drawing No. 2 of 9

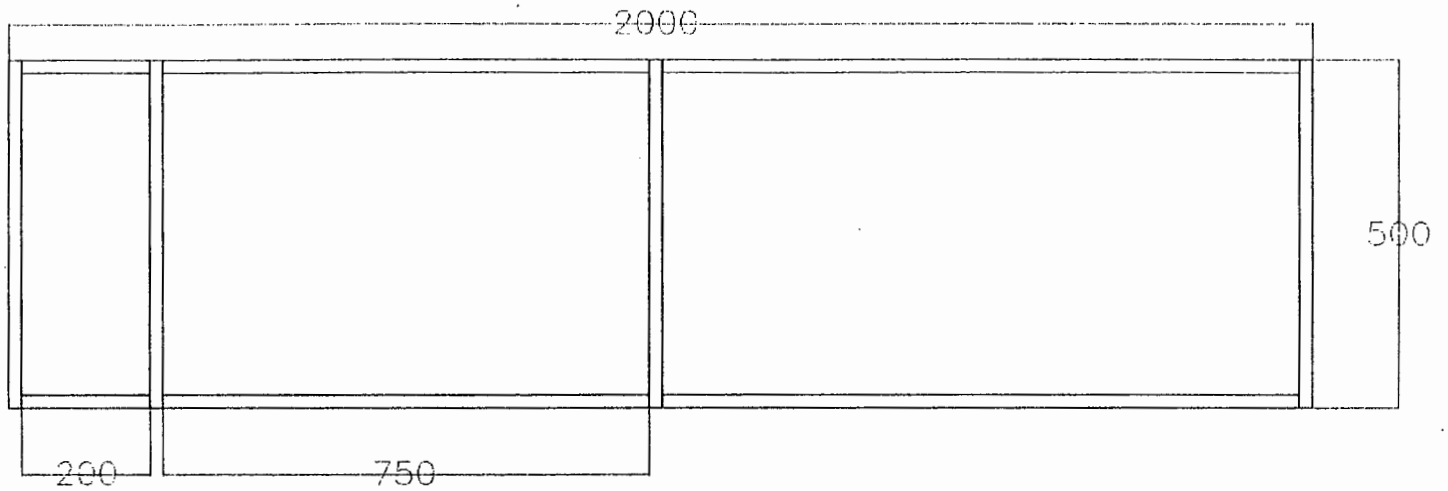

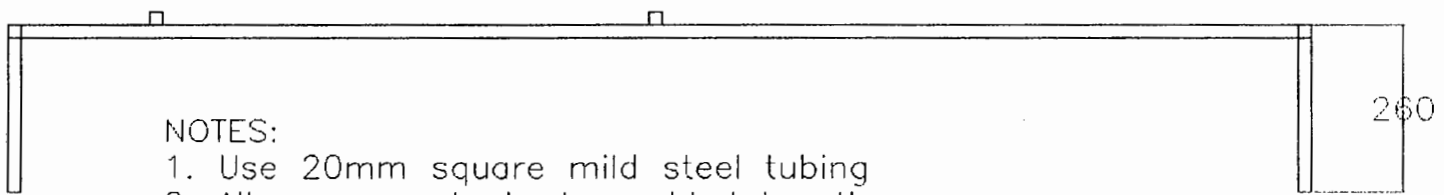

NOTES:
1. Use 20mm square mild steel tubing
2. All components to be welded together.
3. No. of components required = 1.

DEPARTMENT OF MECHANICAL ENGINEERING, UNIVERSITY OF CAPE TOWN		
TOP MOUNTING FRAME		
Supervisor : Prof. A.T. Sayers	Date: 18 May 1997	Drawn by Kamalluddien Parker
Project : MSc. Mechanical Engineering	Scale : 1 : 11.3	Drawing No. 3 of 9

Base bracket

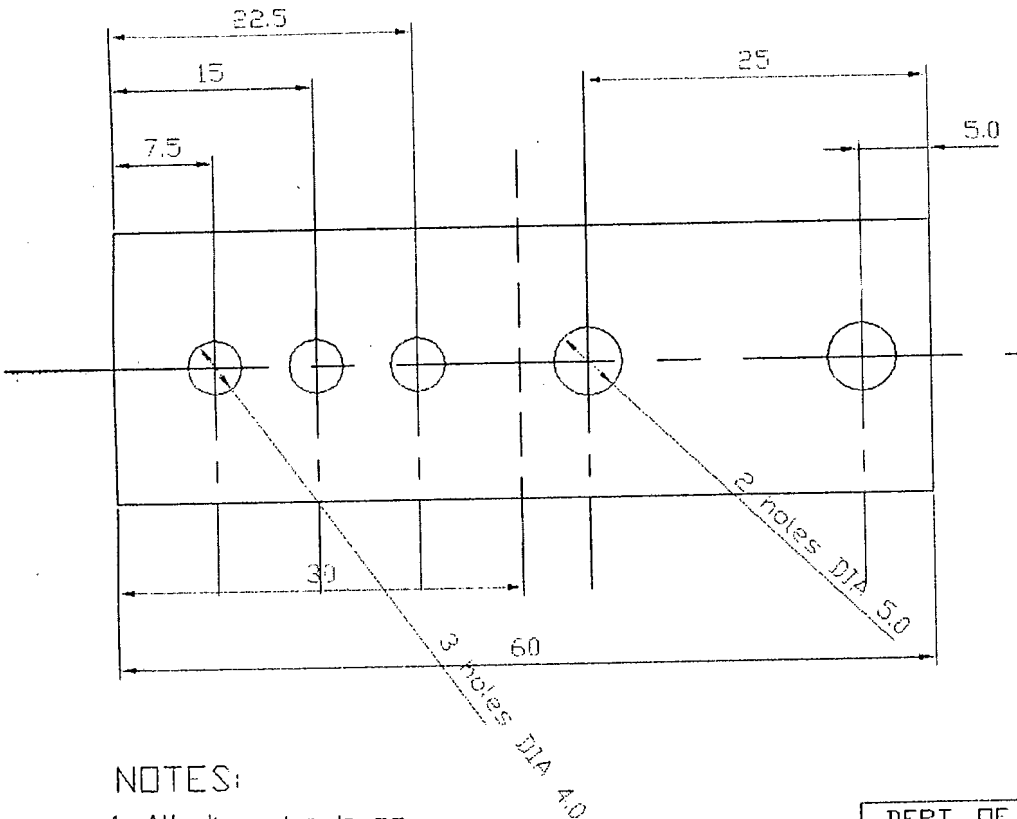

Fastening plate

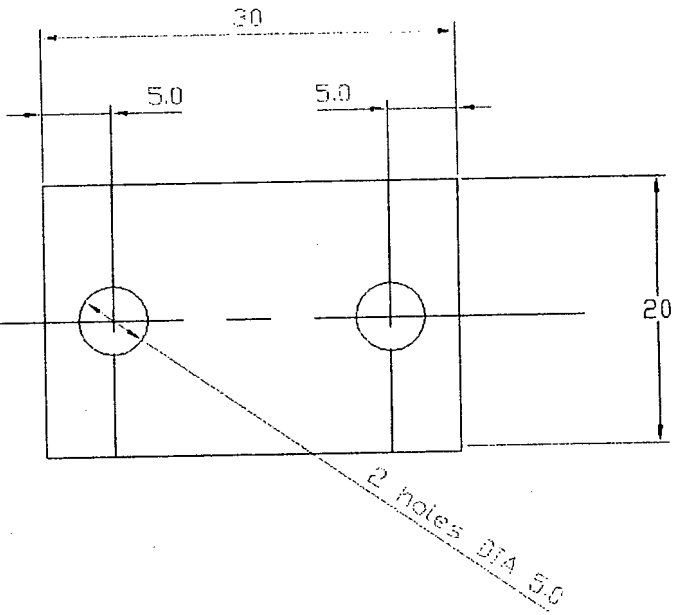

NOTES:

1. All dimension in mm.
2. The DIA 4 holes must be countersunk for 25 x 8 chipboard screws.
3. Use as material 2 mm mild steel.
4. Fold above bracket along dashed line by 90 degrees.
5. Surface finish to be smooth : 4 - 3 microns.
6. No. of components required = 4 of each

DEPT. OF MECHANICAL ENGINEERING, UNIVERSITY OF CAPE TOWN	
TITLE: BASE BRACKET + FASTENING PLATE	
Drawn by: Kamalluddien Parker	
Supervisor : Prof. A.T Sayers	
Date : 18 May 1997	Project : MSc. Mech. Eng.
Scale : 2 : 1	Drawing No. 4 of 9

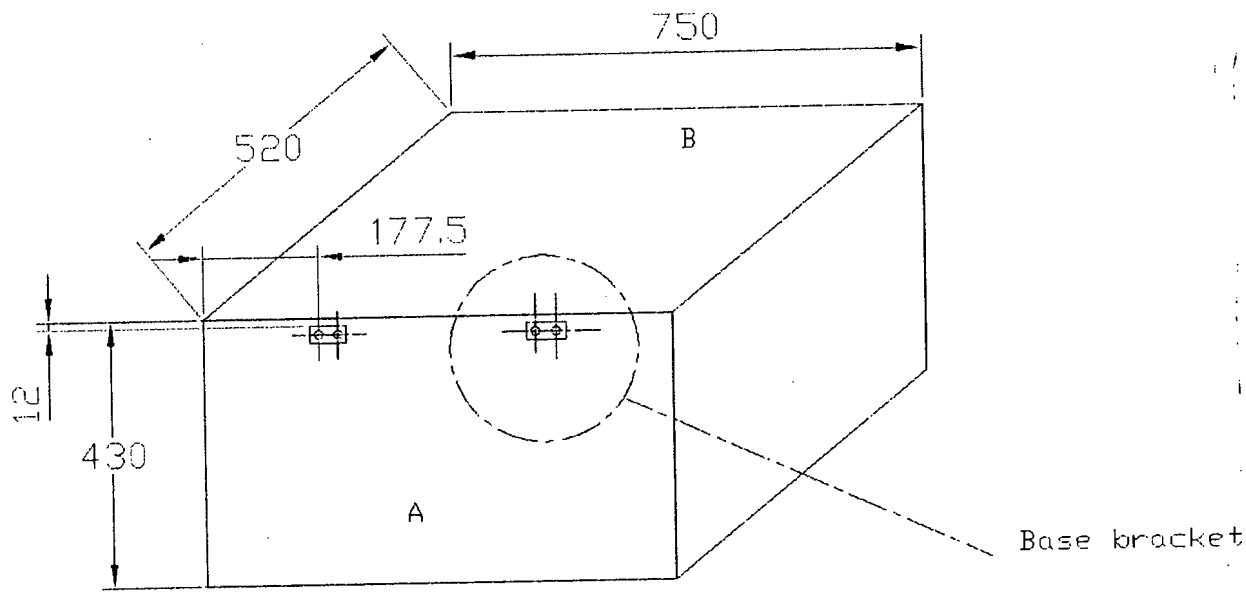

NOTES:

1. Use 20 mm chipboard as material.
2. The Base has no top or bottom cover, only 4 sides.
3. Base brackets are positioned as shown.
4. Base brackets on outer sides A and B.
5. Drill holes for base bracket screws as shown.
6. Base bracket screws are 20 x 8 chipboard screws.

DEPT. OF MECHANICAL ENGINEERING, UNIVERSITY OF CAPE TOWN
TITLE: BASE SECTION
Drawn by: Kamalluddien Parker
Supervisor : Prof. A.T Sayers
Date : 18 May 1997 — Project : MSc. Mech. Eng
Scale : 1 : 4 — Drawing No. 5 of 9

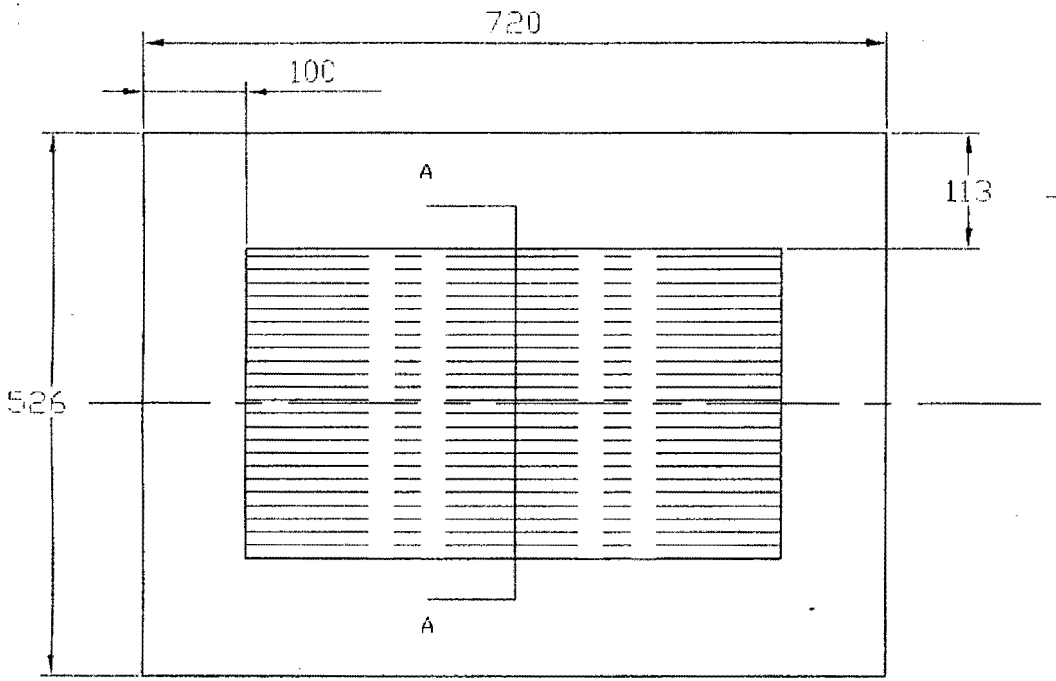

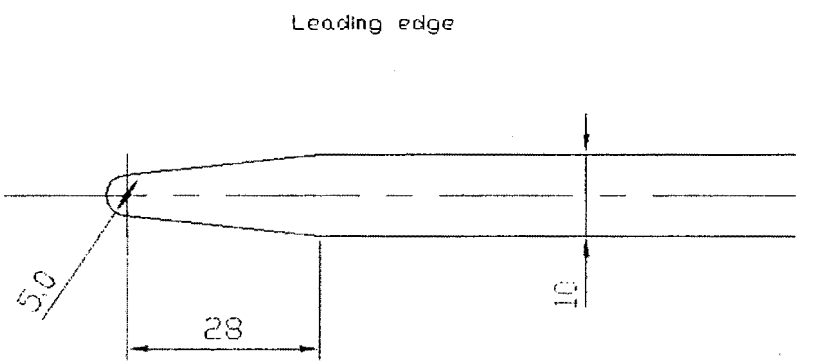

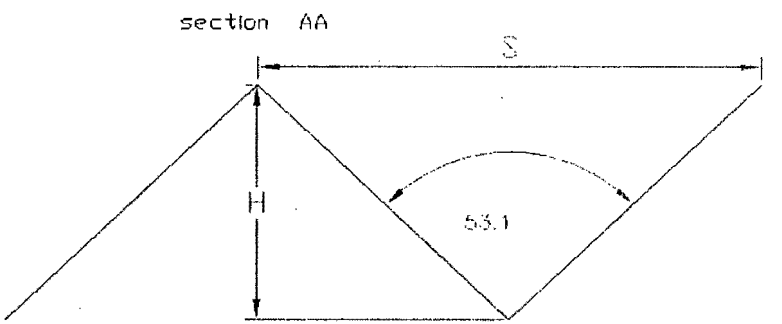

NOTES:

1. Use 10 mm Perspex Board.
2. Machine grooves on 1 side only
3. Grooves must be clean of grease and dirt.
4. Grooves are symmetric.
5. For this test section
   H = 0.51
   S = 0.51
6. All dimensions in mm.

DEPT. OF MECHANICAL ENGINEERING, UNIVERSITY OF CAPE TOWN	
TITLE: TEST PLATE MODEL No. #1	
Drawn by: Kanalluddien Parker	
Supervisor : Prof. A.T Sayers	
Date : 18 May 1997	Project : MSc. Mech. Eng.
Scale : None	Drawing No. 6 of 9

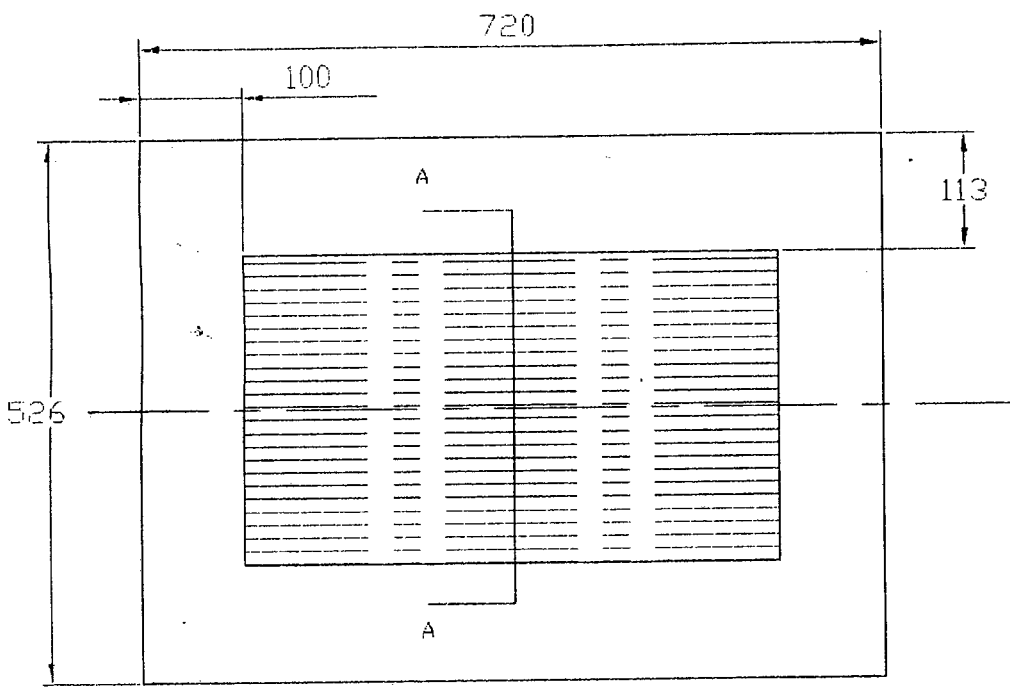

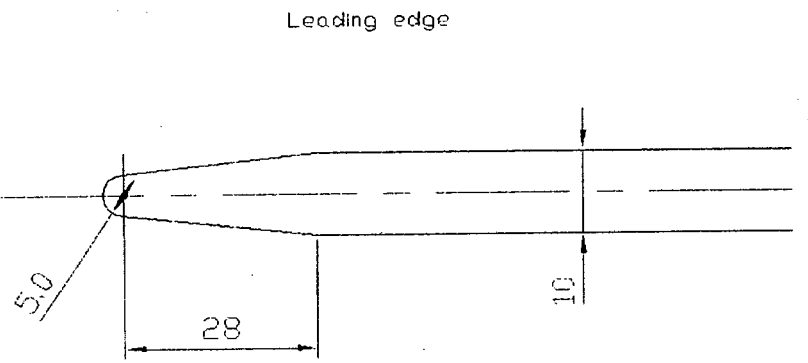

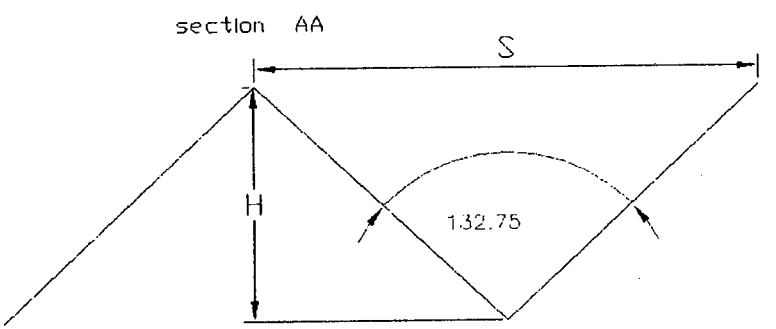

NOTES:

1. Use 10 mm Perspex Board.
2. Machine grooves on 1 side only.
3. Grooves must be clean of grease and dirt.
4. Grooves are symmetric.
5. For this test section
   H = 0.25
   S = 1.14
6. All dimensions in mm.

DEPT. OF MECHANICAL ENGINEERING, UNIVERSITY OF CAPE TOWN	
TITLE: TEST PLATE MODEL No. #2	
Drawn by: Kanalluddien Parker	
Supervisor : Prof. A.T Sayers	
Date : 18 May 1997	Project : MSc. Mech. Eng.
Scale : None	Drawing No. 7 of 9

extention arm (4 of)

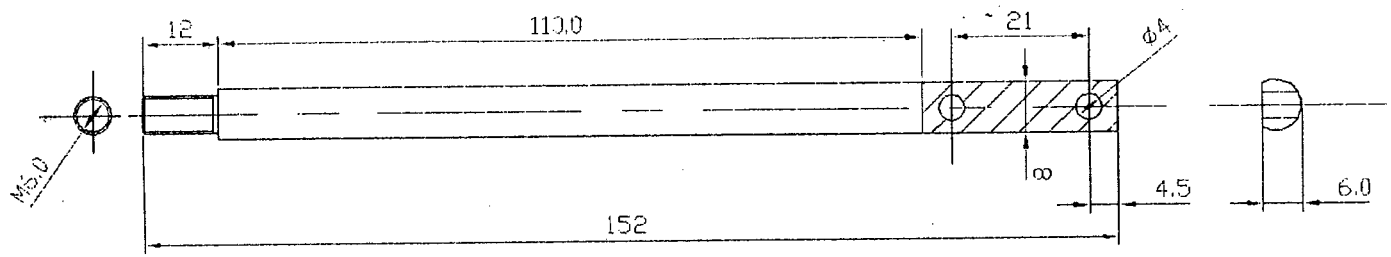

fastening plate (4 of)

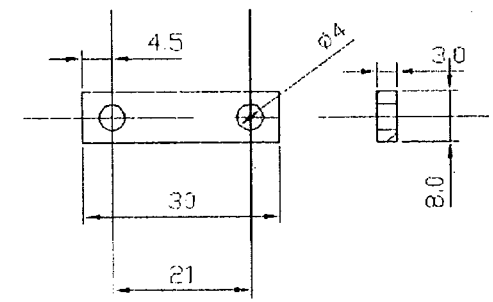

NOTES:

1. All unspecified radii to be 1 mm.
2. All dimensions in mm.
3. All surface finishes to be smooth.
4. Remove all burrs from holes and edges.
5. Use 8mm mild steel rod.
6. No. of components required = 4
7. Assume a scale of 1 : 1.5

MECHANICAL ENGINEERING, UNIVERSITY OF CAPE TOWN	
test surface bracket (extension arm + fastening plate)	
drawn by: Kamalluddien Parker	Date: 18 May 1997
Supervisor: Prof. A.T.Sayers	Drawing No. 8 of 9

profile 1: riblet #2

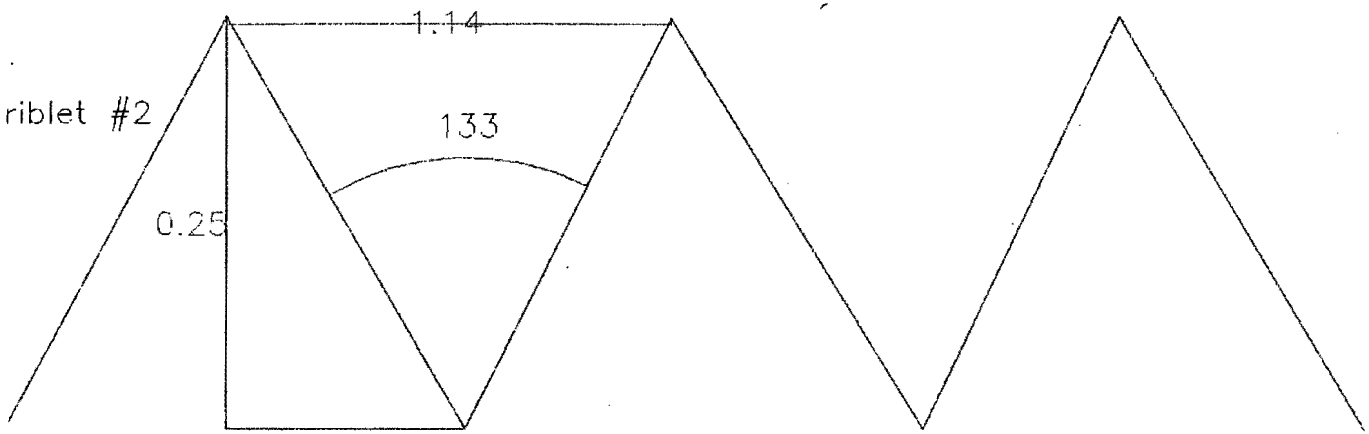

Profile 2: riblet #1

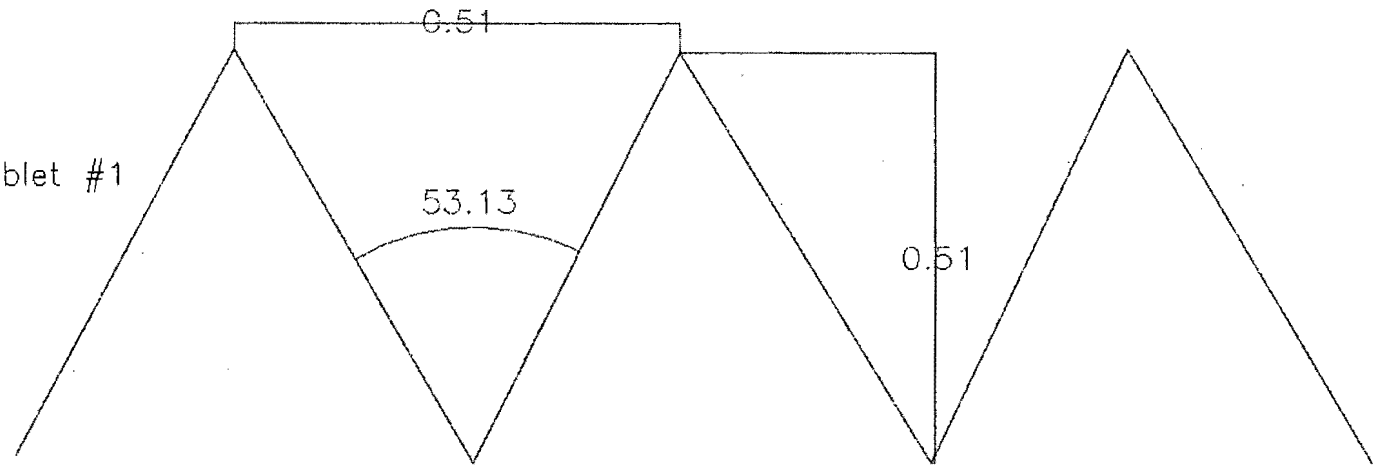

DEPARTMENT OF MECHANICAL ENGINEERING, UNIVERSITY OF CAPE TOWN		
Profiles for Machining		
Supervisor : Prof. A.T. Sayers	Date: 18 May 1997	Drawn by Kamalluddien Parker
Project : MSc. Mechanical Engineering	Scale ; None	Drawing No. 9 of 9

APPENDIX B:

Boundary Layer Data

smooth plate

y(ref) = 0.15 mm

T = 16.5 ° C = 289.5 K

P = 762.4 mm Hg = 101.645 kPa

v = 7.88 Pa = 3.589 m/s

ρ = 1.223 kg/m^3

ν = 1.47E-05 m^2/s

x(from L.E.) = 110 mm

y (mm)	*ΔP*	*v(probe)*	*y(abs) mm*	*v(correct)*	**Dimensionless forms** *y/ δ*	*v/u*
0	0	0	0	0	0	0
0	1.51	1.571	0.15	1.701	0.028302	0.473780175
0.2	2.15	1.875	0.35	1.997	0.066038	0.556385444
0.4	2.81	2.143	0.55	2.260	0.103774	0.629442097
0.6	3.49	2.389	0.75	2.499	0.141509	0.696178515
0.8	4.32	2.658	0.95	2.762	0.179245	0.769335758
1	4.75	2.787	1.15	2.888	0.216981	0.80446558
1.2	5.15	2.902	1.35	3.000	0.254717	0.83574222
1.4	5.68	3.047	1.55	3.143	0.292453	0.87536827
1.6	5.88	3.100	1.75	3.195	0.330189	0.889837865
1.8	6.08	3.153	1.95	3.246	0.367925	0.904063399
2	6.68	3.305	2.15	3.394	0.40566	0.945390512
2.2	6.89	3.356	2.35	3.444	0.443396	0.959413204
2.4	7.04	3.393	2.55	3.480	0.481132	0.969298985
2.6	7.07	3.400	2.75	3.487	0.518868	0.971263463
2.8	7.09	3.405	2.95	3.492	0.556604	0.9725708
3	7.1	3.407	3.15	3.494	0.59434	0.973223776
3.2	7.11	3.409	3.35	3.496	0.632075	0.973876294
3.4	7.12	3.412	3.55	3.499	0.669811	0.974528352
3.6	7.1	3.407	3.75	3.494	0.707547	0.973223776
3.8	7.14	3.417	3.95	3.503	0.745283	0.975831097
4	7.2	3.431	4.15	3.517	0.783019	0.979728422
4.2	7.25	3.443	4.35	3.529	0.820755	0.982963806
4.4	7.3	3.455	4.55	3.540	0.858491	0.986188052
5	7.32	3.459	5.15	3.545	0.971698	0.987474657
5.2	7.35	3.466	5.35	3.552	1.009434	0.989401274
5.4	7.3	3.455	5.55	3.540	1.04717	0.986188052
5.6	7.34	3.464	5.75	3.550	1.084906	0.988759506
5.8	7.31	3.457	5.95	3.543	1.122642	0.986831574
6	7.32	3.459	6.15	3.545	1.160377	0.987474657
6.2	7.26	3.445	6.35	3.531	1.198113	0.983609542
6.4	7.4	3.478	6.55	3.563	1.235849	0.992603586
6.6	7.42	3.483	6.75	3.568	1.273585	0.993881481
6.8	7.46	3.492	6.95	3.577	1.311321	0.996432114
7	7.48	3.497	7.15	3.582	1.349057	0.997704866
7.2	7.48	3.497	7.35	3.582	1.386792	0.997704866
7.4	7.42	3.483	7.55	3.568	1.424528	0.993881481
7.6	7.4	3.478	7.75	3.563	1.462264	0.992603586

7.8	7.5	3.502	7.95	3.586	1.5	0.998975917
8	7.51	3.504	8.15	3.589	1.537736	0.999610808
8.5	7.3	3.455	8.65	3.540	1.632075	0.986188052
9	7.48	3.497	9.15	3.582	1.726415	0.997704866
9.5	7.51	3.504	9.65	3.589	1.820755	0.999610808
10	7.41	3.481	10.15	3.566	1.915094	0.993242749
10.5	7.46	3.492	10.65	3.577	2.009434	0.996432114
11	7.26	3.445	11.15	3.531	2.103774	0.983609542
11.5	7.33	3.462	11.65	3.547	2.198113	0.988117301
12	7.41	3.481	12.15	3.566	2.292453	0.993242749
12.8	7.42	3.483	12.95	3.568	2.443396	0.993881481
13.6	7.51	3.504	13.75	3.589	2.59434	0.999610808
14.4	7.37	3.471	14.55	3.557	2.745283	0.990683502
15.2	7.42	3.483	15.35	3.568	2.896226	0.993881481
16	7.25	3.443	16.15	3.529	3.04717	0.982963806
16.8	7.31	3.457	16.95	3.543	3.198113	0.986831574
17.6	7.27	3.448	17.75	3.533	3.349057	0.984254834
18.4	7.42	3.483	18.55	3.568	3.5	0.993881481

x(from L.E.) = 200 mm

y	*Δp*	*v(probe)*	*y(abs)*	*v(correct)*		
0	0	0	0	0	0	0
0	0.86	1.186	0.15	1.324	0.019868	0.368914858
0.1	1.2	1.401	0.25	1.534	0.033113	0.427384239
0.2	1.46	1.545	0.35	1.675	0.046358	0.466643495
0.4	1.95	1.785	0.55	1.910	0.072848	0.53208264
0.6	2.41	1.985	0.75	2.105	0.099338	0.586346467
0.8	2.89	2.174	0.95	2.289	0.125828	0.63768447
1	3.7	2.459	1.15	2.568	0.152318	0.715444455
1.3	4.31	2.654	1.45	2.759	0.192053	0.768498453
1.6	4.93	2.839	1.75	2.939	0.231788	0.818696816
1.9	5.42	2.977	2.05	3.074	0.271523	0.85617139
2.2	5.69	3.050	2.35	3.145	0.311258	0.876097743
2.5	6.06	3.148	2.65	3.241	0.350993	0.90265148
2.9	6.2	3.184	3.05	3.276	0.403974	0.912486583
3.2	6.28	3.204	3.35	3.296	0.443709	0.918056823
3.5	6.38	3.230	3.65	3.321	0.483444	0.924969967
3.8	6.42	3.240	3.95	3.331	0.523179	0.927720042
4.1	6.48	3.255	4.25	3.345	0.562914	0.931829141
4.4	6.59	3.282	4.55	3.372	0.602649	0.939313381
4.7	6.64	3.295	4.85	3.384	0.642384	0.942694652
5	6.78	3.329	5.15	3.418	0.682119	0.95209506
5.3	6.88	3.354	5.45	3.442	0.721854	0.958750343
5.6	6.92	3.363	5.75	3.451	0.761589	0.961398904
5.9	7	3.383	6.05	3.470	0.801325	0.96667316
6.2	7.04	3.393	6.35	3.480	0.84106	0.969298985

6.5	7.03	3.390	6.65	3.477	0.880795	0.96864323
6.8	6.96	3.373	6.95	3.461	0.92053	0.964039821
7.1	7.24	3.440	7.25	3.527	0.960265	0.982317624
7.4	7.34	3.464	7.55	3.550	1	0.988759506
7.7	7.46	3.492	7.85	3.577	1.039735	0.996432114
8	7.41	3.481	8.15	3.566	1.07947	0.993242749
8.5	7.36	3.469	8.65	3.554	1.145695	0.990042606
9	7.38	3.473	9.15	3.559	1.211921	0.991323964
9.5	7.46	3.492	9.65	3.577	1.278146	0.996432114
10	7.5	3.502	10.15	3.586	1.344371	0.998975917
10.5	7.51	3.504	10.65	3.589	1.410596	0.999610808
11	7.52	3.506	11.15	3.591	1.476821	1.000245275
11.5	7.49	3.499	11.65	3.584	1.543046	0.998340604
12	7.48	3.497	12.15	3.582	1.609272	0.997704866
12.8	7.51	3.504	12.95	3.589	1.715232	0.999610808
13.6	7.48	3.497	13.75	3.582	1.821192	0.997704866
14.4	7.5	3.502	14.55	3.586	1.927152	0.998975917
15.2	7.4	3.478	15.35	3.563	2.033113	0.992603586
16	7.38	3.473	16.15	3.559	2.139073	0.991323964
16.8	7.24	3.440	16.95	3.527	2.245033	0.982317624
17.6	7.41	3.481	17.75	3.566	2.350993	0.993242749
18.4	7.48	3.497	18.55	3.582	2.456954	0.997704866

x(from L.E) = 300 mm

y	*Δp*	*y(abs)*	*v(probe)*	*V(correct)*		
0	0	0	0	0	0	0
0	0.78	1.129	0.15	1.269	0.012876	0.353544416
0.2	1.39	1.507	0.35	1.639	0.030043	0.456443561
0.4	2.08	1.844	0.55	1.967	0.04721	0.548013395
0.7	2.56	2.046	0.85	2.164	0.072961	0.602898508
1.1	3.65	2.443	1.25	2.552	0.107296	0.710907986
1.2	3.98	2.551	1.35	2.658	0.11588	0.740300878
1.5	4.75	2.787	1.65	2.888	0.141631	0.80446558
1.8	4.81	2.804	1.95	2.905	0.167382	0.809238822
2.1	5.35	2.957	2.25	3.055	0.193133	0.850924747
2.4	5.59	3.023	2.55	3.119	0.218884	0.868773905
2.7	5.63	3.034	2.85	3.129	0.244635	0.871711238
3	5.94	3.116	3.15	3.210	0.270386	0.894130588
3.3	6.09	3.155	3.45	3.248	0.296137	0.904768488
3.6	6.33	3.217	3.75	3.308	0.321888	0.921520221
3.9	6.48	3.255	4.05	3.345	0.347639	0.931829141
4.2	6.53	3.267	4.35	3.358	0.373391	0.93523888
4.5	6.58	3.280	4.65	3.370	0.399142	0.93863559
4.8	6.63	3.292	4.95	3.382	0.424893	0.942019419
5.1	6.68	3.305	5.25	3.394	0.450644	0.945390512
5.4	6.72	3.315	5.55	3.404	0.476395	0.948078313

5.7	6.78	3.329	5.85	3.418	0.502146	0.95209506
6	6.83	3.342	6.15	3.430	0.527897	0.955428792
6.3	6.91	3.361	6.45	3.449	0.553648	0.960737483
6.6	6.97	3.376	6.75	3.463	0.579399	0.964698863
6.9	6.99	3.380	7.05	3.468	0.60515	0.966015532
7.2	7.12	3.412	7.35	3.499	0.630901	0.974528352
7.5	7.04	3.393	7.65	3.480	0.656652	0.969298985
7.8	7	3.383	7.95	3.470	0.682403	0.96667316
8.1	7.05	3.395	8.25	3.482	0.708155	0.969954275
8.5	7.15	3.419	8.65	3.506	0.742489	0.976481785
9	7.26	3.445	9.15	3.531	0.785408	0.983609542
9.8	7.31	3.457	9.95	3.543	0.854077	0.986831574
10.6	7.32	3.459	10.75	3.545	0.922747	0.987474657
11.4	7.34	3.464	11.55	3.550	0.991416	0.988759506
12.2	7.38	3.473	12.35	3.559	1.060086	0.991323964
13	7.38	3.473	13.15	3.559	1.128755	0.991323964
13.8	7.36	3.469	13.95	3.554	1.197425	0.990042606
14.6	7.38	3.473	14.75	3.559	1.266094	0.991323964
15.4	7.32	3.459	15.55	3.545	1.334764	0.987474657
16.2	7.3	3.455	16.35	3.540	1.403433	0.986188052
17	7.36	3.469	17.15	3.554	1.472103	0.990042606
18	7.38	3.473	18.15	3.559	1.55794	0.991323964

x(from L.E) = 380 mm

y	*Δp*	*y(abs)*	*v(probe)*	*V(correct)*		
0	0	0	0	0	0	0
0.1	0.96	1.253	0.25	1.390	0.016835	0.387154546
0.3	1.6	1.617	0.45	1.746	0.030303	0.486334599
0.6	2.45	2.001	0.75	2.121	0.050505	0.590809546
0.9	2.97	2.204	1.05	2.318	0.070707	0.64581353
1.2	3.65	2.443	1.35	2.552	0.090909	0.710907986
1.5	4.06	2.576	1.65	2.683	0.111111	0.747240828
1.8	5.18	2.910	1.95	3.009	0.131313	0.83803816
2.1	5.4	2.971	2.25	3.068	0.151515	0.854675824
2.4	5.68	3.047	2.55	3.143	0.171717	0.87536827
2.7	5.79	3.077	2.85	3.171	0.191919	0.883357502
3	6.35	3.222	3.15	3.313	0.212121	0.922901748
3.3	6.39	3.232	3.45	3.323	0.232323	0.925658292
3.6	6.44	3.245	3.75	3.335	0.252525	0.929091867
3.9	6.8	3.334	4.05	3.423	0.272727	0.953430023
4.2	6.86	3.349	4.35	3.437	0.292929	0.957423176
4.5	6.94	3.368	4.65	3.456	0.313131	0.962720314
4.8	6.98	3.378	4.95	3.466	0.333333	0.965357433
5.1	7.02	3.388	5.25	3.475	0.353535	0.967987008
5.4	7.05	3.395	5.55	3.482	0.373737	0.969954275
5.7	7.06	3.397	5.85	3.484	0.393939	0.970609101

6	7.07	3.400	6.15	3.487	0.414141	0.971263463
6.3	7.08	3.402	6.45	3.489	0.434343	0.971917362
6.6	7.1	3.407	6.75	3.494	0.454545	0.973223776
6.9	7.06	3.397	7.05	3.484	0.474747	0.970609101
7.2	7.12	3.412	7.35	3.499	0.494949	0.974528352
7.5	7.13	3.414	7.65	3.501	0.515152	0.975179953
7.8	7.12	3.412	7.95	3.499	0.535354	0.974528352
8.1	7.16	3.421	8.25	3.508	0.555556	0.977132019
8.4	7.14	3.417	8.55	3.503	0.575758	0.975831097
8.7	7.15	3.419	8.85	3.506	0.59596	0.976481785
9	7.12	3.412	9.15	3.499	0.616162	0.974528352
9.8	7.15	3.419	9.95	3.506	0.670034	0.976481785
10.6	7.19	3.428	10.75	3.515	0.723906	0.979079999
11.4	7.22	3.436	11.55	3.522	0.777778	0.98102392
12.2	7.18	3.426	12.35	3.513	0.83165	0.978431125
13	7.29	3.452	13.15	3.538	0.885522	0.985544088
14	7.31	3.457	14.15	3.543	0.952862	0.986831574
15	7.37	3.471	15.15	3.557	1.020202	0.990683502
16	7.33	3.462	16.15	3.547	1.087542	0.988117301
17	7.38	3.473	17.15	3.559	1.154882	0.991323964
18	7.4	3.478	18.15	3.563	1.222222	0.992603586

x(from L.E)= 490 mm

y	*Δp*	*y(abs)*	*v(probe)*	*V(correct)*		
0	0	0	0	0	0	0
0	0.98	1.266	0.15	1.403	0.008646	0.390686572
0.1	1.65	1.642	0.25	1.770	0.014409	0.493156889
0.3	1.99	1.804	0.45	1.928	0.025937	0.537039498
0.5	2.56	2.046	0.65	2.164	0.037464	0.602898508
0.7	2.93	2.189	0.85	2.304	0.048991	0.641762873
0.8	3.39	2.354	0.95	2.466	0.054755	0.686800601
0.9	3.65	2.443	1.05	2.552	0.060519	0.710907986
1	3.91	2.528	1.15	2.636	0.066282	0.734170986
1.3	4.27	2.642	1.45	2.747	0.083573	0.76513948
1.6	4.65	2.757	1.75	2.859	0.100865	0.796442683
1.9	4.96	2.848	2.05	2.948	0.118156	0.821043273
2.2	5.68	3.047	2.35	3.143	0.135447	0.87536827
2.5	5.77	3.071	2.65	3.166	0.152738	0.881910596
2.8	5.89	3.103	2.95	3.197	0.170029	0.890554834
3.1	6.18	3.179	3.25	3.271	0.18732	0.911088417
3.4	6.38	3.230	3.55	3.321	0.204611	0.924969967
3.7	6.44	3.245	3.85	3.335	0.221902	0.929091867
4	6.61	3.287	4.15	3.377	0.239193	0.940667424
4.3	6.7	3.310	4.45	3.399	0.256484	0.946735415
4.6	6.72	3.315	4.75	3.404	0.273775	0.948078313
4.9	6.63	3.292	5.05	3.382	0.291066	0.942019419

5.2	6.79	3.332	5.35	3.420	0.308357	0.952762787
5.5	6.78	3.329	5.65	3.418	0.325648	0.95209506
5.8	6.82	3.339	5.95	3.428	0.342939	0.954763024
6.1	6.83	3.342	6.25	3.430	0.360231	0.955428792
6.4	6.87	3.351	6.55	3.440	0.377522	0.958087001
6.7	6.89	3.356	6.85	3.444	0.394813	0.959413204
7	6.9	3.359	7.15	3.447	0.412104	0.960075583
7.3	6.91	3.361	7.45	3.449	0.429395	0.960737483
7.6	6.95	3.371	7.75	3.459	0.446686	0.963380305
7.9	6.98	3.378	8.05	3.466	0.463977	0.965357433
8.2	7.05	3.395	8.35	3.482	0.481268	0.969954275
8.5	7.08	3.402	8.65	3.489	0.498559	0.971917362
8.8	7.09	3.405	8.95	3.492	0.51585	0.9725708
9.1	7.06	3.397	9.25	3.484	0.533141	0.970609101
9.4	7.1	3.407	9.55	3.494	0.550432	0.973223776
9.7	7.08	3.402	9.85	3.489	0.567723	0.971917362
10.5	7.14	3.417	10.65	3.503	0.613833	0.975831097
11.3	7.19	3.428	11.45	3.515	0.659942	0.979079999
12.1	7.23	3.438	12.25	3.524	0.706052	0.981670995
12.9	7.25	3.443	13.05	3.529	0.752161	0.982963806
13.7	7.28	3.450	13.85	3.536	0.798271	0.984899682
14.7	7.34	3.464	14.85	3.550	0.855908	0.988759506
15.7	7.28	3.450	15.85	3.536	0.913545	0.984899682
16.7	7.31	3.457	16.85	3.543	0.971182	0.986831574
17.7	7.39	3.476	17.85	3.561	1.028818	0.991963992
18.7	7.4	3.478	18.85	3.563	1.086455	0.992603586

x(from LE) = 590 mm

y	*Δp*	*y(abs)*	*v(probe)*	*V(correct)*		
0	0	0	0	0	0	0
0	0.5	0.904	0.15	1.049	0.007407	0.292297014
0.2	1.01	1.285	0.35	1.421	0.017284	0.395917709
0.3	1.34	1.480	0.45	1.612	0.022222	0.44899974
0.6	2.03	1.822	0.75	1.946	0.037037	0.541946784
0.9	2.79	2.136	1.05	2.252	0.051852	0.627363235
1.2	3.57	2.416	1.35	2.526	0.066667	0.703584514
1.5	4.35	2.667	1.65	2.771	0.081481	0.771841875
1.8	5.14	2.899	1.95	2.998	0.096296	0.834975421
2.1	5.25	2.930	2.25	3.028	0.111111	0.843369635
2.4	5.39	2.968	2.55	3.066	0.125926	0.853927002
2.7	5.79	3.077	2.85	3.171	0.140741	0.883357502
3	6.12	3.163	3.15	3.256	0.155556	0.906880288
3.3	6.48	3.255	3.45	3.345	0.17037	0.931829141
3.6	6.7	3.310	3.75	3.399	0.185185	0.946735415
3.9	6.8	3.334	4.05	3.423	0.2	0.953430023
4.2	6.86	3.349	4.35	3.437	0.214815	0.957423176

4.5	6.97	3.376	4.65	3.463	0.22963	0.964698863
4.8	7.02	3.388	4.95	3.475	0.244444	0.967987008
5.1	7.13	3.414	5.25	3.501	0.259259	0.975179953
5.4	7.19	3.428	5.55	3.515	0.274074	0.979079999
5.7	7.28	3.450	5.85	3.536	0.288889	0.984899682
6	7.27	3.448	6.15	3.533	0.303704	0.984254834
6.3	7.29	3.452	6.45	3.538	0.318519	0.985544088
6.6	7.36	3.469	6.75	3.554	0.333333	0.990042606
6.9	7.28	3.450	7.05	3.536	0.348148	0.984899682
7.2	7.19	3.428	7.35	3.515	0.362963	0.979079999
7.5	7.23	3.438	7.65	3.524	0.377778	0.981670995
7.8	7.28	3.450	7.95	3.536	0.392593	0.984899682
8.1	7.24	3.440	8.25	3.527	0.407407	0.982317624
8.8	7.26	3.445	8.95	3.531	0.441975	0.983609542
9.6	7.2	3.431	9.75	3.517	0.481481	0.979728422
10.4	7.21	3.433	10.55	3.520	0.520988	0.980376396
11.2	7.29	3.452	11.35	3.538	0.560494	0.985544088
12	7.28	3.450	12.15	3.536	0.6	0.984899682
12.8	7.31	3.457	12.95	3.543	0.639506	0.986831574
13.6	7.26	3.445	13.75	3.531	0.679012	0.983609542
14.4	7.23	3.438	14.55	3.524	0.718519	0.981670995
15.4	7.28	3.450	15.55	3.536	0.767901	0.984899682
16.4	7.28	3.450	16.55	3.536	0.817284	0.984899682
17.4	7.3	3.455	17.55	3.540	0.866667	0.986188052
18.4	7.33	3.462	18.55	3.547	0.916049	0.988117301
19.4	7.32	3.459	19.55	3.545	0.965432	0.987474657
20.4	7.36	3.469	20.55	3.554	1.014815	0.990042606

Riblet surface #1

		T =	16.5	° C =	289.5 K
y(ref) =	0.2 mm	P =	762.4	mm Hg =	101.645 kPa
		V =	7.88	Pa =	3.589 m/s
		ρ =	1.223	kg/m^3	
		ν =	1.47E-05	m^2/s	

x(from L.E) = 110 mm

y (mm)	*Δp*	*v(probe)*	*y(abs)*	*v(correct)*	**Dimensionless forms** *y/ δ*	*v/u*
0	0	0	0	0	0	0
0	1.35	1.486	0.2	1.617	0.038314	0.450499
0.2	1.98	1.799	0.4	1.924	0.076628	0.535805
0.4	2.72	2.109	0.6	2.226	0.114943	0.620028
0.6	3.79	2.489	0.8	2.597	0.153257	0.723534
0.8	4.2	2.620	1	2.726	0.191571	0.759223
1	4.99	2.856	1.2	2.956	0.229885	0.823383
1.2	5.75	3.066	1.4	3.161	0.268199	0.880461
1.4	6.17	3.176	1.6	3.268	0.306513	0.910388
1.6	6.41	3.237	1.8	3.328	0.344828	0.927033
1.8	6.61	3.287	2	3.377	0.383142	0.940667
2	6.7	3.310	2.2	3.399	0.421456	0.946735
2.2	6.75	3.322	2.4	3.411	0.45977	0.950089
2.4	6.79	3.332	2.6	3.420	0.498084	0.952763
2.6	6.88	3.354	2.8	3.442	0.536398	0.95875
2.8	6.94	3.368	3	3.456	0.574713	0.96272
3	7.1	3.407	3.2	3.494	0.613027	0.973224
3.2	7.03	3.390	3.4	3.477	0.651341	0.968643
3.4	6.97	3.376	3.6	3.463	0.689655	0.964699
3.6	7.04	3.393	3.8	3.480	0.727969	0.969299
3.8	7.01	3.385	4	3.473	0.766284	0.96733
4	7.07	3.400	4.2	3.487	0.804598	0.971263
4.2	7.21	3.433	4.4	3.520	0.842912	0.980376
4.4	7.18	3.426	4.6	3.513	0.881226	0.978431
4.6	7.28	3.450	4.8	3.536	0.91954	0.9849
4.8	7.32	3.459	5	3.545	0.957854	0.987475
5	7.36	3.469	5.2	3.554	0.996169	0.990043
5.5	7.35	3.466	5.7	3.552	1.091954	0.989401
6	7.37	3.471	6.2	3.557	1.187739	0.990684
6.5	7.38	3.473	6.7	3.559	1.283525	0.991324
7	7.28	3.450	7.2	3.536	1.37931	0.9849
7.5	7.17	3.424	7.7	3.510	1.475096	0.977782
8	7.24	3.440	8.2	3.527	1.570881	0.982318
8.8	7.19	3.428	9	3.515	1.724138	0.97908
9.6	7.16	3.421	9.8	3.508	1.877395	0.977132
10.4	7.16	3.421	10.6	3.508	2.030651	0.977132
11.2	7.2	3.431	11.4	3.517	2.183908	0.979728
12	7.3	3.455	12.2	3.540	2.337165	0.986188
12.8	7.24	3.440	13	3.527	2.490421	0.982318

13.6	7.23	3.438	13.8	3.524	2.643678	0.981671
14.4	7.28	3.450	14.6	3.536	2.796935	0.9849
15.2	7.24	3.440	15.4	3.527	2.950192	0.982318
16	7.32	3.459	16.2	3.545	3.103448	0.987475
16.8	7.29	3.452	17	3.538	3.256705	0.985544
17.6	7.27	3.448	17.8	3.533	3.409962	0.984255
18.4	7.31	3.457	18.6	3.543	3.563218	0.986832

x(from L.E) = 200 mm

y (mm)	*Δp*	*v(probe)*	*y(abs)*	*V(correct)*		
0	0	0	0	0	0	0
0.2	0.9	1.213	0.2	1.351	0.026667	0.376332
0.3	1.04	1.304	0.3	1.440	0.04	0.401072
0.4	1.58	1.607	0.4	1.736	0.053333	0.483576
0.6	1.76	1.696	0.6	1.823	0.08	0.507811
0.8	2.25	1.918	0.8	2.040	0.106667	0.568113
1	3.34	2.337	1	2.449	0.133333	0.68206
1.2	3.9	2.525	1.2	2.633	0.16	0.733291
1.4	4.46	2.700	1.4	2.804	0.186667	0.780958
1.6	4.81	2.804	1.6	2.905	0.213333	0.809239
1.8	5.2	2.916	1.8	3.014	0.24	0.839565
2	5.64	3.037	2	3.132	0.266667	0.872444
2.2	5.82	3.085	2.2	3.179	0.293333	0.885523
2.4	5.9	3.106	2.4	3.200	0.32	0.891271
2.6	6	3.132	2.6	3.225	0.346667	0.898402
2.8	6.06	3.148	2.8	3.241	0.373333	0.902651
3	5.98	3.127	3	3.220	0.4	0.89698
3.2	6.08	3.153	3.2	3.246	0.426667	0.904063
3.4	6.14	3.168	3.4	3.261	0.453333	0.908285
3.6	6.24	3.194	3.6	3.286	0.48	0.915276
3.8	6.35	3.222	3.8	3.313	0.506667	0.922902
4	6.58	3.280	4	3.370	0.533333	0.938636
4.2	6.78	3.329	4.2	3.418	0.56	0.952095
4.4	6.89	3.356	4.4	3.444	0.586667	0.959413
4.8	6.99	3.380	4.8	3.468	0.64	0.966016
5.2	7.06	3.397	5.2	3.484	0.693333	0.970609
5.6	7.14	3.417	5.6	3.503	0.746667	0.975831
6.4	7.21	3.433	6.4	3.520	0.853333	0.980376
7.2	7.29	3.452	7.2	3.538	0.96	0.985544
8	7.36	3.469	8	3.554	1.066667	0.990043
8.8	7.32	3.459	8.8	3.545	1.173333	0.987475
9.6	7.34	3.464	9.6	3.550	1.28	0.98876
10.4	7.37	3.471	10.4	3.557	1.386667	0.990684
11.2	7.31	3.457	11.2	3.543	1.493333	0.986832
12	7.34	3.464	12	3.550	1.6	0.98876
12.8	7.29	3.452	12.8	3.538	1.706667	0.985544
13.6	7.28	3.450	13.6	3.536	1.813333	0.9849

14.4	7.28	3.450	14.4	3.536	1.92	0.9849
15.2	7.3	3.455	15.2	3.540	2.026667	0.986188
16	7.32	3.459	16	3.545	2.133333	0.987475
16.8	7.34	3.464	16.8	3.550	2.24	0.98876
17.6	7.39	3.476	17.6	3.561	2.346667	0.991964
18.4	7.41	3.481	18.4	3.566	2.453333	0.993243
19.2	7.37	3.471	19.2	3.557	2.56	0.990684
19.7	7.38	3.473	19.7	3.559	2.626667	0.991324
20.2	7.37	3.471	20.2	3.557	2.693333	0.990684
20.7	7.39	3.476	20.7	3.561	2.76	0.991964
21.1	7.36	3.469	21.1	3.554	2.813333	0.990043
21.5	7.41	3.481	21.5	3.566	2.866667	0.993243
21.9	7.37	3.471	21.9	3.557	2.92	0.990684
22.3	7.39	3.476	22.3	3.561	2.973333	0.991964
22.7	7.36	3.469	22.7	3.554	3.026667	0.990043

x(from L.E.) = 300 mm

y (mm)	*Δp*	*v(probe)*	*y(abs)*	*V(correct)*		
0	0	0	0	0	0	0
0	0.69	1.062	0.2	1.204	0.017544	0.335277
0.2	1.23	1.418	0.4	1.551	0.035088	0.432118
0.4	2.13	1.866	0.6	1.989	0.052632	0.554008
0.6	2.97	2.204	0.8	2.318	0.070175	0.645814
0.8	3.45	2.375	1	2.486	0.087719	0.692444
1	3.74	2.473	1.2	2.581	0.105263	0.719052
1.2	3.92	2.532	1.4	2.639	0.122807	0.73505
1.4	4.44	2.694	1.6	2.798	0.140351	0.779309
1.6	4.65	2.757	1.8	2.859	0.157895	0.796443
1.8	5.05	2.873	2	2.973	0.175439	0.82804
2	5.57	3.018	2.2	3.114	0.192982	0.867301
2.2	5.75	3.066	2.4	3.161	0.210526	0.880461
2.4	5.81	3.082	2.6	3.176	0.22807	0.884802
2.6	5.89	3.103	2.8	3.197	0.245614	0.890555
2.8	5.96	3.121	3	3.215	0.263158	0.895557
3	6.19	3.181	3.2	3.273	0.280702	0.911788
3.2	6.28	3.204	3.4	3.296	0.298246	0.918057
3.4	6.35	3.222	3.6	3.313	0.315789	0.922902
3.6	6.42	3.240	3.8	3.331	0.333333	0.92772
3.8	6.44	3.245	4	3.335	0.350877	0.929092
4	6.76	3.324	4.2	3.413	0.368421	0.950758
4.2	6.8	3.334	4.4	3.423	0.385965	0.95343
4.4	6.77	3.327	4.6	3.416	0.403509	0.951427
4.8	6.8	3.334	5	3.423	0.438596	0.95343
5.2	6.82	3.339	5.4	3.428	0.473684	0.954763
5.6	6.88	3.354	5.8	3.442	0.508772	0.95875
6	6.9	3.359	6.2	3.447	0.54386	0.960076
6.4	6.86	3.349	6.6	3.437	0.578947	0.957423
7.2	7	3.383	7.4	3.470	0.649123	0.966673

8	7.07	3.400	8.2	3.487	0.719298	0.971263
8.8	7.08	3.402	9	3.489	0.789474	0.971917
9.6	7.16	3.421	9.8	3.508	0.859649	0.977132
10.4	7.28	3.450	10.6	3.536	0.929825	0.9849
11.2	7.36	3.469	11.4	3.554	1	0.990043
12	7.38	3.473	12.2	3.559	1.070175	0.991324
12.8	7.35	3.466	13	3.552	1.140351	0.989401
13.6	7.42	3.483	13.8	3.568	1.210526	0.993881
14.4	7.44	3.488	14.6	3.573	1.280702	0.995158
15.2	7.45	3.490	15.4	3.575	1.350877	0.995795
16	7.36	3.469	16.2	3.554	1.421053	0.990043
16.8	7.39	3.476	17	3.561	1.491228	0.991964
17.6	7.43	3.485	17.8	3.570	1.561404	0.99452
18.4	7.39	3.476	18.6	3.561	1.631579	0.991964

x(from L.E) = 380 mm

y (mm)	*Δp*	*v(probe)*	*y(abs)*	*V(correct)*		
0	0	0	0	0	0	0
0	0.44	0.848	0.2	0.995	0.013699	0.277067
0.1	0.95	1.246	0.3	1.383	0.020548	0.385375
0.2	1.26	1.435	0.4	1.568	0.027397	0.436795
0.4	2.1	1.853	0.6	1.976	0.041096	0.55042
0.6	2.74	2.116	0.8	2.233	0.054795	0.622133
0.8	3.77	2.483	1	2.591	0.068493	0.721744
1	4.01	2.560	1.2	2.667	0.082192	0.742911
1.2	4.59	2.739	1.4	2.842	0.09589	0.791587
1.4	5.04	2.870	1.6	2.970	0.109589	0.827266
1.6	5.4	2.971	1.8	3.068	0.123288	0.854676
1.8	5.56	3.015	2	3.111	0.136986	0.866564
2	5.62	3.031	2.2	3.127	0.150685	0.870978
2.2	5.76	3.069	2.4	3.163	0.164384	0.881186
2.4	6.06	3.148	2.6	3.241	0.178082	0.902651
2.6	6.15	3.171	2.8	3.263	0.191781	0.908987
2.8	5.98	3.127	3	3.220	0.205479	0.89698
3	6.02	3.137	3.2	3.230	0.219178	0.899821
3.2	6.15	3.171	3.4	3.263	0.232877	0.908987
3.4	6.28	3.204	3.6	3.296	0.246575	0.918057
3.6	6.3	3.209	3.8	3.301	0.260274	0.919444
3.8	6.42	3.240	4	3.331	0.273973	0.92772
4	6.46	3.250	4.2	3.340	0.287671	0.930462
4.2	6.5	3.260	4.4	3.350	0.30137	0.933195
4.4	6.42	3.240	4.6	3.331	0.315068	0.92772
4.8	6.51	3.262	5	3.353	0.342466	0.933877
5.2	6.64	3.295	5.4	3.384	0.369863	0.942695
5.6	6.71	3.312	5.8	3.401	0.39726	0.947407
6.4	6.79	3.332	6.6	3.420	0.452055	0.952763
7.2	6.83	3.342	7.4	3.430	0.506849	0.955429

8	6.9	3.359	8.2	3.447	0.561644	0.960076
8.8	6.92	3.363	9	3.451	0.616438	0.961399
9.6	6.98	3.378	9.8	3.466	0.671233	0.965357
10.4	6.99	3.380	10.6	3.468	0.726027	0.966016
11.2	7.03	3.390	11.4	3.477	0.780822	0.968643
12	7.1	3.407	12.2	3.494	0.835616	0.973224
12.8	7.19	3.428	13	3.515	0.890411	0.97908
13.6	7.29	3.452	13.8	3.538	0.945205	0.985544
14.4	7.36	3.469	14.6	3.554	1	0.990043
15.2	7.35	3.466	15.4	3.552	1.054795	0.989401
16	7.39	3.476	16.2	3.561	1.109589	0.991964
16.8	7.42	3.483	17	3.568	1.164384	0.993881
17.6	7.36	3.469	17.8	3.554	1.219178	0.990043
18.4	7.37	3.471	18.6	3.557	1.273973	0.990684

x(from L.E.)= 490 mm

y (mm)	*Δp*	*v(probe)*	*y(abs)*	*V(correct)*		
0	0	0	0	0	0	0
0	0.39	0.798	0.2	0.946	0.011765	0.263561
0.2	0.91	1.220	0.4	1.358	0.023529	0.37816
0.4	1.37	1.497	0.6	1.628	0.035294	0.453482
0.6	1.86	1.744	0.8	1.869	0.047059	0.52074
0.8	2.42	1.989	1	2.109	0.058824	0.587466
1	2.89	2.174	1.2	2.289	0.070588	0.637684
1.2	3.22	2.294	1.4	2.407	0.082353	0.670535
1.4	3.64	2.439	1.6	2.549	0.094118	0.709997
1.6	4.35	2.667	1.8	2.771	0.105882	0.771842
1.8	4.59	2.739	2	2.842	0.117647	0.791587
2	4.77	2.793	2.2	2.894	0.129412	0.80606
2.2	5.36	2.960	2.4	3.058	0.141176	0.851676
2.4	5.87	3.098	2.6	3.192	0.152941	0.88912
2.6	5.29	2.941	2.8	3.039	0.164706	0.8464
2.8	5.35	2.957	3	3.055	0.176471	0.850925
3	5.6	3.026	3.2	3.122	0.188235	0.869509
3.2	5.76	3.069	3.4	3.163	0.2	0.881186
3.4	5.82	3.085	3.6	3.179	0.211765	0.885523
3.6	6.09	3.155	3.8	3.248	0.223529	0.904768
3.8	6.38	3.230	4	3.321	0.235294	0.92497
4	6.64	3.295	4.2	3.384	0.247059	0.942695
4.8	6.78	3.329	5	3.418	0.294118	0.952095
5.2	6.8	3.334	5.4	3.423	0.317647	0.95343
5.6	6.85	3.346	5.8	3.435	0.341176	0.956759
6.4	6.9	3.359	6.6	3.447	0.388235	0.960076
7.2	7.04	3.393	7.4	3.480	0.435294	0.969299
8	7.12	3.412	8.2	3.499	0.482353	0.974528
8.8	7.13	3.414	9	3.501	0.529412	0.97518
9.6	7.15	3.419	9.8	3.506	0.576471	0.976482

10.4	7.17	3.424	10.6	3.510	0.623529	0.977782
11.2	7.18	3.426	11.4	3.513	0.670588	0.978431
12	7.16	3.421	12.2	3.508	0.717647	0.977132
12.8	7.21	3.433	13	3.520	0.764706	0.980376
13.6	7.25	3.443	13.8	3.529	0.811765	0.982964
14.4	7.23	3.438	14.6	3.524	0.858824	0.981671
15.2	7.29	3.452	15.4	3.538	0.905882	0.985544
16	7.31	3.457	16.2	3.543	0.952941	0.986832
16.8	7.34	3.464	17	3.550	1	0.98876
17.6	7.39	3.476	17.8	3.561	1.047059	0.991964
18.4	7.41	3.481	18.6	3.566	1.094118	0.993243
19.2	7.4	3.478	19.4	3.563	1.141176	0.992604

x(from L.E) = 590 mm

y (mm)	*Δp*	*v(probe)*	*y(abs)*	*V(correct)*		
0	0	0	0	0	0	0
0	0.42	0.829	0.2	0.976	0.01005	0.271762
0.2	0.98	1.266	0.4	1.403	0.020101	0.390687
0.3	1.29	1.452	0.5	1.585	0.025126	0.441416
0.4	1.37	1.497	0.6	1.628	0.030151	0.453482
0.5	1.78	1.706	0.7	1.832	0.035176	0.510426
0.7	2.33	1.952	0.9	2.073	0.045226	0.577308
1.1	3.08	2.244	1.3	2.358	0.065327	0.656814
1.5	3.96	2.544	1.7	2.651	0.085427	0.738555
1.9	4.88	2.825	2.1	2.925	0.105528	0.81477
2.3	5.35	2.957	2.5	3.055	0.125628	0.850925
2.7	5.45	2.985	2.9	3.082	0.145729	0.85841
3.5	5.7	3.053	3.7	3.148	0.18593	0.876827
4.3	6.24	3.194	4.5	3.286	0.226131	0.915276
5.1	6.48	3.255	5.3	3.345	0.266332	0.931829
5.9	6.68	3.305	6.1	3.394	0.306533	0.945391
6.7	6.84	3.344	6.9	3.432	0.346734	0.956094
7.5	6.98	3.378	7.7	3.466	0.386935	0.965357
8.3	6.93	3.366	8.5	3.454	0.427136	0.96206
9.1	6.93	3.366	9.3	3.454	0.467337	0.96206
9.9	7.08	3.402	10.1	3.489	0.507538	0.971917
10.7	7.02	3.388	10.9	3.475	0.547739	0.967987
11.5	7.05	3.395	11.7	3.482	0.58794	0.969954
12.3	6.99	3.380	12.5	3.468	0.628141	0.966016
13.1	7.03	3.390	13.3	3.477	0.668342	0.968643
13.9	7.09	3.405	14.1	3.492	0.708543	0.972571
14.7	7.12	3.412	14.9	3.499	0.748744	0.974528
15.5	7.16	3.421	15.7	3.508	0.788945	0.977132
16.3	7.2	3.431	16.5	3.517	0.829146	0.979728
17.1	7.18	3.426	17.3	3.513	0.869347	0.978431
17.9	7.29	3.452	18.1	3.538	0.909548	0.985544
18.7	7.3	3.455	18.9	3.540	0.949749	0.986188

19.5	7.33	3.462	19.7	3.547	0.98995	0.988117
20	7.36	3.469	20.2	3.554	1.015075	0.990043

Riblet surface #2

y(ref) = 0.15 mm

T =	16 ° C =	289 K
P =	762.3 mm Hg =	101.632 kPa
V =	7.88 Pa =	3.586 m/s
ρ =	1.225 kg/m^3	
ν =	1.47E-05 m^2/s	

x(from L.E) = 110 mm

y (mm)	*Δp*	*v(probe)*	*y(abs)*	*V(correct)*	**Dimensionless forms** *y/ δ*	*v/u*
0	0	0	0	0	0	0
0	0.8	1.143	0.15	1.282	0.029412	0.35721
0.3	2	1.807	0.45	1.931	0.088235	0.537878
0.6	2.88	2.168	0.75	2.284	0.147059	0.636189
0.9	3.8	2.490	1.05	2.599	0.205882	0.723885
1.2	4.31	2.652	1.35	2.757	0.264706	0.767922
1.5	5.07	2.877	1.65	2.976	0.323529	0.828961
1.8	5.41	2.972	1.95	3.069	0.382353	0.854778
2.1	5.89	3.101	2.25	3.195	0.441176	0.889881
2.4	6.05	3.142	2.55	3.236	0.5	0.901262
2.7	6.19	3.179	2.85	3.271	0.558824	0.911097
3	6.34	3.217	3.15	3.308	0.617647	0.921512
3.3	6.58	3.277	3.45	3.367	0.676471	0.937923
3.6	6.88	3.351	3.75	3.439	0.735294	0.958022
3.9	6.96	3.371	4.05	3.458	0.794118	0.963307
4.2	7.06	3.395	4.35	3.482	0.852941	0.969871
4.5	7.12	3.409	4.65	3.496	0.911765	0.973787
4.8	7.22	3.433	4.95	3.519	0.970588	0.980278
5.1	7.32	3.457	5.25	3.542	1.029412	0.986723
5.4	7.38	3.471	5.55	3.556	1.088235	0.990569
5.7	7.35	3.464	5.85	3.549	1.147059	0.988648
6	7.36	3.466	6.15	3.552	1.205882	0.989289
6.3	7.37	3.468	6.45	3.554	1.264706	0.98993
6.6	7.35	3.464	6.75	3.549	1.323529	0.988648
6.9	7.37	3.468	7.05	3.554	1.382353	0.98993
7.2	7.28	3.447	7.35	3.533	1.441176	0.98415
7.5	7.32	3.457	7.65	3.542	1.5	0.986723
7.8	7.37	3.468	7.95	3.554	1.558824	0.98993
8.1	7.31	3.454	8.25	3.540	1.617647	0.986081
8.4	7.29	3.449	8.55	3.535	1.676471	0.984794
8.8	7.28	3.447	8.95	3.533	1.754902	0.98415
9.6	7.28	3.447	9.75	3.533	1.911765	0.98415
10.4	7.31	3.454	10.55	3.540	2.068627	0.986081
11.2	7.3	3.452	11.35	3.538	2.22549	0.985438
12	7.29	3.449	12.15	3.535	2.382353	0.984794
12.8	7.27	3.445	12.95	3.531	2.539216	0.983506
13.6	7.32	3.457	13.75	3.542	2.696078	0.986723
14.4	7.27	3.445	14.55	3.531	2.852941	0.983506
15.2	7.24	3.438	15.35	3.524	3.009804	0.98157

16	7.27	3.445	16.15	3.531	3.166667	0.983506
16.8	7.22	3.433	16.95	3.519	3.323529	0.980278
17.8	7.26	3.442	17.95	3.528	3.519608	0.982861
18.8	7.32	3.457	18.95	3.542	3.715686	0.986723

x (from L.E.) = 200 mm

y (mm)	*Δp*	*v(probe)*	*y(abs)*	*V(correct)*		
0	0	0	0	0	0	0
0	0.68	1.054	0.15	1.195	0.02027	0.332946
0.3	1.41	1.517	0.45	1.648	0.060811	0.459054
0.6	2.61	2.064	0.75	2.182	0.101351	0.607859
0.9	3.9	2.523	1.05	2.631	0.141892	0.732742
1.2	4.19	2.615	1.35	2.721	0.182432	0.757805
1.5	5.01	2.860	1.65	2.959	0.222973	0.824317
1.8	5.24	2.925	1.95	3.023	0.263514	0.841974
2.1	5.68	3.045	2.25	3.140	0.304054	0.874706
2.4	5.85	3.090	2.55	3.184	0.344595	0.887012
2.7	6.01	3.132	2.85	3.225	0.385135	0.898431
3	6.14	3.166	3.15	3.258	0.425676	0.907597
3.3	6.26	3.197	3.45	3.288	0.466216	0.915973
3.6	6.37	3.224	3.75	3.316	0.506757	0.92358
3.9	6.48	3.252	4.05	3.343	0.547297	0.931122
4.2	6.52	3.262	4.35	3.353	0.587838	0.933849
4.5	6.63	3.290	4.65	3.379	0.628378	0.941304
4.8	6.71	3.309	4.95	3.399	0.668919	0.946688
5.1	6.79	3.329	5.25	3.418	0.709459	0.952039
5.4	6.84	3.341	5.55	3.430	0.75	0.955368
5.7	6.98	3.375	5.85	3.463	0.790541	0.964624
6	7.08	3.399	6.15	3.487	0.831081	0.971178
6.3	7.14	3.414	6.45	3.501	0.871622	0.975089
6.6	7.2	3.428	6.75	3.515	0.912162	0.978983
6.9	7.28	3.447	7.05	3.533	0.952703	0.98415
7.2	7.34	3.461	7.35	3.547	0.993243	0.988007
7.5	7.37	3.468	7.65	3.554	1.033784	0.98993
7.8	7.39	3.473	7.95	3.558	1.074324	0.991209
8.1	7.42	3.480	8.25	3.565	1.114865	0.993125
8.4	7.43	3.482	8.55	3.568	1.155405	0.993763
8.8	7.35	3.464	8.95	3.549	1.209459	0.988648
9.6	7.34	3.461	9.75	3.547	1.317568	0.988007
10.4	7.36	3.466	10.55	3.552	1.425676	0.989289
11.2	7.32	3.457	11.35	3.542	1.533784	0.986723
12	7.34	3.461	12.15	3.547	1.641892	0.988007
12.8	7.35	3.464	12.95	3.549	1.75	0.988648
13.6	7.42	3.480	13.75	3.565	1.858108	0.993125
14.4	7.38	3.471	14.55	3.556	1.966216	0.990569
15.2	7.42	3.480	15.35	3.565	2.074324	0.993125

16	7.44	3.485	16.15	3.570	2.182432	0.9944
16.8	7.38	3.471	16.95	3.556	2.290541	0.990569
17.8	7.41	3.478	17.95	3.563	2.425676	0.992487
18.8	7.42	3.480	18.95	3.565	2.560811	0.993125

x(from L.E) = 300 mm

y (mm)	*Δp*	*v(probe)*	*y(abs)*	*V(correct)*		
0	0	0	0	0	0	0
0	0.42	0.828	0.15	0.975	0.013333	0.271582
0.3	1.26	1.434	0.45	1.567	0.04	0.436483
0.6	1.96	1.789	0.75	1.913	0.066667	0.532938
0.9	3.2	2.285	1.05	2.398	0.093333	0.668097
1.2	3.74	2.471	1.35	2.579	0.12	0.718514
1.5	4.61	2.743	1.65	2.845	0.146667	0.792613
1.8	5.04	2.868	1.95	2.968	0.173333	0.826643
2.1	5.32	2.947	2.25	3.044	0.2	0.848025
2.4	5.74	3.061	2.55	3.156	0.226667	0.87907
2.7	5.99	3.127	2.85	3.220	0.253333	0.897012
3	6.24	3.191	3.15	3.283	0.28	0.914582
3.3	6.49	3.255	3.45	3.345	0.306667	0.931805
3.6	6.74	3.317	3.75	3.406	0.333333	0.948698
3.9	6.87	3.349	4.05	3.437	0.36	0.957359
4.2	6.8	3.332	4.35	3.420	0.386667	0.952706
4.5	6.74	3.317	4.65	3.406	0.413333	0.948698
4.8	6.7	3.307	4.95	3.396	0.44	0.946017
5.1	6.86	3.346	5.25	3.435	0.466667	0.956696
5.4	7	3.380	5.55	3.468	0.493333	0.965938
5.7	7.07	3.397	5.85	3.484	0.52	0.970525
6	6.98	3.375	6.15	3.463	0.546667	0.964624
6.3	7.06	3.395	6.45	3.482	0.573333	0.969871
6.6	7.12	3.409	6.75	3.496	0.6	0.973787
6.9	7.18	3.423	7.05	3.510	0.626667	0.977687
7.2	7.21	3.431	7.35	3.517	0.653333	0.979631
7.5	7.26	3.442	7.65	3.528	0.68	0.982861
7.8	7.29	3.449	7.95	3.535	0.706667	0.984794
8.1	7.25	3.440	8.25	3.526	0.733333	0.982216
8.4	7.23	3.435	8.55	3.522	0.76	0.980924
8.8	7.27	3.445	8.95	3.531	0.795556	0.983506
9.6	7.19	3.426	9.75	3.512	0.866667	0.978335
10.4	7.29	3.449	10.55	3.535	0.937778	0.984794
11.2	7.38	3.471	11.35	3.556	1.008889	0.990569
12	7.34	3.461	12.15	3.547	1.08	0.988007
12.8	7.41	3.478	12.95	3.563	1.151111	0.992487
13.6	7.37	3.468	13.75	3.554	1.222222	0.98993
14.4	7.39	3.473	14.55	3.558	1.293333	0.991209
15.2	7.46	3.489	15.35	3.574	1.364444	0.995674

16	7.39	3.473	16.15	3.558	1.435556	0.991209
16.8	7.34	3.461	16.95	3.547	1.506667	0.988007
17.8	7.44	3.485	17.95	3.570	1.595556	0.9944
18.8	7.45	3.487	18.95	3.572	1.684444	0.995037

x(from L.E) = 380 mm

y (mm)	*Δp*	*v(probe)*	*y(abs)*	*V(correct)*		
0	0	0	0	0	0	0
0	0.1	0.404	0.15	0.561	0.010381	0.156238
0.3	0.93	1.232	0.45	1.370	0.031142	0.381519
0.6	1.68	1.656	0.75	1.784	0.051903	0.496841
0.9	2.29	1.933	1.05	2.055	0.072664	0.57231
1.2	3.1	2.249	1.35	2.363	0.093426	0.658304
1.5	3.88	2.517	1.65	2.624	0.114187	0.73098
1.8	4.79	2.796	1.95	2.897	0.134948	0.807043
2.1	5.18	2.908	2.25	3.006	0.155709	0.837406
2.4	5.31	2.944	2.55	3.042	0.176471	0.847271
2.7	5.48	2.991	2.85	3.087	0.197232	0.859991
3	5.88	3.098	3.15	3.192	0.217993	0.889164
3.3	6.02	3.135	3.45	3.228	0.238754	0.899139
3.6	6.25	3.194	3.75	3.286	0.259516	0.915278
3.9	6.34	3.217	4.05	3.308	0.280277	0.921512
4.2	6.57	3.275	4.35	3.365	0.301038	0.937245
4.5	6.71	3.309	4.65	3.399	0.321799	0.946688
4.8	6.8	3.332	4.95	3.420	0.342561	0.952706
5.1	6.68	3.302	5.25	3.391	0.363322	0.944673
5.4	6.65	3.295	5.55	3.384	0.384083	0.942653
5.7	6.78	3.327	5.85	3.415	0.404844	0.951372
6	6.86	3.346	6.15	3.435	0.425606	0.956696
6.3	6.99	3.378	6.45	3.465	0.446367	0.965281
6.6	6.87	3.349	6.75	3.437	0.467128	0.957359
6.9	6.85	3.344	7.05	3.432	0.487889	0.956032
7.2	6.94	3.366	7.35	3.454	0.508651	0.961989
7.5	6.95	3.368	7.65	3.456	0.529412	0.962648
7.8	6.98	3.375	7.95	3.463	0.550173	0.964624
8.1	7.04	3.390	8.25	3.477	0.570934	0.968562
8.4	7.01	3.383	8.55	3.470	0.591696	0.966595
8.8	7.1	3.404	8.95	3.491	0.619377	0.972484
9.6	7.07	3.397	9.75	3.484	0.67474	0.970525
10.4	7.09	3.402	10.55	3.489	0.730104	0.971831
11.2	7.18	3.423	11.35	3.510	0.785467	0.977687
12	7.08	3.399	12.15	3.487	0.84083	0.971178
12.8	7.19	3.426	12.95	3.512	0.896194	0.978335
13.6	7.28	3.447	13.75	3.533	0.951557	0.98415
14.4	7.35	3.464	14.55	3.549	1.00692	0.988648
15.2	7.38	3.471	15.35	3.556	1.062284	0.990569

16	7.41	3.478	16.15	3.563	1.117647	0.992487
16.8	7.42	3.480	16.95	3.565	1.17301	0.993125
17.8	7.39	3.473	17.95	3.558	1.242215	0.991209
18.8	7.43	3.482	18.95	3.568	1.311419	0.993763

x(from L.E) = 490 mm

y (mm)	*Δp*	*v(probe)*	*y(abs)*	*V(correct)*		
0	0	0	0	0	0	0
0	0.26	0.651	0.15	0.803	0.008982	0.223556
0.3	0.89	1.205	0.45	1.343	0.026946	0.374231
0.6	1.69	1.661	0.75	1.788	0.04491	0.49818
0.9	2.89	2.172	1.05	2.288	0.062874	0.637212
1.2	3.76	2.477	1.35	2.586	0.080838	0.720309
1.5	4.25	2.634	1.65	2.739	0.098802	0.762882
1.8	4.84	2.811	1.95	2.912	0.116766	0.811003
2.1	5.31	2.944	2.25	3.042	0.134731	0.847271
2.4	5.46	2.985	2.55	3.082	0.152695	0.858505
2.7	5.89	3.101	2.85	3.195	0.170659	0.889881
3	5.99	3.127	3.15	3.220	0.188623	0.897012
3.3	6.16	3.171	3.45	3.263	0.206587	0.908999
3.6	6.31	3.209	3.75	3.301	0.224551	0.919439
3.9	6.45	3.245	4.05	3.335	0.242515	0.929072
4.2	6.29	3.204	4.35	3.296	0.260479	0.918054
4.5	6.48	3.252	4.65	3.343	0.278443	0.931122
4.8	6.44	3.242	4.95	3.333	0.296407	0.928387
5.1	6.42	3.237	5.25	3.328	0.314371	0.927016
5.4	6.51	3.260	5.55	3.350	0.332335	0.933168
5.7	6.59	3.280	5.85	3.370	0.350299	0.9386
6	6.48	3.252	6.15	3.343	0.368263	0.931122
6.3	6.39	3.230	6.45	3.321	0.386228	0.924956
6.6	6.49	3.255	6.75	3.345	0.404192	0.931805
6.9	6.59	3.280	7.05	3.370	0.422156	0.9386
7.2	6.76	3.322	7.35	3.411	0.44012	0.950036
7.5	6.96	3.371	7.65	3.458	0.458084	0.963307
7.8	6.88	3.351	7.95	3.439	0.476048	0.958022
8.1	7.01	3.383	8.25	3.470	0.494012	0.966595
8.4	7.06	3.395	8.55	3.482	0.511976	0.969871
8.8	7.12	3.409	8.95	3.496	0.535928	0.973787
9.6	7.16	3.419	9.75	3.505	0.583832	0.976389
10.4	7.09	3.402	10.55	3.489	0.631737	0.971831
11.2	7.12	3.409	11.35	3.496	0.679641	0.973787
12	7.2	3.428	12.15	3.515	0.727545	0.978983
12.8	7.17	3.421	12.95	3.508	0.775449	0.977038
13.6	7.19	3.426	13.75	3.512	0.823353	0.978335
14.4	7.27	3.445	14.55	3.531	0.871257	0.983506
15.2	7.22	3.433	15.35	3.519	0.919162	0.980278

16	7.37	3.468	16.15	3.554	0.967066	0.98993
16.8	7.33	3.459	16.95	3.545	1.01497	0.987365
17.8	7.39	3.473	17.95	3.558	1.07485	0.991209
18.8	7.41	3.478	18.95	3.563	1.134731	0.992487

x (from LE) = 590 mm

y (mm)	*Δp*	*v(probe)*	*y(abs)*	*V(correct)*		
0	0	0	0	0	0	0
0	0.36	0.767	0.15	0.915	0.007595	0.254872
0.3	1.14	1.364	0.45	1.499	0.022785	0.417439
0.6	2.08	1.843	0.75	1.966	0.037975	0.547613
0.9	2.87	2.164	1.05	2.280	0.053165	0.635164
1.2	3.73	2.467	1.35	2.576	0.068354	0.717615
1.5	4.03	2.565	1.65	2.671	0.083544	0.744089
1.8	4.48	2.704	1.95	2.807	0.098734	0.782015
2.1	4.92	2.834	2.25	2.934	0.113924	0.817297
2.4	5.14	2.896	2.55	2.995	0.129114	0.834346
2.7	5.28	2.936	2.85	3.034	0.144304	0.845005
3	5.6	3.023	3.15	3.119	0.159494	0.868852
3.3	6.01	3.132	3.45	3.225	0.174684	0.898431
3.6	6.36	3.222	3.75	3.313	0.189873	0.922891
3.9	6.42	3.237	4.05	3.328	0.205063	0.927016
4.2	6.46	3.247	4.35	3.338	0.220253	0.929756
4.5	6.48	3.252	4.65	3.343	0.235443	0.931122
4.8	6.49	3.255	4.95	3.345	0.250633	0.931805
5.1	6.45	3.245	5.25	3.335	0.265823	0.929072
5.4	6.48	3.252	5.55	3.343	0.281013	0.931122
5.7	6.5	3.257	5.85	3.348	0.296203	0.932487
6	6.54	3.267	6.15	3.357	0.311392	0.935209
6.3	6.6	3.282	6.45	3.372	0.326582	0.939277
6.6	6.73	3.314	6.75	3.403	0.341772	0.948029
6.9	6.79	3.329	7.05	3.418	0.356962	0.952039
7.2	6.74	3.317	7.35	3.406	0.372152	0.948698
7.5	6.84	3.341	7.65	3.430	0.387342	0.955368
7.8	6.78	3.327	7.95	3.415	0.402532	0.951372
8.1	6.91	3.358	8.25	3.446	0.417722	0.960007
9	7.08	3.399	9.15	3.487	0.463291	0.971178
9.8	7.1	3.404	9.95	3.491	0.503797	0.972484
10.6	7.06	3.395	10.75	3.482	0.544304	0.969871
11.4	7.1	3.404	11.55	3.491	0.58481	0.972484
12	7.12	3.409	12.15	3.496	0.61519	0.973787
12.8	7.15	3.416	12.95	3.503	0.655696	0.975739
13.6	7.17	3.421	13.75	3.508	0.696203	0.977038
14.4	7.21	3.431	14.55	3.517	0.736709	0.979631
15.6	7.28	3.447	15.75	3.533	0.797468	0.98415
16.6	7.27	3.445	16.75	3.531	0.848101	0.983506
17.6	7.31	3.454	17.75	3.540	0.898734	0.986081

18.6	7.29	3.449	18.75	3.535	0.949367	0.984794
19	7.33	3.459	19.15	3.545	0.96962	0.987365
19.5	7.37	3.468	19.65	3.554	0.994937	0.98993
20	7.35	3.464	20.15	3.549	1.020253	0.988648
20.5	7.37	3.468	20.65	3.554	1.04557	0.98993
21	7.38	3.471	21.15	3.556	1.070886	0.990569

Plots for the 1/7th power rule

v	y/δ @590 mm	y/δ @490 mm	y/δ @380 mm	y/δ @300 mm	y/δ @200 mm	y/δ @110 mm	v/u
0	0	0	0	0	0	0	0
0.1	1.30194E-11	1.30977E-11	1.24865E-11	1.31738E-11	1.46966E-11	1.29771E-11	0.027855
0.2	1.66648E-09	1.6765E-09	1.59827E-09	1.68624E-09	1.88116E-09	1.66107E-09	0.05571
0.3	2.84733E-08	2.86446E-08	2.73079E-08	2.88111E-08	3.21414E-08	2.83809E-08	0.083565
0.4	2.13309E-07	2.14592E-07	2.04578E-07	2.15839E-07	2.40789E-07	2.12617E-07	0.111421
0.5	1.01714E-06	1.02326E-06	9.75506E-07	1.0292E-06	1.14817E-06	1.01384E-06	0.139276
0.6	3.64459E-06	3.66651E-06	3.49541E-06	3.68782E-06	4.1141E-06	3.63276E-06	0.167131
0.7	1.0722E-05	1.07865E-05	1.02831E-05	1.08492E-05	1.21033E-05	1.06872E-05	0.194986
0.8	2.73036E-05	2.74678E-05	2.6186E-05	2.76274E-05	3.0821E-05	2.7215E-05	0.222841
0.9	6.22712E-05	6.26458E-05	5.97224E-05	6.30098E-05	7.02933E-05	6.20691E-05	0.250696
1	0.000130194	0.000130977	0.000124865	0.000131738	0.000146966	0.000129771	0.278552
1.1	0.00025371	0.000255237	0.000243326	0.00025672	0.000286395	0.000252887	0.306407
1.2	0.000466507	0.000469314	0.000447413	0.00047204	0.000526605	0.000464993	0.334262
1.3	0.000816946	0.00082186	0.000783508	0.000826635	0.000922189	0.000814294	0.362117
1.4	0.001372416	0.001380673	0.001316243	0.001388695	0.001549219	0.001367962	0.389972
1.5	0.00222448	0.002237862	0.002133431	0.002250864	0.00251105	0.00221726	0.417827
1.6	0.003494858	0.003515883	0.003351813	0.003536311	0.003945085	0.003483514	0.445682
1.7	0.005342347	0.005374486	0.005123684	0.005405713	0.006030578	0.005325007	0.473538
1.8	0.007970713	0.008018664	0.00764447	0.008065254	0.008997545	0.007944842	0.501393
1.9	0.011637638	0.011707649	0.011161307	0.011775673	0.013136864	0.011599865	0.529248
2	0.01666478	0.016765035	0.015982688	0.016862443	0.018811631	0.016610691	0.557103
2.1	0.02344902	0.023590088	0.022489248	0.02372715	0.026469854	0.02337291	0.584958
2.2	0.032474943	0.032670311	0.031145738	0.03286013	0.036658547	0.032369537	0.612813
2.3	0.044328647	0.044595327	0.042514269	0.044854433	0.050039313	0.044184767	0.640669
2.4	0.059712921	0.060072152	0.057268862	0.060421181	0.067405475	0.059519107	0.668524
2.5	0.079463866	0.079941917	0.076211397	0.080406393	0.089700847	0.079205945	0.696379
2.6	0.104569026	0.105198109	0.100289	0.105809327	0.118040196	0.10422962	0.724234
2.7	0.136187101	0.137006398	0.130612942	0.137802427	0.153731489	0.13574507	0.752089

2.8	0.17566929	0.17672611	0.168479119	0.177752917	0.198299995	0.175099109	0.779944
2.9	0.224582345	0.225933424	0.215390155	0.227246134	0.253514305	0.223853404	0.807799
3	0.284733397	0.286446343	0.273079215	0.288110642	0.321414354	0.283809221	0.835655
3.1	0.35819662	0.360351518	0.343535577	0.362445218	0.404341522	0.357033999	0.86351
3.2	0.447341794	0.450032985	0.429032025	0.45264775	0.504970878	0.445889829	0.891365
3.3	0.55486484	0.558202886	0.532154136	0.561446136	0.626345647	0.553063881	0.91922
3.4	0.68382039	0.687934227	0.655831515	0.691931237	0.771913975	0.681600872	0.947075
3.5	0.837656451	0.84269576	0.803371043	0.84759196	0.945568062	0.834937618	0.97493
3.51	0.854553864	0.859694828	0.819576842	0.864689794	0.964642295	0.851780186	0.977716
3.52	0.871742604	0.876986974	0.836062044	0.882082411	0.984045385	0.868913135	0.980501
3.53	0.889226844	0.894576399	0.852830651	0.899774033	1.003782043	0.886340626	0.983287
3.54	0.907010806	0.912467348	0.869886713	0.917768932	1.023857035	0.904066865	0.986072
3.55	0.925098759	0.930664118	0.887234323	0.936071428	1.04427518	0.922096109	0.988858
3.56	0.943495021	0.949171052	0.904877624	0.95468589	1.065041352	0.940432661	0.991643
3.564	0.950940829	0.956661653	0.912018674	0.962220013	1.073446371	0.947854302	0.992758
3.568	0.958436946	0.964202867	0.919207974	0.969805042	1.08190818	0.955326089	0.993872
3.572	0.965983656	0.971794977	0.926445795	0.977441264	1.090427099	0.962848303	0.994986
3.576	0.973581242	0.97943827	0.933732411	0.985128966	1.099003449	0.97042123	0.9961
3.58	0.98122999	0.987133033	0.941068095	0.992868436	1.107637551	0.978045152	0.997214
3.584	0.988930187	0.994879554	0.948453121	1.000659965	1.116329731	0.985720355	0.998329
3.588	0.99668212	1.002678122	0.955887767	1.008503845	1.125080312	0.993447128	0.999443
3.589	0.998628222	1.004635931	0.957754214	1.010473029	1.127277121	0.995386913	0.999721
3.58989	1.00036299	1.006381136	0.959417978	1.012228374	1.129235372	0.99711605	0.999969

APPENDIX C:

Experimental Velocity Profiles at various x-stations

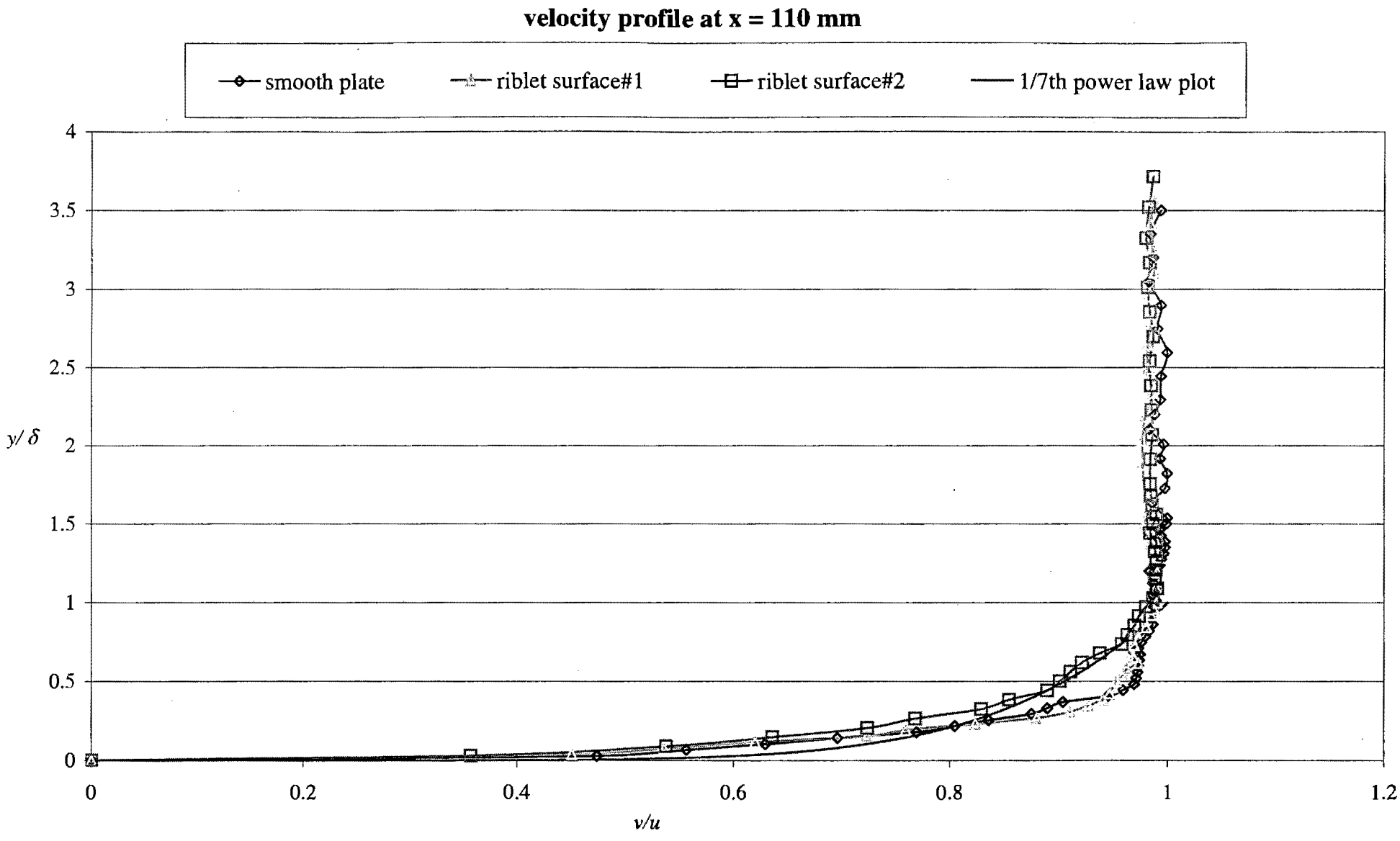
velocity profile at x = 110 mm
smooth plate
riblet surface#1
riblet surface#2
1/7th power law plot
y/δ
v/u
0
0.5
1
1.5
2
2.5
3
3.5
4
0
0.2
0.4
0.6
0.8
1
1.2

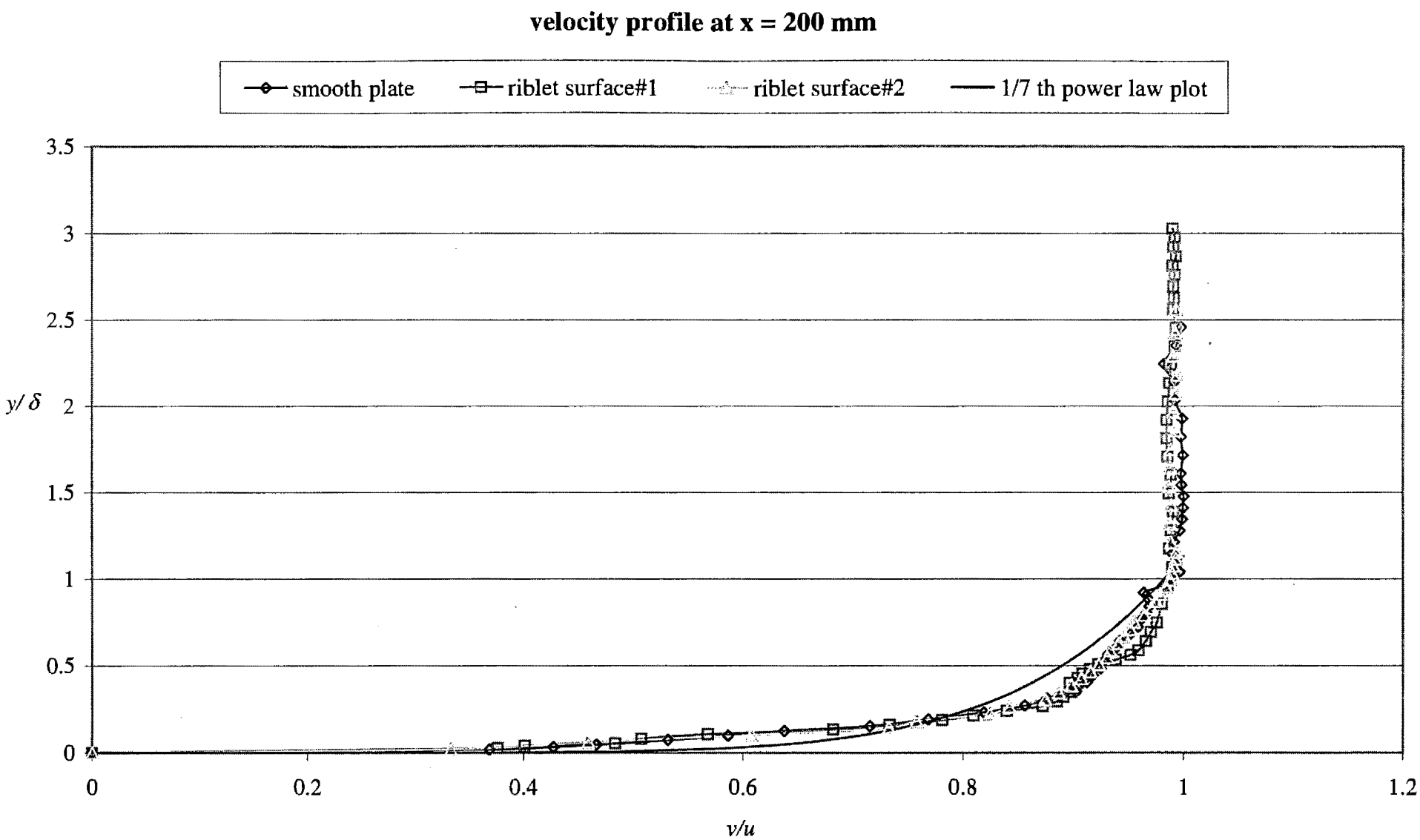
velocity profile at x = 200 mm
smooth plate
riblet surface#1
riblet surface#2
1/7 th power law plot
3.5
3
2.5
2
1.5
1
0.5
0
y/δ
0
0.2
0.4
0.6
0.8
1
1.2
v/u

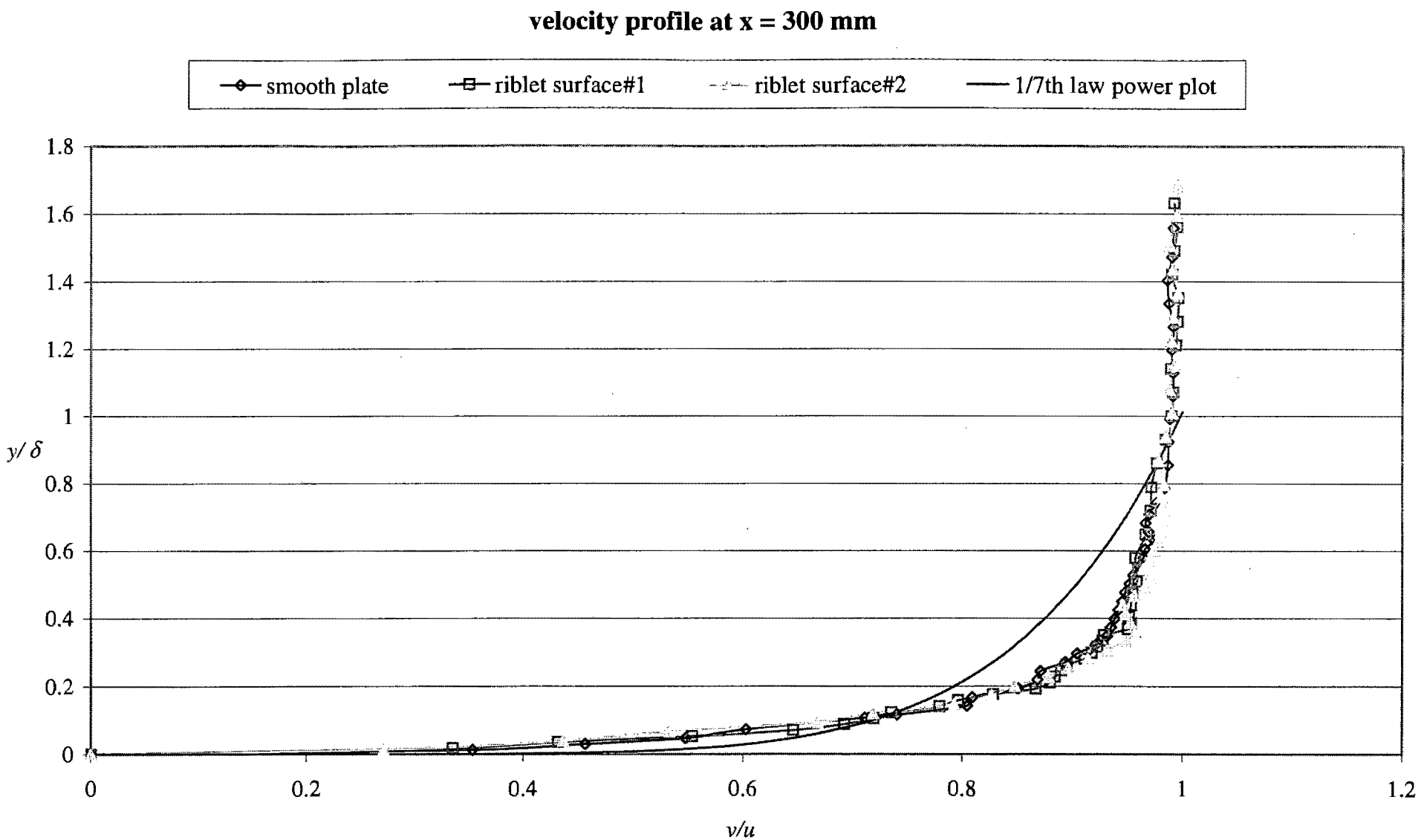
velocity profile at x = 300 mm
smooth plate
riblet surface#1
riblet surface#2
1/7th law power plot
1.8
1.6
1.4
1.2
1
0.8
0.6
0.4
0.2
0
y/ δ
0
0.2
0.4
0.6
0.8
1
1.2
v/u

velocity profile at x = 380 mm

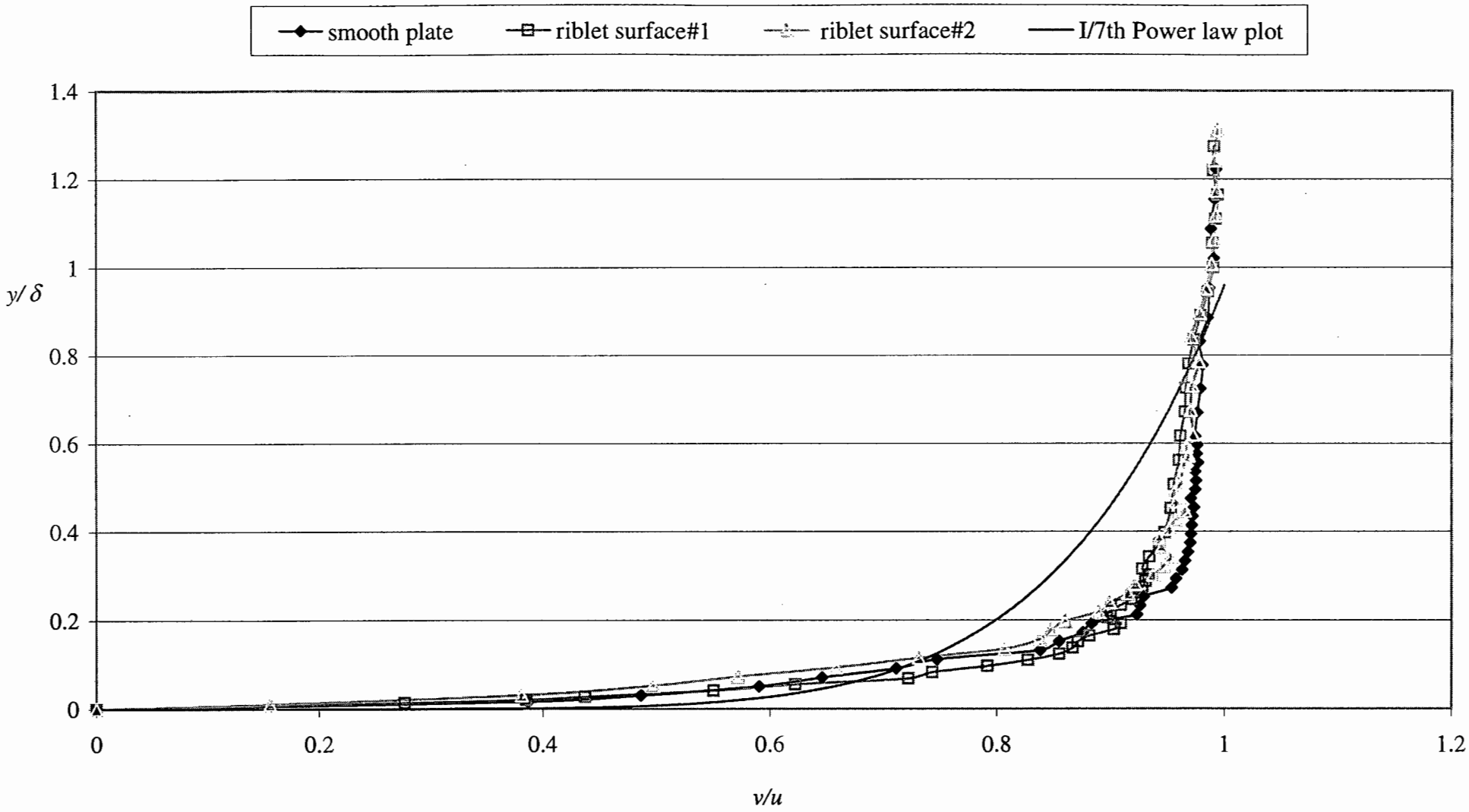

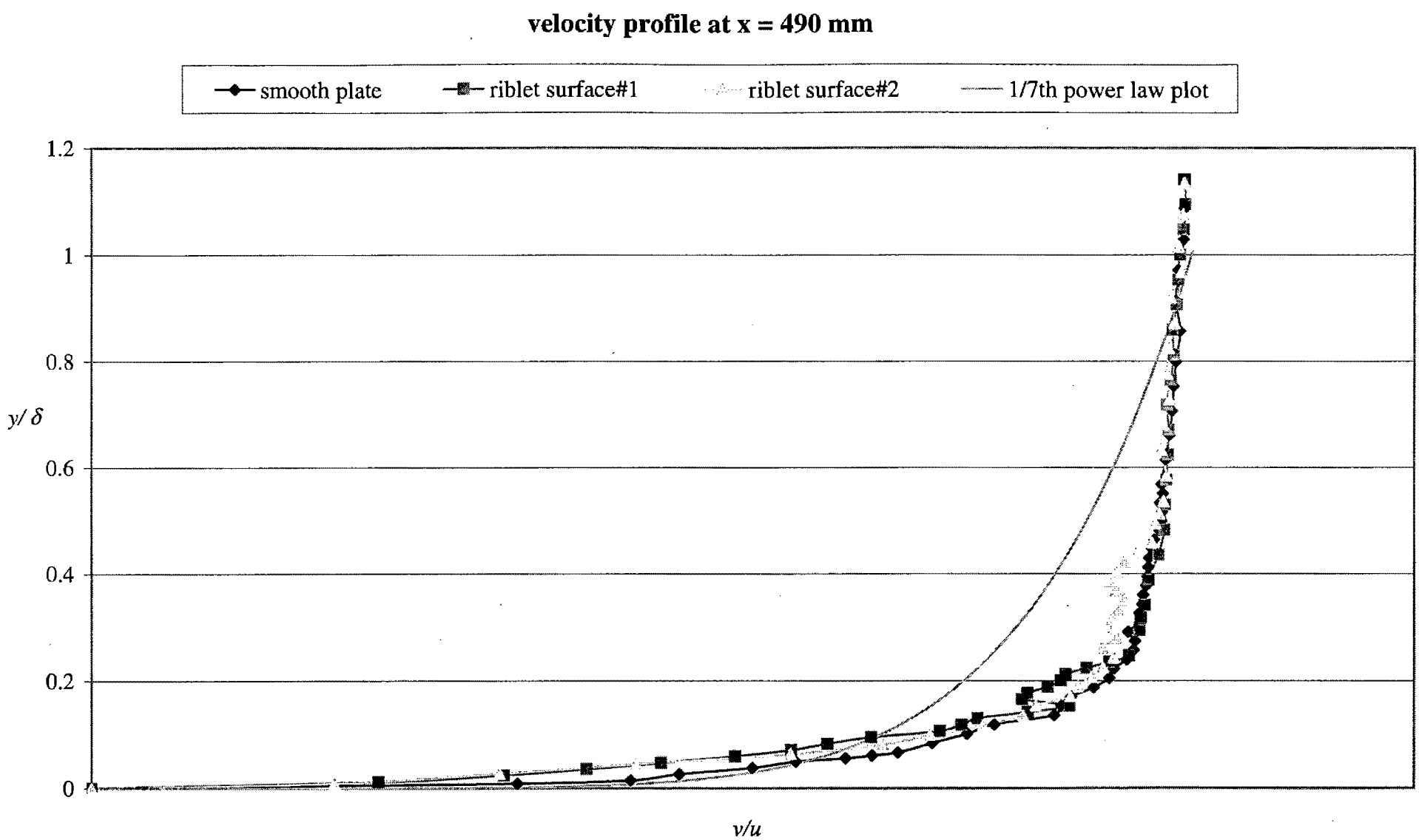
velocity profile at x = 490 mm
smooth plate
riblet surface#1
riblet surface#2
1/7th power law plot
1.2
1
0.8
0.6
0.4
0.2
0
y/ δ
v/u

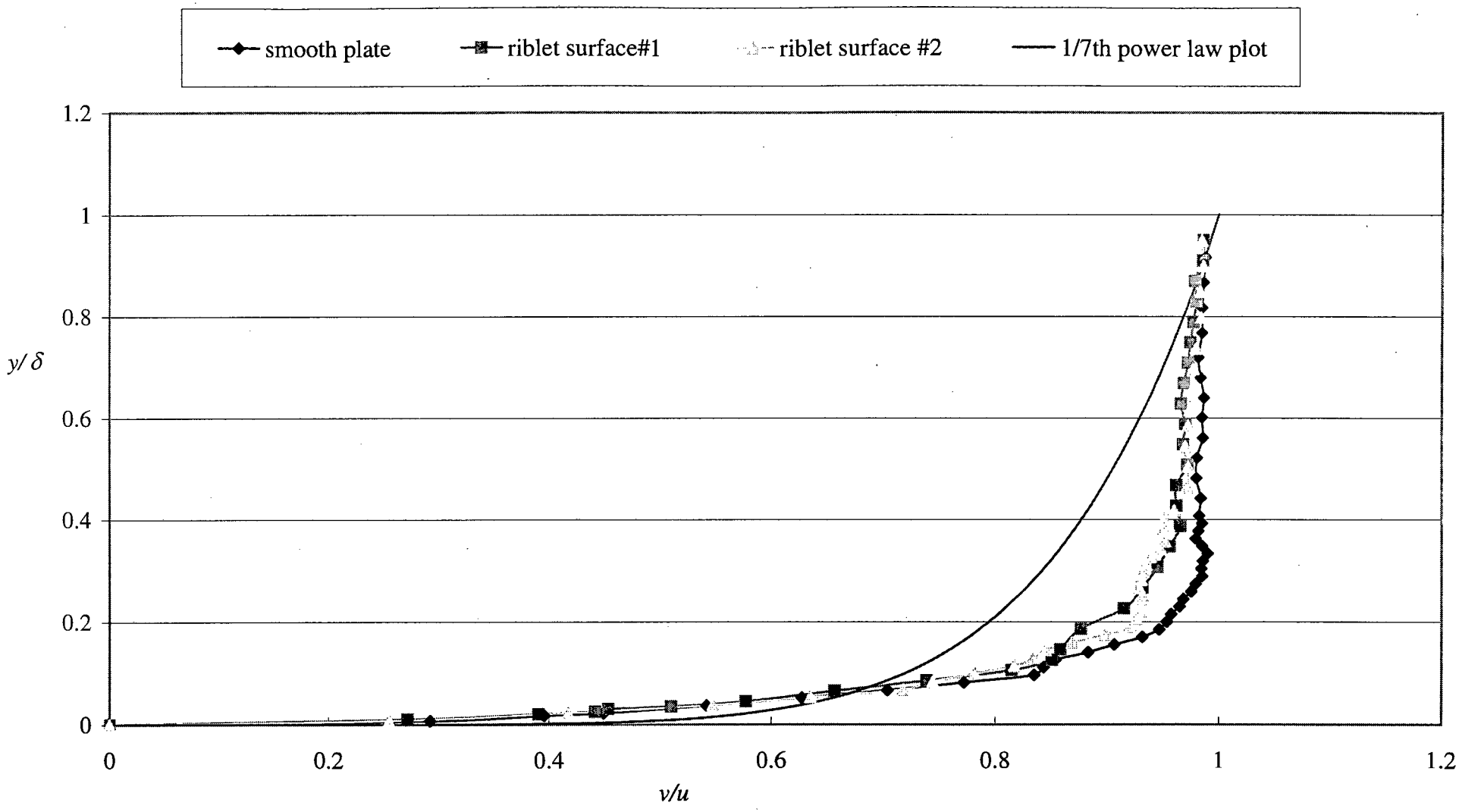
velocity profile at x = 590 mm
smooth plate
riblet surface#1
riblet surface #2
1/7th power law plot
1.2
1
0.8
0.6
0.4
0.2
0
y/ δ
0
0.2
0.4
0.6
0.8
1
1.2
v/u

APPENDIX D:

Shear stress/Laminar sublayer Profiles

velocity in the laminar sublayer region, at x = 110 mm

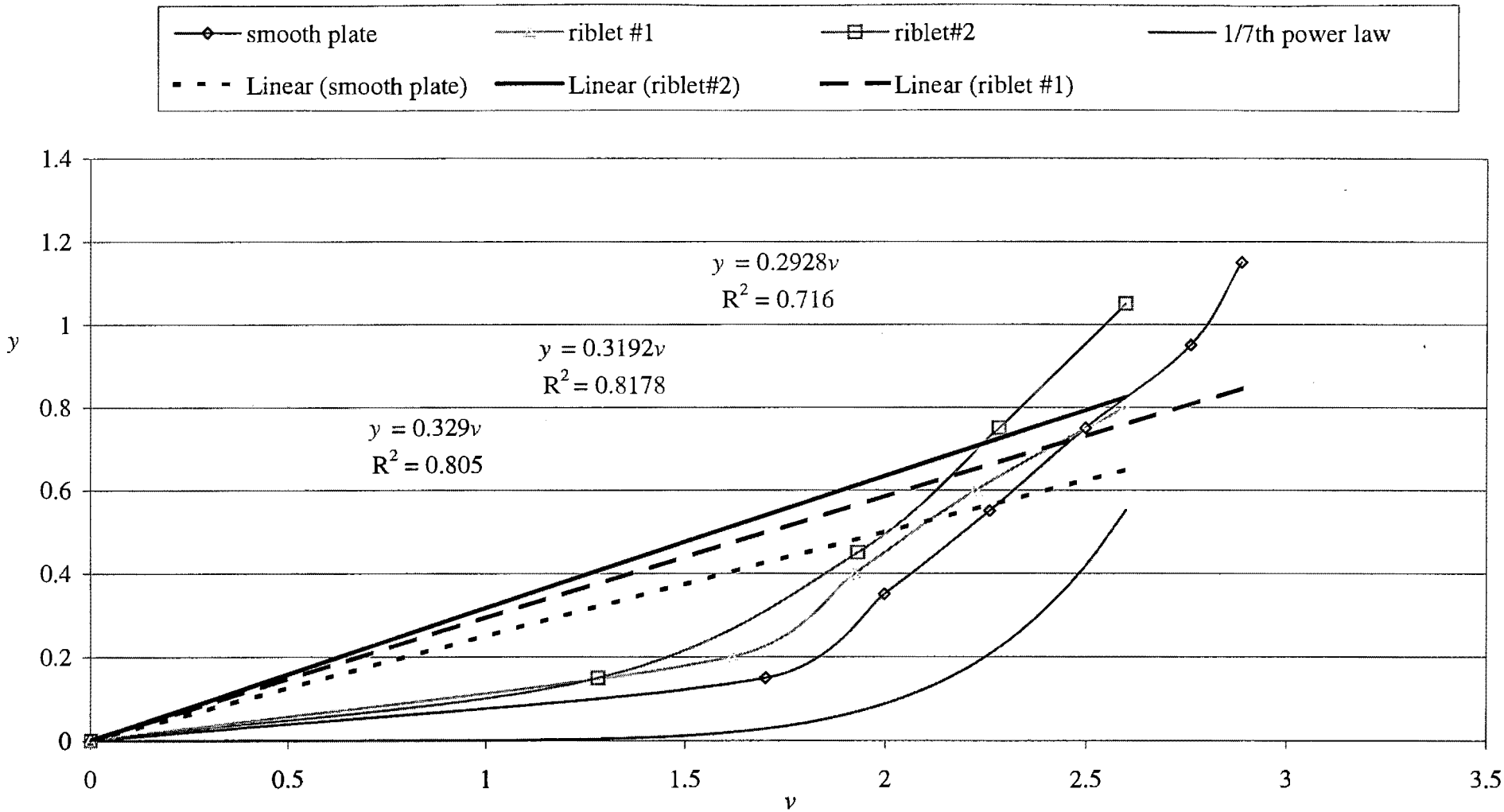

velocity profile in the laminar sublayer, at x = 200 mm

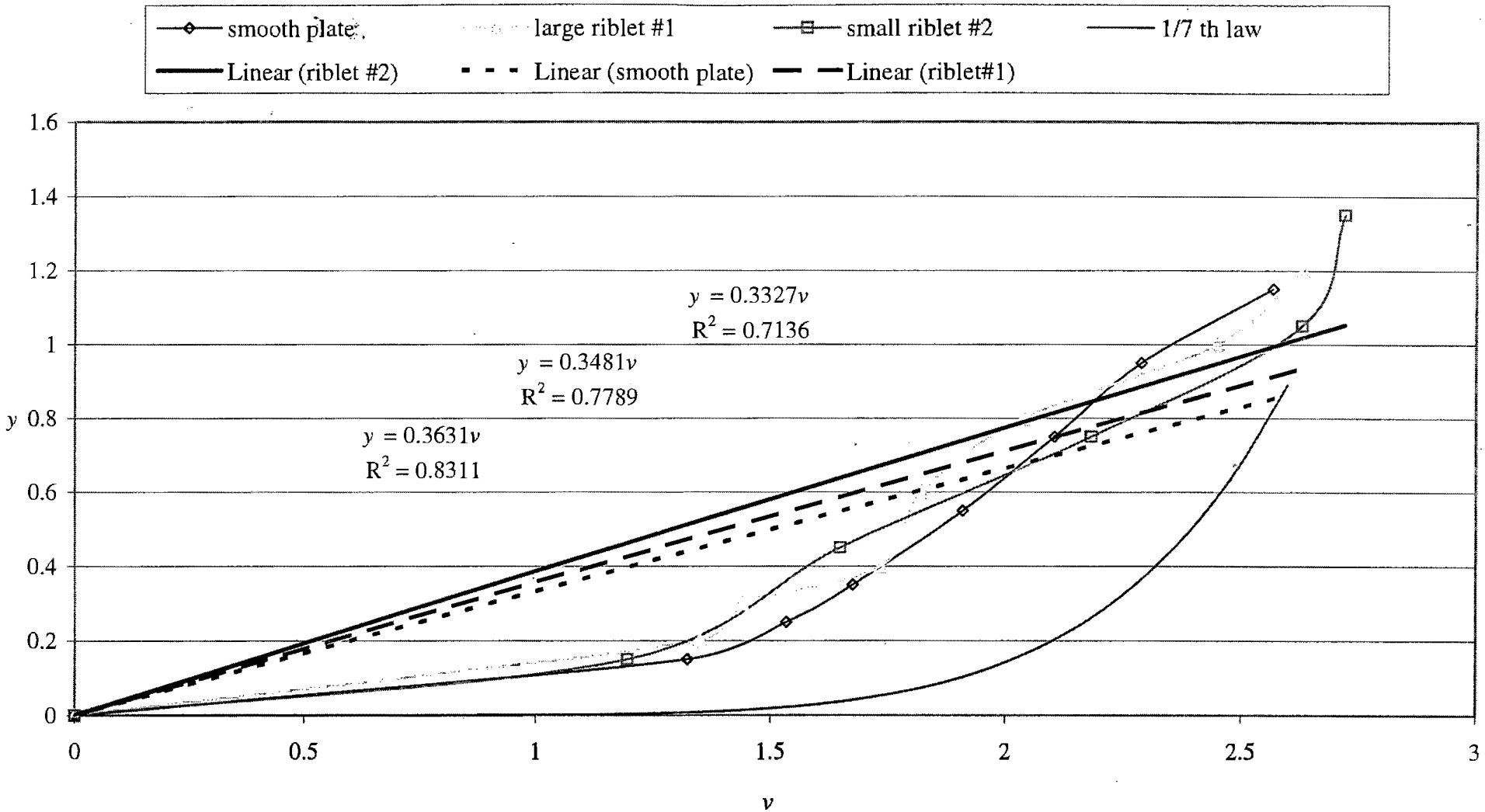

velocity profile in the laminar sublayer region, at x = 300 mm

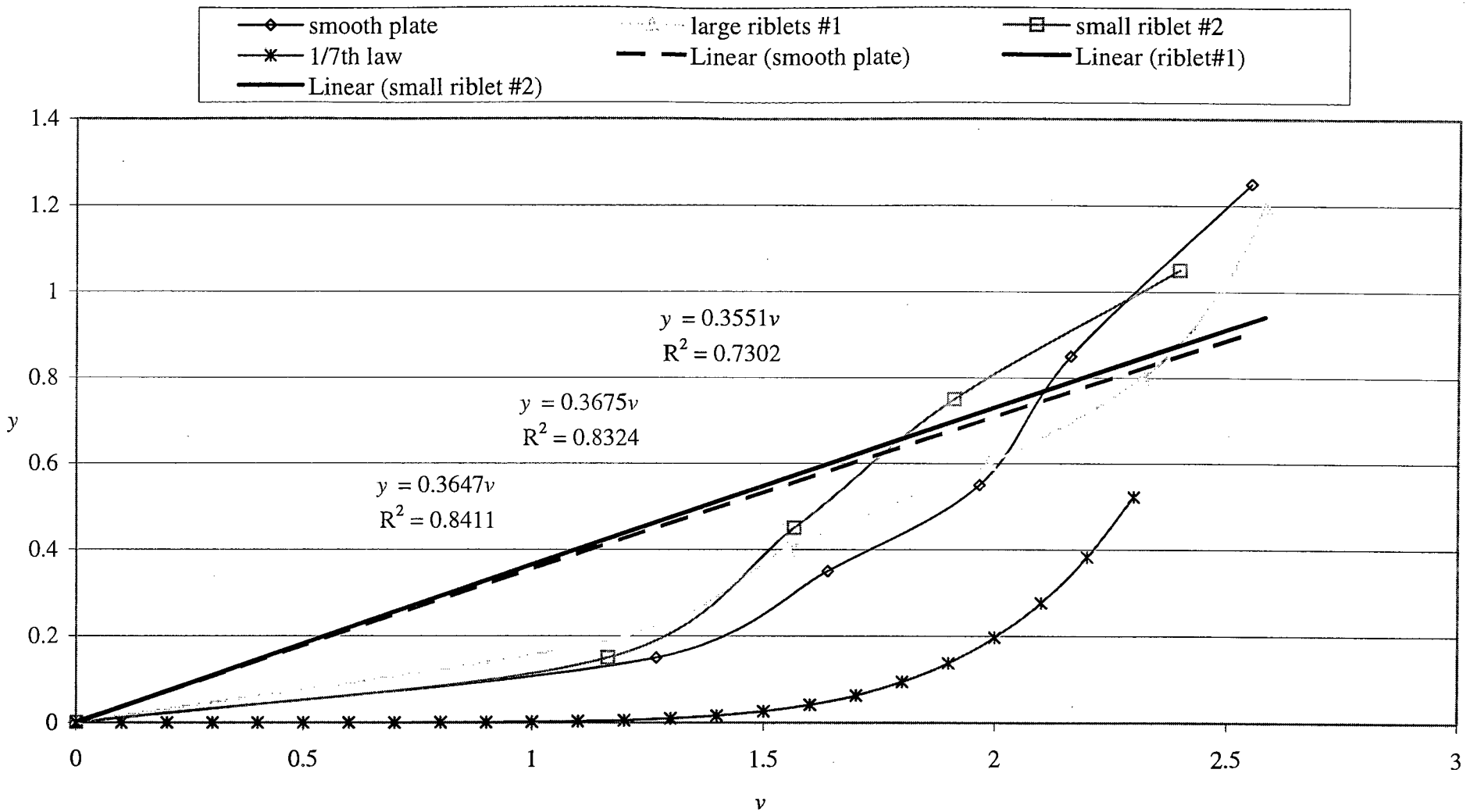

velocity profile in the laminar sublayer region, at x = 380 mm

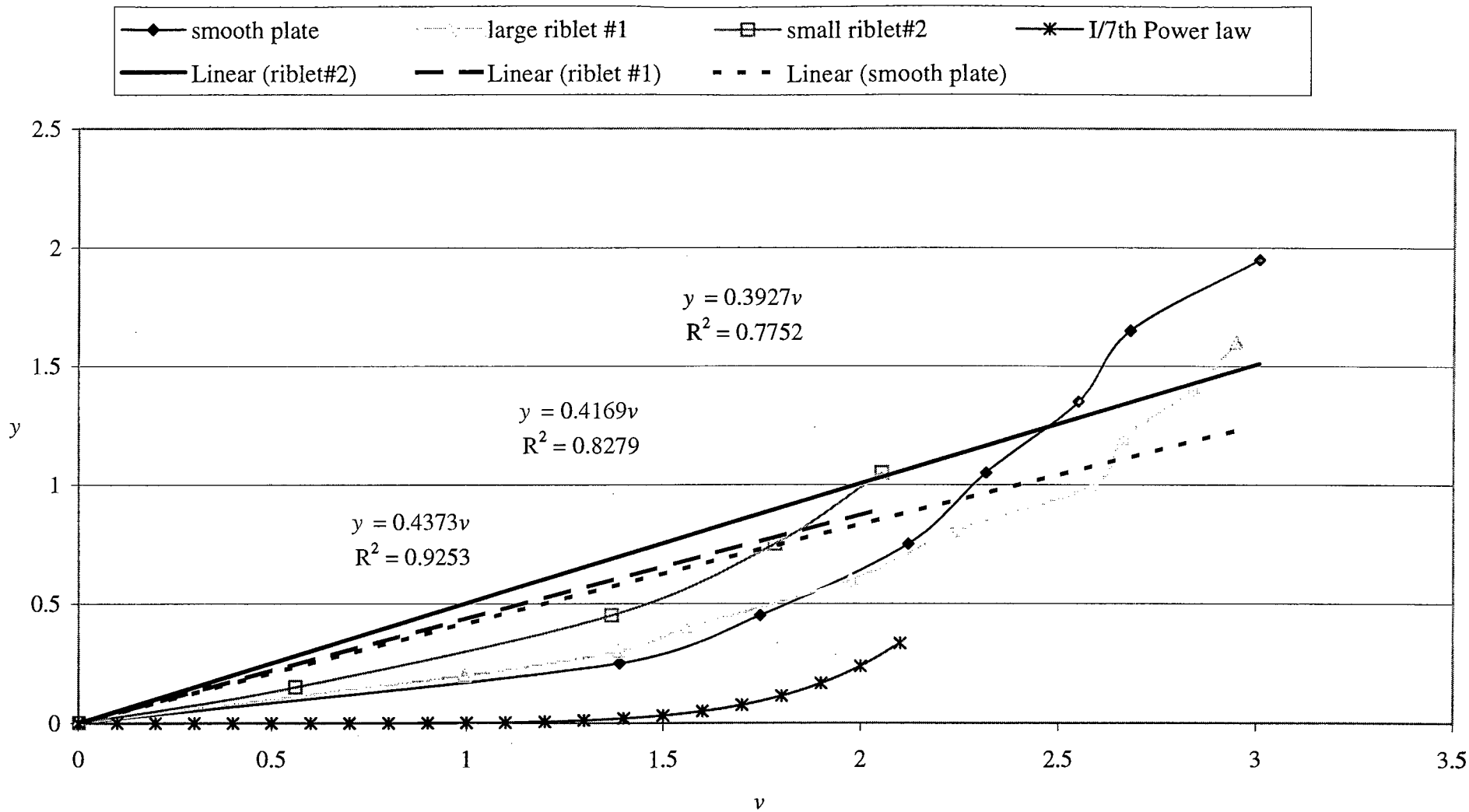

velocity profile in the laminar sublayer region, at x = 490 mm

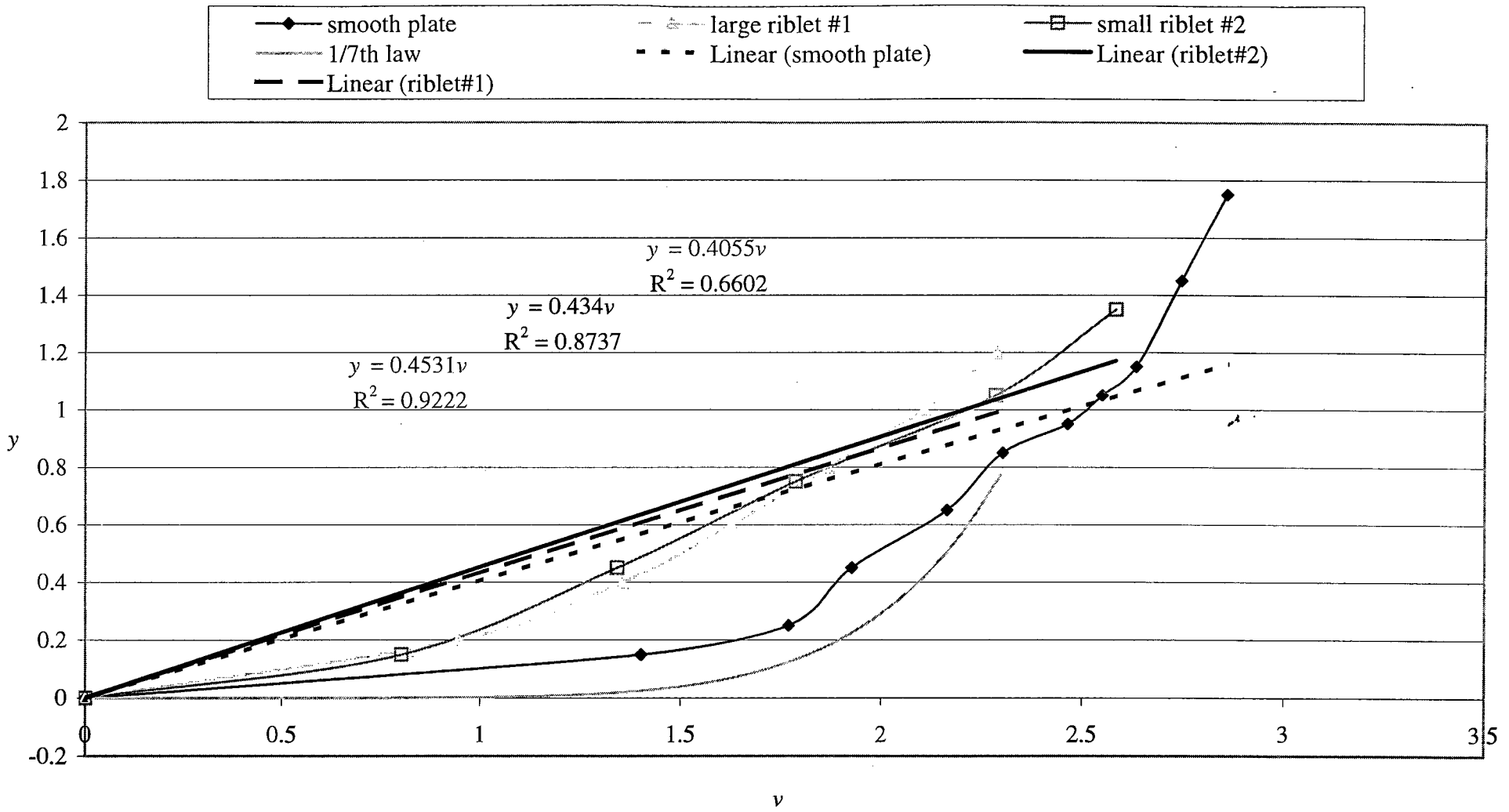

velocity profile in the laminar sublayer region, at x = 590 mm

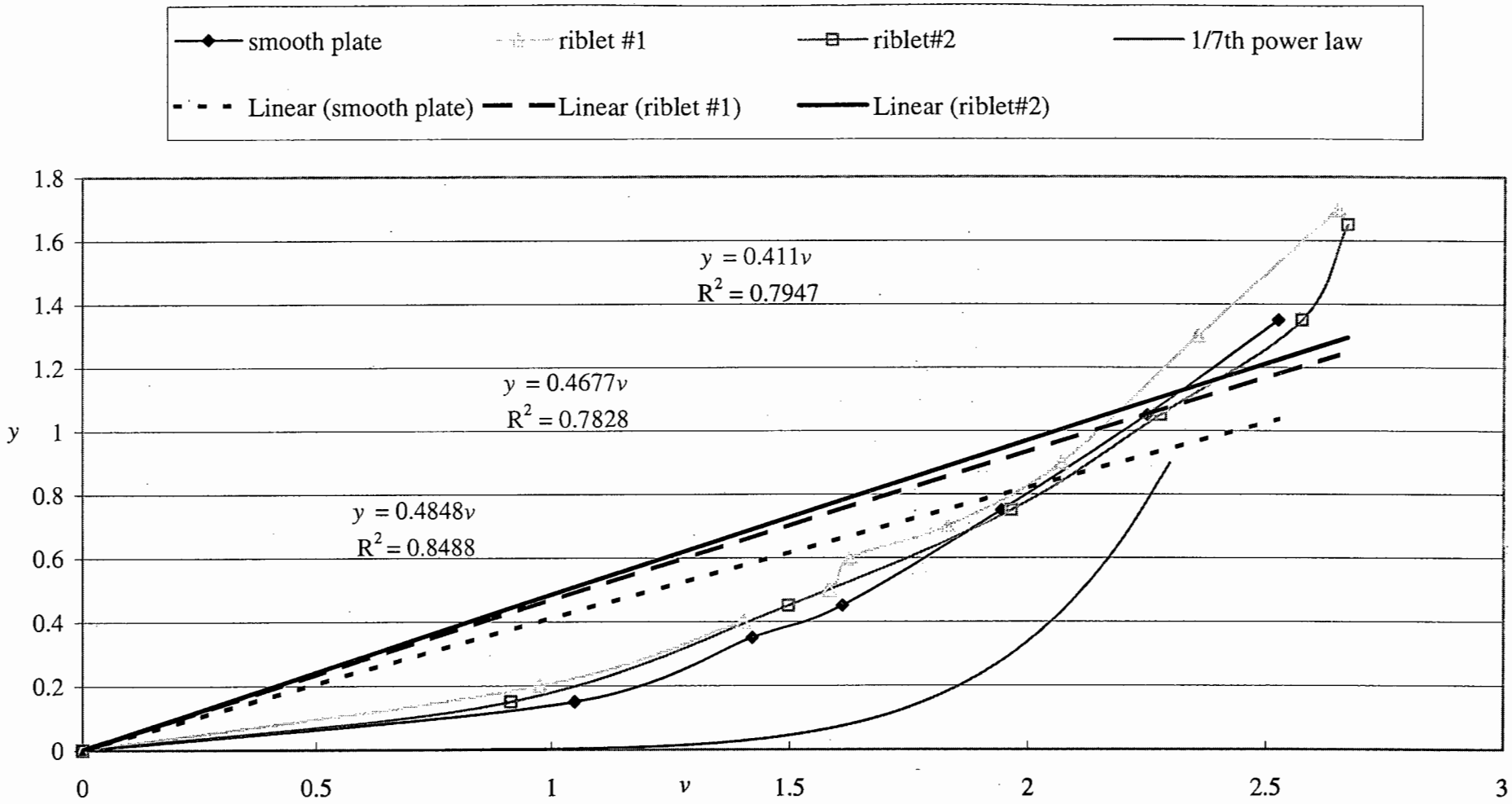

DIRECT DRAG RESULTS: smooth plate

ΔP	x mm	$\mu\varepsilon 1$	$\mu\varepsilon 2$	$\mu\varepsilon 3$	$\mu\varepsilon 4$	average $\mu\varepsilon$	drag force N1	drag force N2	air velocity	C_D	Re (x10^5)
1.42		7	6	8	9	7.5	0.0045	0.004733	1.534413	0.021558	0.50106
2.28		8	7	9	10	8.5	0.0051	0.005364	1.94431	0.015217	0.63492
3.64		10	9	10	12	10.25	0.00615	0.006468	2.45668	0.011494	0.80223
4.73		12	10	11	14	11.75	0.00705	0.007414	2.800455	0.010139	0.91449
5.17		13	12	13	15	13.25	0.00795	0.008361	2.927812	0.010461	0.95608
6.06		14	13	14	16	14.25	0.00855	0.008992	3.169818	0.009598	1.03511
7.96		16	14	16	17	15.75	0.00945	0.009938	3.632909	0.008076	1.18633
8.46		18	17	18	19	18	0.0108	0.011358	3.74527	0.008684	1.22302
10.1		19	18	20	21	19.5	0.0117	0.012305	4.092217	0.00788	1.33632
12.1		21	20	22	23	21.5	0.0129	0.013567	4.479099	0.007252	1.46266
13.87		22	21	23	24	22.5	0.0135	0.014198	4.795526	0.006621	1.56599
14.44		24	22	24	25	23.75	0.01425	0.014986	4.893072	0.006713	1.59784
16.05		27	25	27	28	26.75	0.01605	0.016879	5.158643	0.006803	1.68456
18.23		30	28	30	31	29.75	0.01785	0.018772	5.49783	0.006661	1.79532
19.81		32	30	32	33	31.75	0.01905	0.020034	5.731129	0.006542	1.87151
	51	43	43	44	45	43.75	0.02625	0.027606	6.534747	0.006933	2.13393
	66	56	55	57	58	56.5	0.0339	0.035652	7.433882	0.006919	2.42754
	80	71	70	74	75	72.5	0.0435	0.045748	8.184434	0.007325	2.67264
	89	77	75	78	80	77.5	0.0465	0.048903	8.632541	0.007038	2.81897
	97	83	82	83	85	83.25	0.04995	0.052531	9.012173	0.006937	2.94294
	115	104	101	104	105	103.5	0.0621	0.065309	9.812792	0.007274	3.20438

g =	9.81 m/s^2	$S = b \times l$	0.147 m^2
ρ =	1.206 kg/m^3	μ =	1.81E-05 Pa.s
T =	293 K		
P =	101.434 kPa		
s =	0.505		

DIRECT DRAG RESULTS: riblet surface #1

ΔP	x mm	$\mu\varepsilon$ 1	$\mu\varepsilon$ 2	$\mu\varepsilon$ 3	$\mu\varepsilon$ 4	average $\mu\varepsilon$	drag force N1	drag force N2	air velocity	C_D	Re (x10^5)
1.1		5	6	5	6	5.5	0.003476	0.003388	1.350499	0.020952	0.44101
2.47		8	8	8	9	8.25	0.005214	0.005082	2.023702	0.013997	0.66084
4.91		11	11	10	12	11	0.006952	0.006776	2.853243	0.009388	0.93173
6.24		13	14	13	14	13.5	0.008532	0.008316	3.21655	0.009066	1.05037
7.9		15	15	14	15	14.75	0.009322	0.009086	3.619191	0.007824	1.18185
8.94		16	17	16	15	16	0.010112	0.009856	3.850053	0.0075	1.25724
10.01		18	18	18	17	17.75	0.011218	0.010934	4.073944	0.007431	1.33035
11.95		20	21	20	20	20.25	0.012798	0.012474	4.451249	0.007101	1.45356
13.74		22	23	22	21	22	0.013904	0.013552	4.772999	0.00671	1.55863
14.82		24	24	24	22	23.5	0.014852	0.014476	4.957036	0.006645	1.61873
17.05		26	27	27	25	26.25	0.01659	0.01617	5.316921	0.006452	1.73625
18.98		29	29	29	30	29.25	0.018486	0.018018	5.609783	0.006458	1.83188
	44	33	34	33	35	33.75	0.02133	0.02079	6.069739	0.006365	1.98208
	64	52	54	52	55	53.25	0.033654	0.032802	7.320381	0.006904	2.39048
	77	64	66	65	66	65.25	0.041238	0.040194	8.02951	0.007032	2.62205
	94	75	78	76	77	76.5	0.048348	0.047124	8.871715	0.006753	2.89707
	110	91	93	92	93	92.25	0.058302	0.056826	9.5971	0.006959	3.13395
	121	104	105	103	105	104.25	0.065886	0.064218	10.06552	0.007149	3.28691

g = 9.81 m/s^2

ρ = 1.206 kg/m^3

T = 293 K

P = 101.434 kPa

s = 0.505

$S = b \times l$ 0.147 m^2

μ = 1.81E-05 Pa.s

DIRECT DRAG RESULTS: riblet surface #2

ΔP	x mm	$\mu\varepsilon$ 1	$\mu\varepsilon$ 2	$\mu\varepsilon$ 3	$\mu\varepsilon$ 4		average $\mu\varepsilon$	drag force N1	drag force N2	air velocity	C_D	Re (x10^5)
0.85			3	5	4	5	4.25	0.002508	0.002635	1.187155	0.021088	0.38767
2.22			7	8	7	8	7.5	0.004425	0.00465	1.918556	0.014249	0.62651
4.44			10	10	10	10	10	0.0059	0.0062	2.713248	0.009499	0.88601
6.33			13	13	12	13	12.75	0.007523	0.007905	3.239663	0.008495	1.05792
7.39			13	14	13	14	13.5	0.007965	0.00837	3.50042	0.007705	1.14307
8.68			15	15	14	15	14.75	0.008703	0.009145	3.793655	0.007167	1.23882
9.74			16	17	15	16	16	0.00944	0.00992	4.018625	0.006928	1.31229
11.4			18	19	17	18	18	0.01062	0.01116	4.347608	0.00666	1.41972
13.8			21	23	21	22	21.75	0.012833	0.013485	4.783409	0.006647	1.56203
16.86			25	26	24	25	25	0.01475	0.0155	5.287212	0.006254	1.72655
19.58			29	29	28	28	28.5	0.016815	0.01767	5.697762	0.006139	1.86061
	42		32	32	32	33	32.25	0.019028	0.019995	5.930186	0.006413	1.93651
	50		37	39	38	38	38	0.02242	0.02356	6.470363	0.006347	2.11291
	62		46	48	46	47	46.75	0.027583	0.028985	7.205092	0.006298	2.35283
	77		61	63	61	63	62	0.03658	0.03844	8.02951	0.006725	2.62205
	95		77	78	76	79	77.5	0.045725	0.04805	8.91878	0.006813	2.91244
	111		91	93	91	93	92	0.05428	0.05704	9.640624	0.006922	3.14816

g =	9.81	m/s^2
ρ =	1.206	kg/m^3
T =	293	K
P =	101.434	kPa
s =	0.505	
$S = b \times l$	0.147	m^2
μ =	1.81E-05	Pa.s

APPENDIX F:

Calibration Data

Strain gauge calibration data points: smooth plate

trial 1							trial 2						
Mass grams	$\mu\varepsilon$ 1	$\mu\varepsilon$ 2	$\mu\varepsilon$ 3	$\mu\varepsilon$ 4	force N	average strain $\mu\varepsilon$	Mass grams	$\mu\varepsilon$ 1	$\mu\varepsilon$ 2	$\mu\varepsilon$ 3	$\mu\varepsilon$ 4	force N	average strain $\mu\varepsilon$
2.95	43	43	44	45	0.02894	43.75	2.95	43	44	45	45	0.02894	44.25
1.29	19	16	21	18	0.01265	18.5	1.29	19	17	21	18	0.01265	18.75
2.13	31	37	33	30	0.02090	32.75	2.13	31	37	33	32	0.02090	33.25
3.57	62	57	64	62	0.03502	61.25	3.57	62	57	64	60	0.03502	60.75
3.7	63	58	64	62	0.03630	61.75	3.7	63	58	64	62	0.03630	61.75
3.36	61	57	63	61	0.03296	60.5	3.36	60	57	62	61	0.03296	60
5.61	95	91	88	96	0.05503	92.5	5.61	94	91	89	96	0.05503	92.5
7.5	118	123	121	119	0.07358	120.25	7.5	120	123	121	119	0.07358	120.75
5.54	94	89	86	95	0.05435	91	5.54	93	89	88	95	0.05435	91.25
4.48	72	66	72	72	0.04395	70.5	4.48	70	66	72	72	0.04395	70
16.46	271	270	273	274	0.16147	272	16.46	254	252	255	257	0.16147	254.5
18.22	297	297	299	300	0.17874	298.25	18.22	274	276	277	279	0.17874	276.5
19.5	319	320	323	323	0.19130	321.25	19.5	296	296	298	300	0.19130	297.5
22.44	367	368	369	369	0.22014	368.25	22.44	344	343	347	347	0.22014	345.25
20.9	345	344	345	346	0.20503	345	20.9	317	319	321	320	0.20503	319.25
24.8	401	401	403	405	0.24329	402.5	24.8	381	380	383	384	0.24329	382
6.89	112	112	113	114	0.06759	112.75	6.89	105	105	106	107	0.06759	105.75
7.98	129	129	130	130	0.07828	129.5	7.98	122	123	125	123	0.07828	123.25
10.2	167	168	168	170	0.10006	168.25	10.2	156	155	156	156	0.10006	155.75
11.7	193	197	197	193	0.11478	195	11.7	193	197	192	195	0.11478	194.25
18.1	292	296	298	295	0.17756	295.25	18.1	292	289	298	295	0.17756	293.5
14.68	234	230	232	229	0.14401	231.25	14.68	234	230	232	229	0.14401	231.25
0.68	10	11	9	10	0.00667	10	0.68	10	11	10	10	0.00667	10.25
1.21	16	22	20	17	0.01187	18.75	1.21	16	22	21	17	0.01187	19
2.15	35	31	33	34	0.02109	33.25	2.15	35	31	34	34	0.02109	33.5
1.86	28	32	31	29	0.01825	30	1.86	28	32	30	29	0.01825	29.75

trial 3: large masses on smooth flat plate						
20	52	51	47	42	0.19620	48
34.68	72	73	64	59	0.34021	67
17.69	49	47	43	41	0.17354	45
21.05	53	53	49	46	0.20650	50.25
39.98	95	97	87	78	0.39220	89.25
44.68	98	102	91	82	0.43831	93.25
63.61	137	145	128	114	0.62401	131
69.15	146	153	135	120	0.67836	138.5
76.65	150	155	138	129	0.75194	143
80.22	161	168	147	133	0.78696	152.25
85.83	171	182	160	142	0.84199	163.75
90.31	178	188	167	148	0.88594	170.25
102.01	206	218	192	171	1.00072	196.75
120.11	255	272	238	212	1.17828	244.25
15.4	41	39	36	32	0.15107	37
22.9	56	55	50	44	0.22465	51.25
26.47	62	60	55	49	0.25967	56.5
32.01	73	72	63	55	0.31402	65.75
36.49	82	73	64	57	0.35797	69
42.1	81	84	73	64	0.41300	75.5
62.1	127	133	116	102	0.60920	119.5
79.79	152	163	140	130	0.78274	146.25
98.82	196	210	181	158	0.96942	186.25

Strain gauge calibration data points: riblet surface #1

trial 1: Mass grams	με 1	με 2	με 3	με 4	force N	average stain με	trial 2: Mass grams	με 1	με 2	με 3	με 4	force N	average stain με
2.95	46	48	47	46	0.02894	46.75	2.95	47	49	47	47	0.02894	47.5
1.29	17	19	18	19	0.01265	18.25	1.29	21	22	21	21	0.01265	21.25
2.13	33	34	34	33	0.02090	33.5	2.13	33	34	33	34	0.02090	33.5
3.57	56	57	58	56	0.03502	56.75	3.57	57	57	58	56	0.03502	57
3.7	57	57	58	57	0.03630	57.25	3.7	59	57	58	57	0.03630	57.75
3.36	52	52	52	51	0.03296	51.75	3.36	53	53	55	51	0.03296	53
5.61	87	89	88	86	0.05503	87.5	5.61	90	89	88	87	0.05503	88.5
7.5	117	118	117	115	0.07358	116.75	7.5	117	118	118	116	0.07358	117.25
5.54	86	89	88	87	0.05435	87.5	5.54	88	89	88	88	0.05435	88.25
4.48	69	70	69	68	0.04395	69	4.48	70	71	69	69	0.04395	69.75
11.7	181	184	184	182	0.11478	182.75	11.7	183	187	185	184	0.11478	184.75
18.1	279	283	281	278	0.17756	280.25	18.1	287	289	286	288	0.17756	287.5
16.46	252	254	255	252	0.16147	253.25	16.46	261	264	265	262	0.16147	263
18.22	283	285	286	284	0.17874	284.5	18.22	292	295	296	294	0.17874	294.25
19.5	300	304	305	301	0.19130	302.5	19.5	305	304	309	308	0.19130	306.5
22.44	347	351	351	348	0.22014	349.25	22.44	357	361	361	358	0.22014	359.25
20.9	321	324	323	320	0.20503	322	20.9	331	334	333	329	0.20503	331.75
24.8	385	390	388	386	0.24329	387.25	24.8	395	395	398	396	0.24329	396
6.89	105	107	107	105	0.06759	106	6.89	115	117	117	115	0.06759	116
7.98	126	126	127	125	0.07828	126	7.98	126	128	127	125	0.07828	126.5
10.2	157	158	158	156	0.10006	157.25	10.2	163	167	165	165	0.10006	165
14.68	227	227	228	225	0.14401	226.75	14.68	229	231	234	231	0.14401	231.25
0.68	12	12	12	11	0.00667	11.75	0.68	12	12	11	11	0.00667	11.5
1.21	20	21	20	19	0.01187	20	1.21	20	21	19	19	0.01187	19.75
2.15	32	34	33	32	0.02109	32.75	2.15	33	35	33	32	0.02109	33.25
1.86	29	31	30	28	0.01825	29.5	1.86	30	32	30	28	0.01825	30

Strain gauge calibration data points: riblet surface #2

trial 1: Mass grams	με 1	με 2	με 3	με 4	force N	average strain με
2.95	49	50	47	49	0.02894	48.75
1.29	20	22	19	21	0.01265	20.5
2.13	36	35	34	35	0.02090	35
3.57	60	61	57	59	0.03502	59.25
3.7	64	64	60	62	0.03630	62.5
3.36	56	55	54	56	0.03296	55.25
5.61	93	94	92	93	0.05503	93
7.5	126	129	123	125	0.07358	125.75
5.54	92	92	91	92	0.05435	91.75
4.48	75	76	74	74	0.04395	74.75
11.7	195	197	192	193	0.11478	194.25
18.1	298	299	297	301	0.17756	298.75
16.46	272	273	279	280	0.16147	276
18.22	302	300	301	304	0.17874	301.75
19.5	326	327	324	326	0.19130	325.75
22.44	378	378	375	379	0.22014	377.5
20.9	348	348	346	347	0.20503	347.25
24.8	411	413	410	414	0.24329	412
6.89	120	120	118	119	0.06759	119.25
7.98	136	136	134	137	0.07828	135.75
10.2	176	177	175	177	0.10006	176.25
14.68	246	245	243	244	0.14401	244.5
0.68	12	12	11	13	0.00667	12
1.21	20	20	19	20	0.01187	19.75
2.15	37	36	34	35	0.02109	35.5
1.86	31	33	30	31	0.01825	31.25

trial 2: Mass grams	με 1	με 2	με 3	με 4	force N	average strain με
2.95	48	50	46	50	0.02894	48.5
1.29	20	22	19	21	0.01265	20.5
2.13	34	35	33	35	0.02090	34.25
3.57	56	57	55	57	0.03502	56.25
3.7	60	62	59	62	0.03630	60.75
3.36	51	54	51	53	0.03296	52.25
5.61	92	93	90	92	0.05503	91.75
7.5	121	125	121	124	0.07358	122.75
5.54	85	87	85	87	0.05435	86
4.48	76	76	75	76	0.04395	75.75
11.7	182	185	181	187	0.11478	183.75
18.1	282	283	280	285	0.17756	282.5
14.68	227	230	228	231	0.14401	229
0.68	12	12	11	13	0.00667	12
1.21	22	23	19	23	0.01187	21.75
2.15	35	35	34	35	0.02109	34.75
1.86	27	28	28	29	0.01825	28
16.46	257	261	256	262	0.16147	259
18.22	281	280	279	285	0.17874	281.25
19.5	309	310	307	311	0.19130	309.25
22.44	351	353	349	354	0.22014	351.75
20.9	332	330	329	334	0.20503	331.25
24.8	395	394	392	395	0.24329	394
6.89	109	109	107	110	0.06759	108.75
7.98	121	122	119	121	0.07828	120.75
10.2	162	163	160	163	0.10006	162

APPENDIX G:

Addition Sharkskin Electron Microscopy photographs

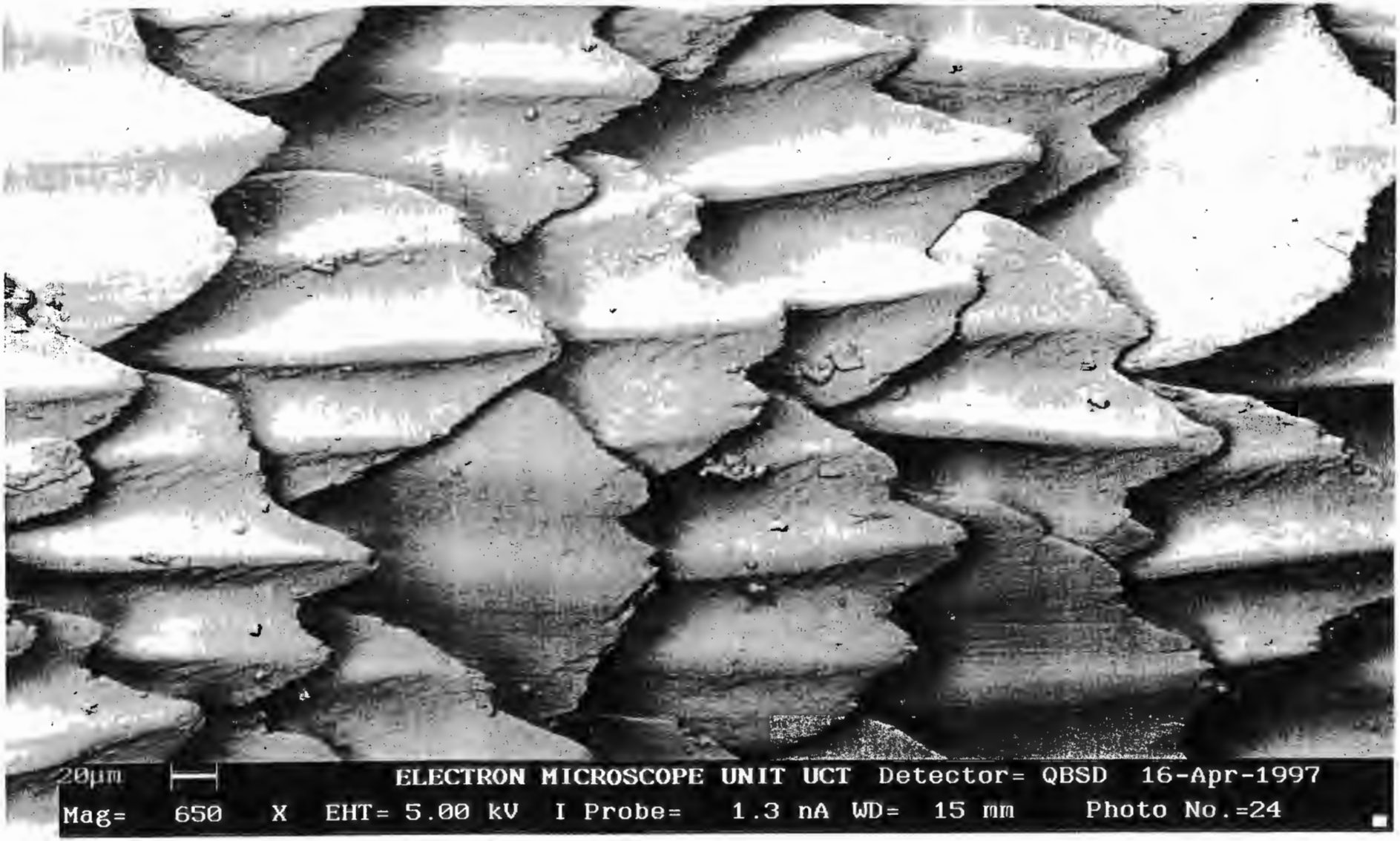
20µm
ELECTRON MICROSCOPE UNIT UCT Detector= QBSD 16-Apr-1997
Mag= 650 X EHT= 5.00 kV I Probe= 1.3 nA WD= 15 mm Photo No.=24

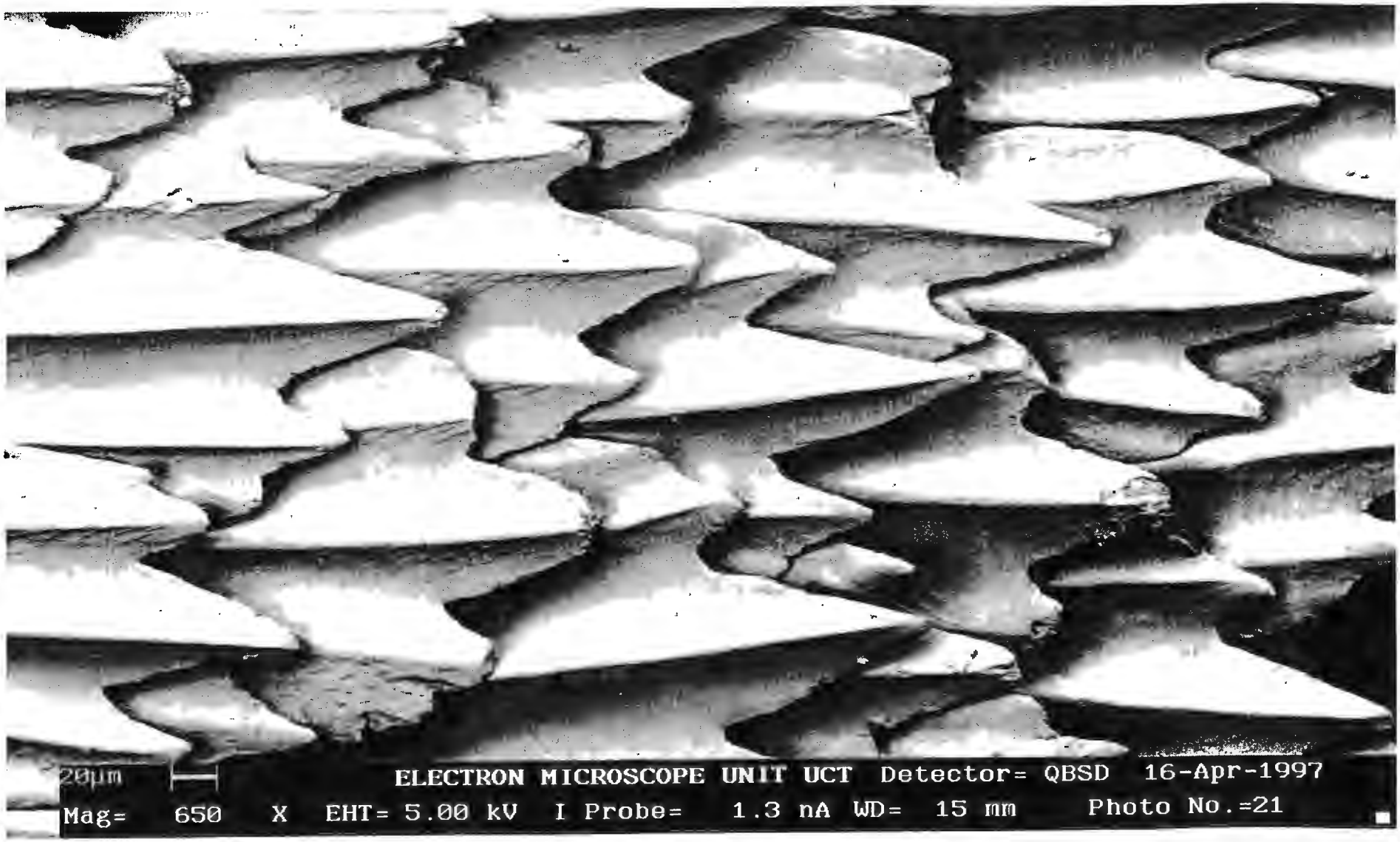
20µm
ELECTRON MICROSCOPE UNIT UCT Detector= QBSD 16-Apr-1997
Mag= 650 X EHT= 5.00 kV I Probe= 1.3 nA WD= 15 mm Photo No.=21

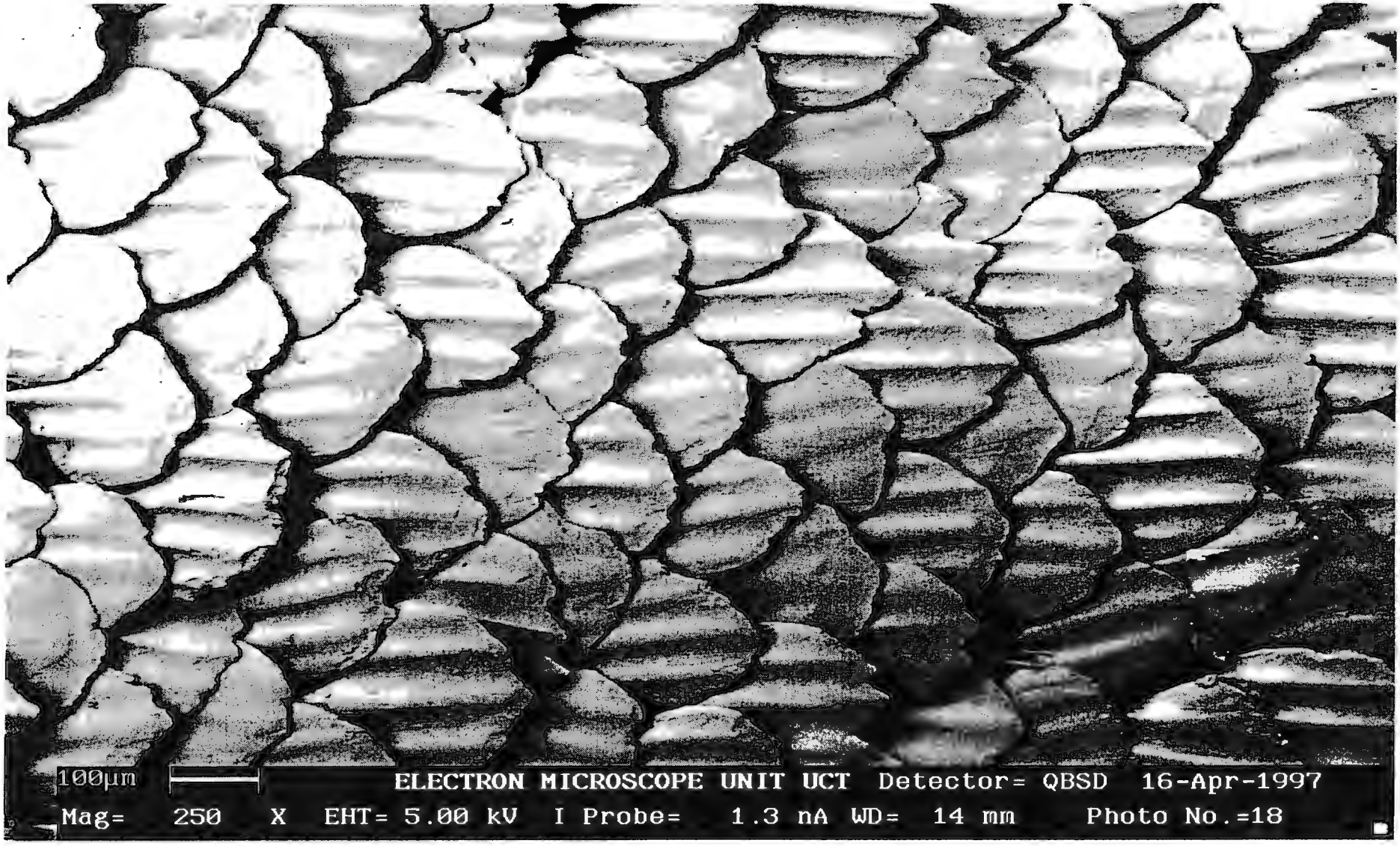
100µm
ELECTRON MICROSCOPE UNIT UCT Detector= QBSD 16-Apr-1997
Mag= 250 X EHT= 5.00 kV I Probe= 1.3 nA WD= 14 mm Photo No.=18

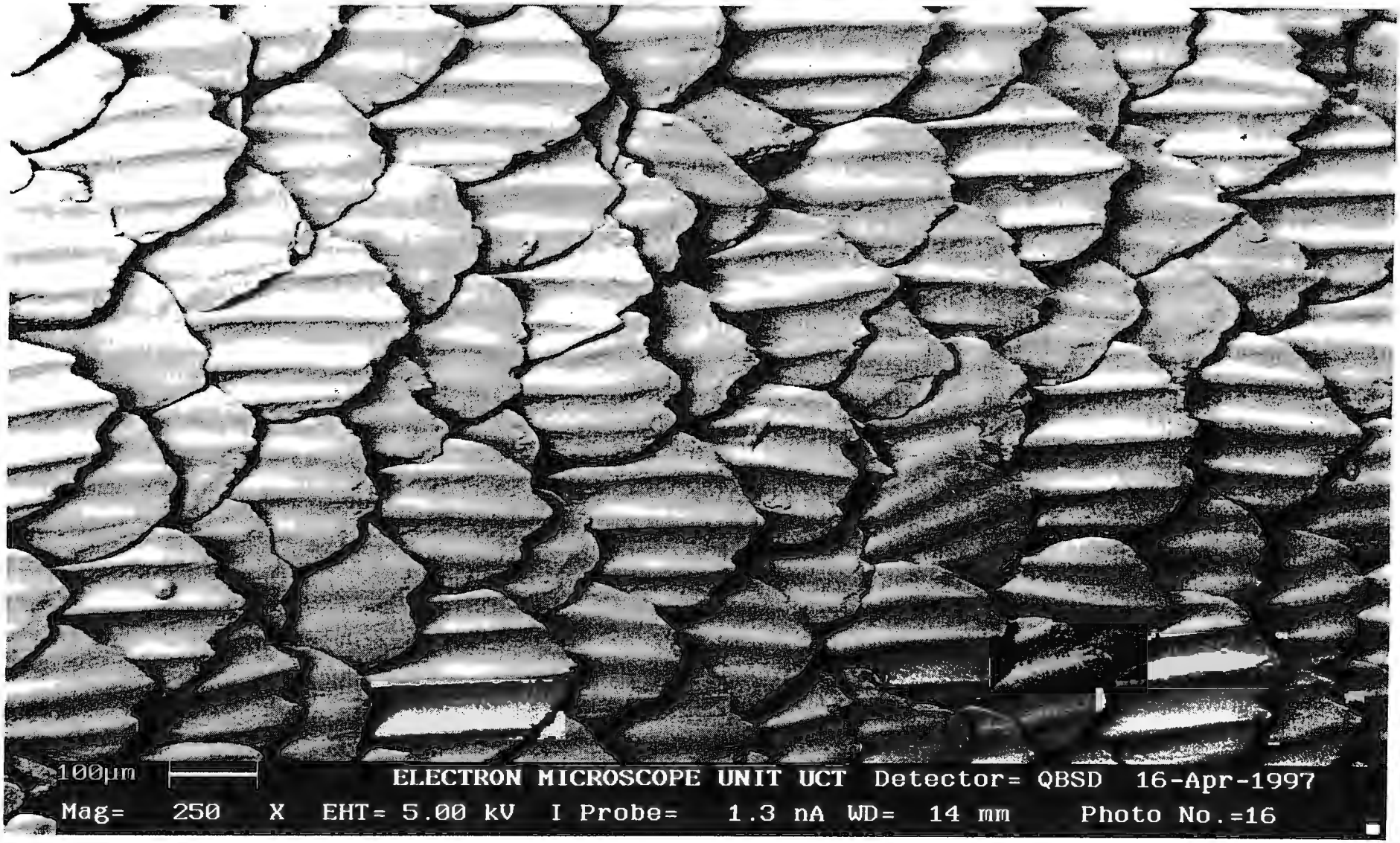
100µm
ELECTRON MICROSCOPE UNIT UCT Detector= QBSD 16-Apr-1997
Mag= 250 X EHT= 5.00 kV I Probe= 1.3 nA WD= 14 mm Photo No.=16

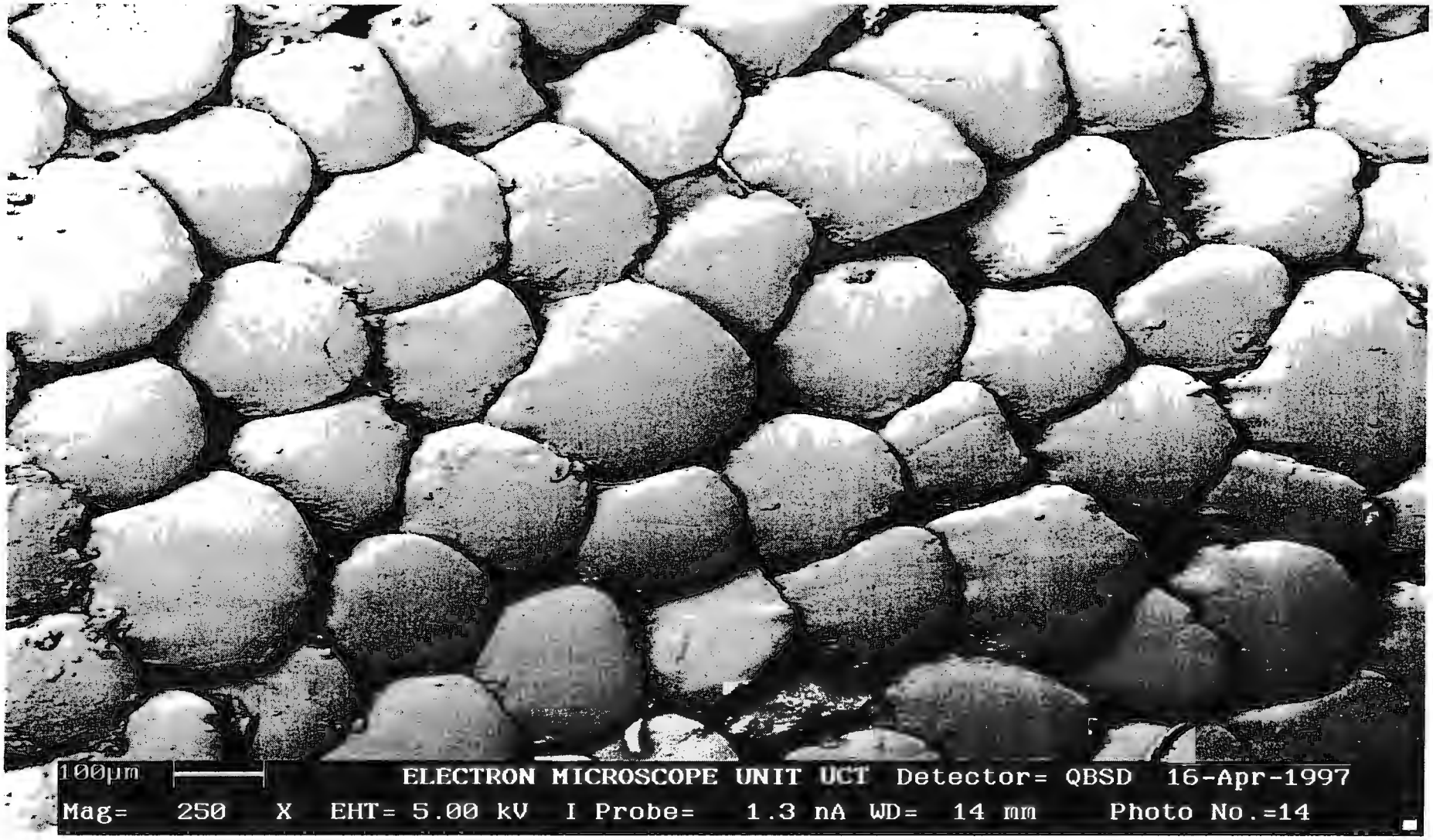
100µm
ELECTRON MICROSCOPE UNIT UCT Detector= QBSD 16-Apr-1997
Mag= 250 X EHT= 5.00 kV I Probe= 1.3 nA WD= 14 mm Photo No.=14

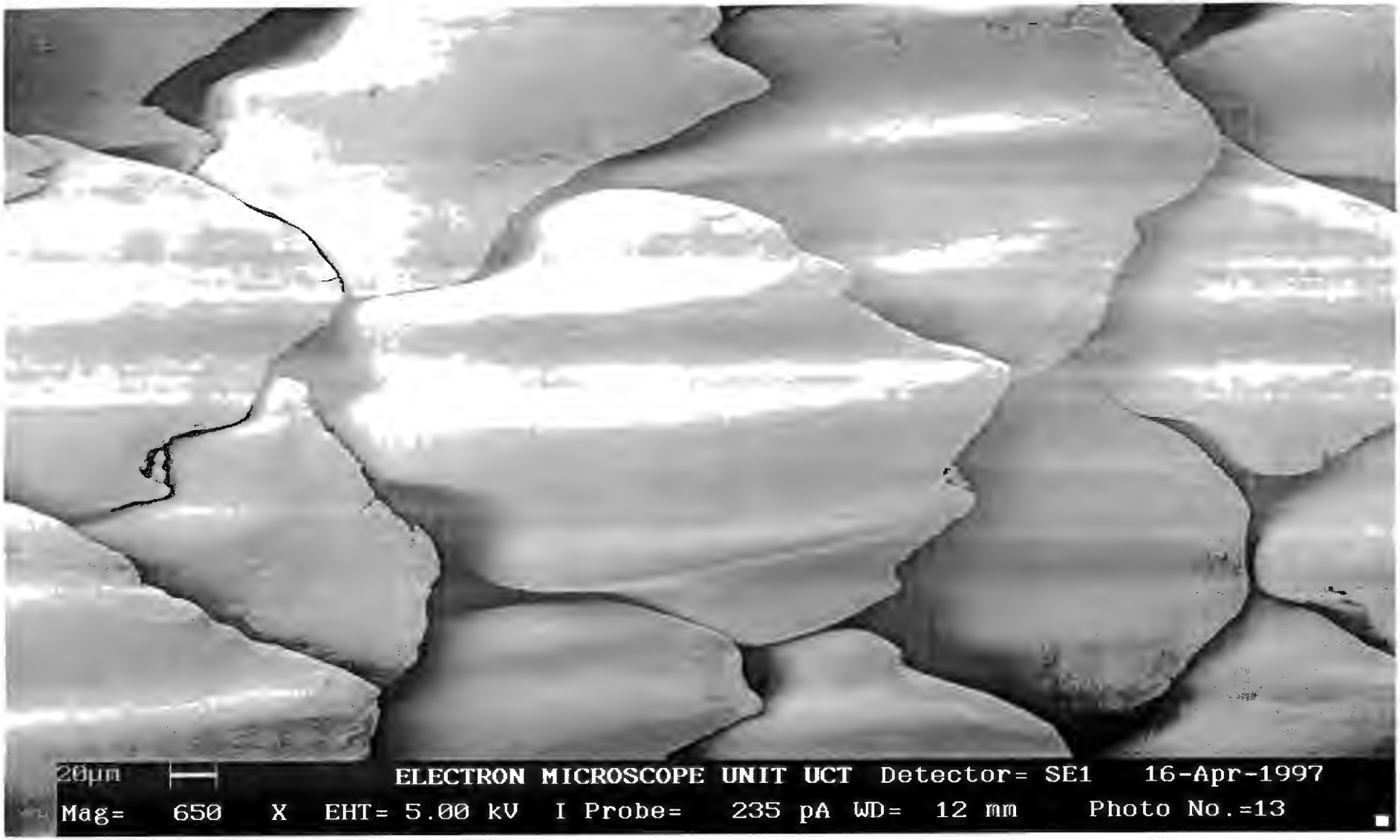
20µm
ELECTRON MICROSCOPE UNIT UCT Detector= SE1 16-Apr-1997
Mag= 650 X EHT= 5.00 kV I Probe= 235 pA WD= 12 mm Photo No.=13


20µm
ELECTRON MICROSCOPE UNIT UCT Detector= QBSD 16-Apr-1997
Mag= 650 X EHT= 5.00 kV I Probe= 1.3 nA WD= 12 mm Photo No.=11

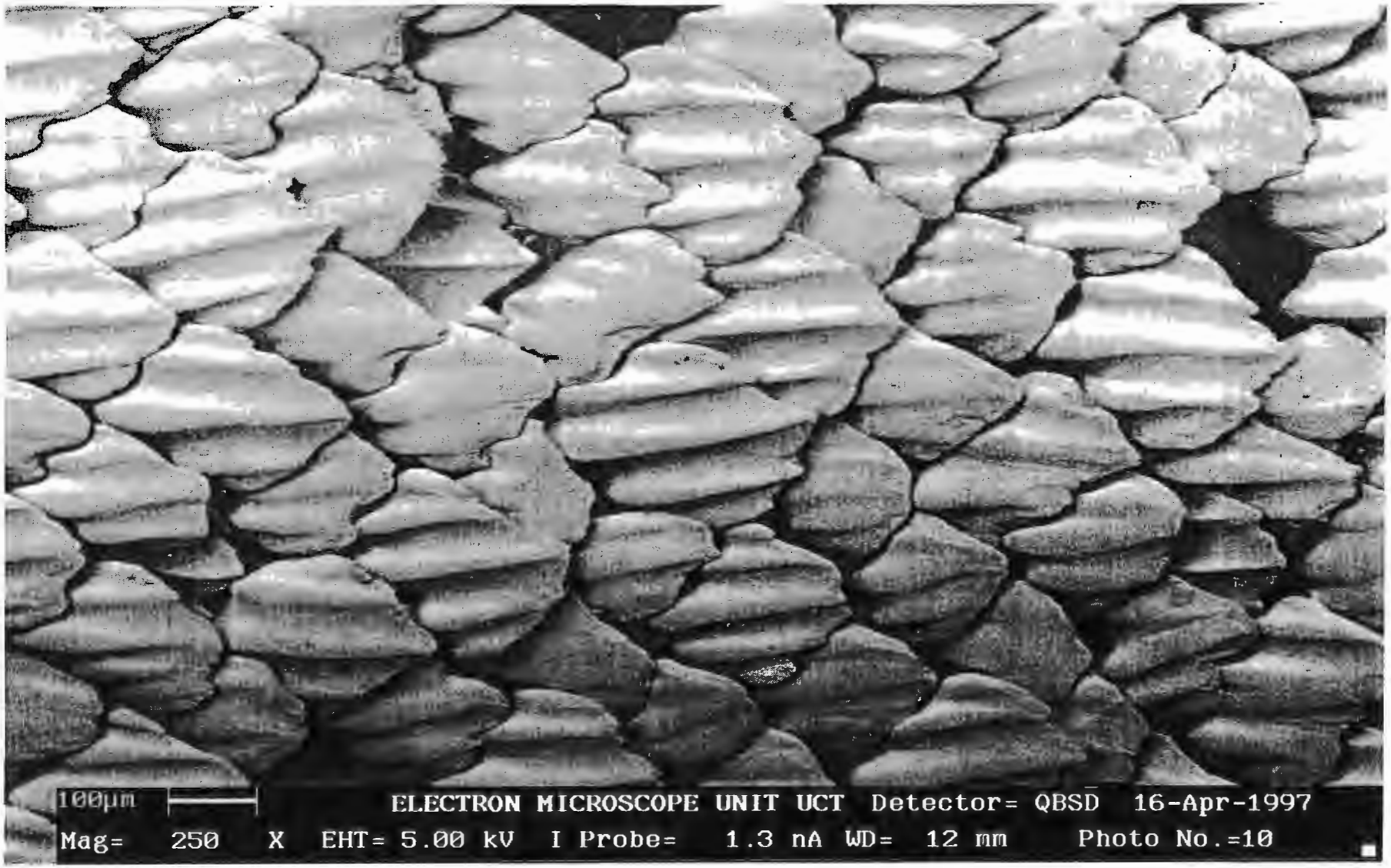
100µm
ELECTRON MICROSCOPE UNIT UCT Detector= QBSD 16-Apr-1997
Mag= 250 X EHT= 5.00 kV I Probe= 1.3 nA WD= 12 mm Photo No.=10

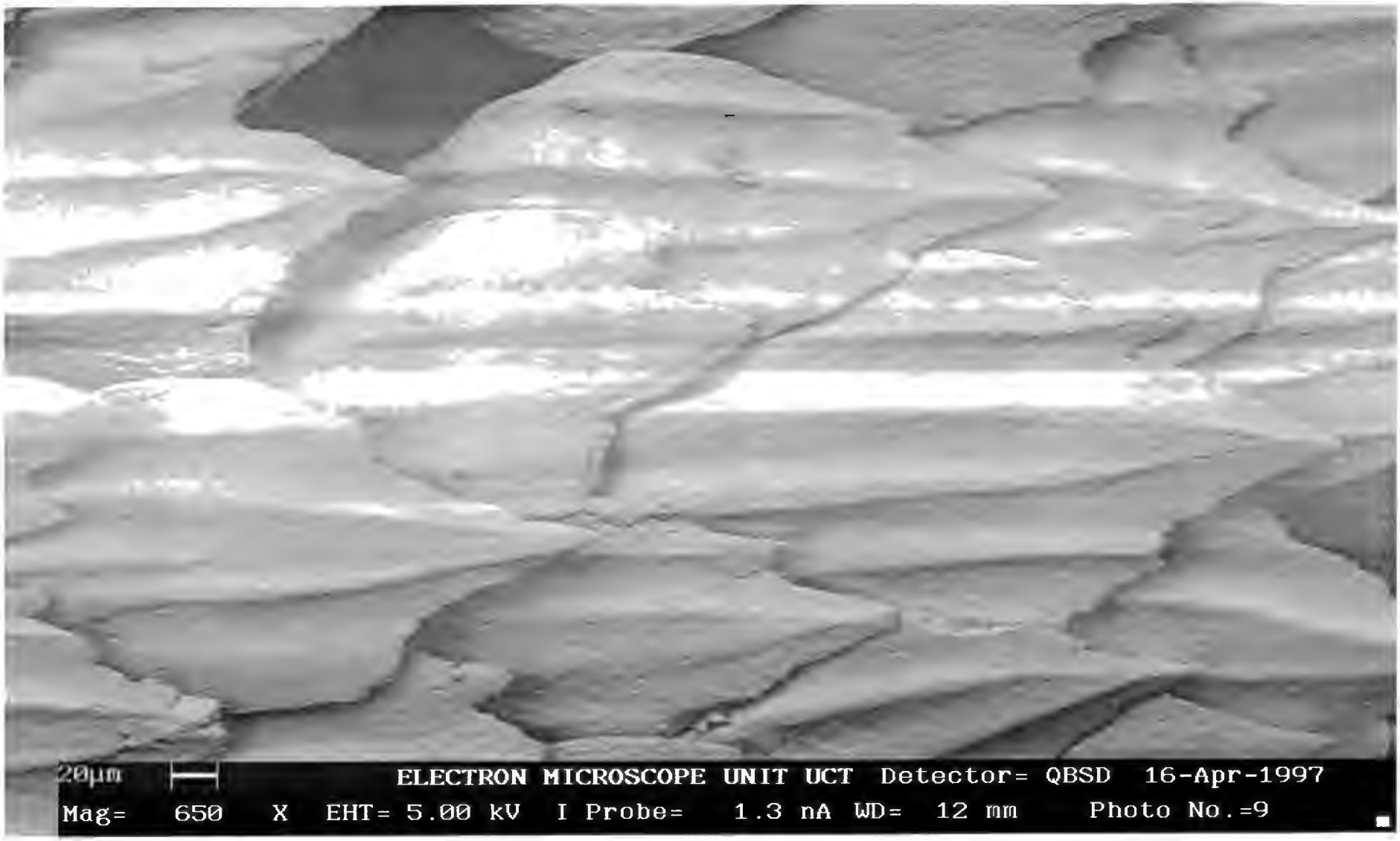
20µm
ELECTRON MICROSCOPE UNIT UCT Detector= QBSD 16-Apr-1997
Mag= 650 X EHT= 5.00 kV I Probe= 1.3 nA WD= 12 mm Photo No.=9

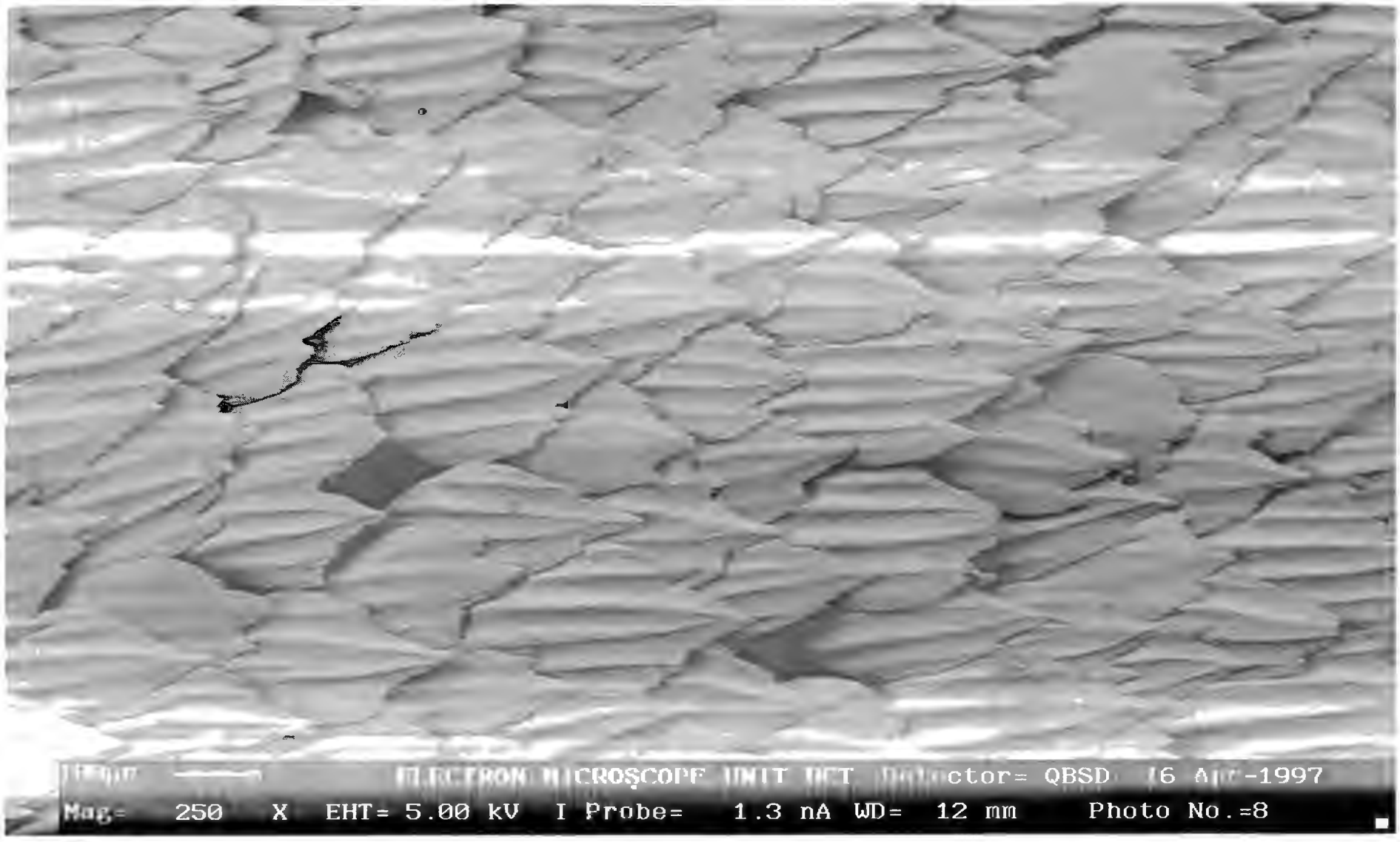
ELECTRON MICROSCOPE UNIT DCT Detector= QBSD 16 Apr-1997
Mag= 250 X EHT= 5.00 kV I Probe= 1.3 nA WD= 12 mm Photo No.=8

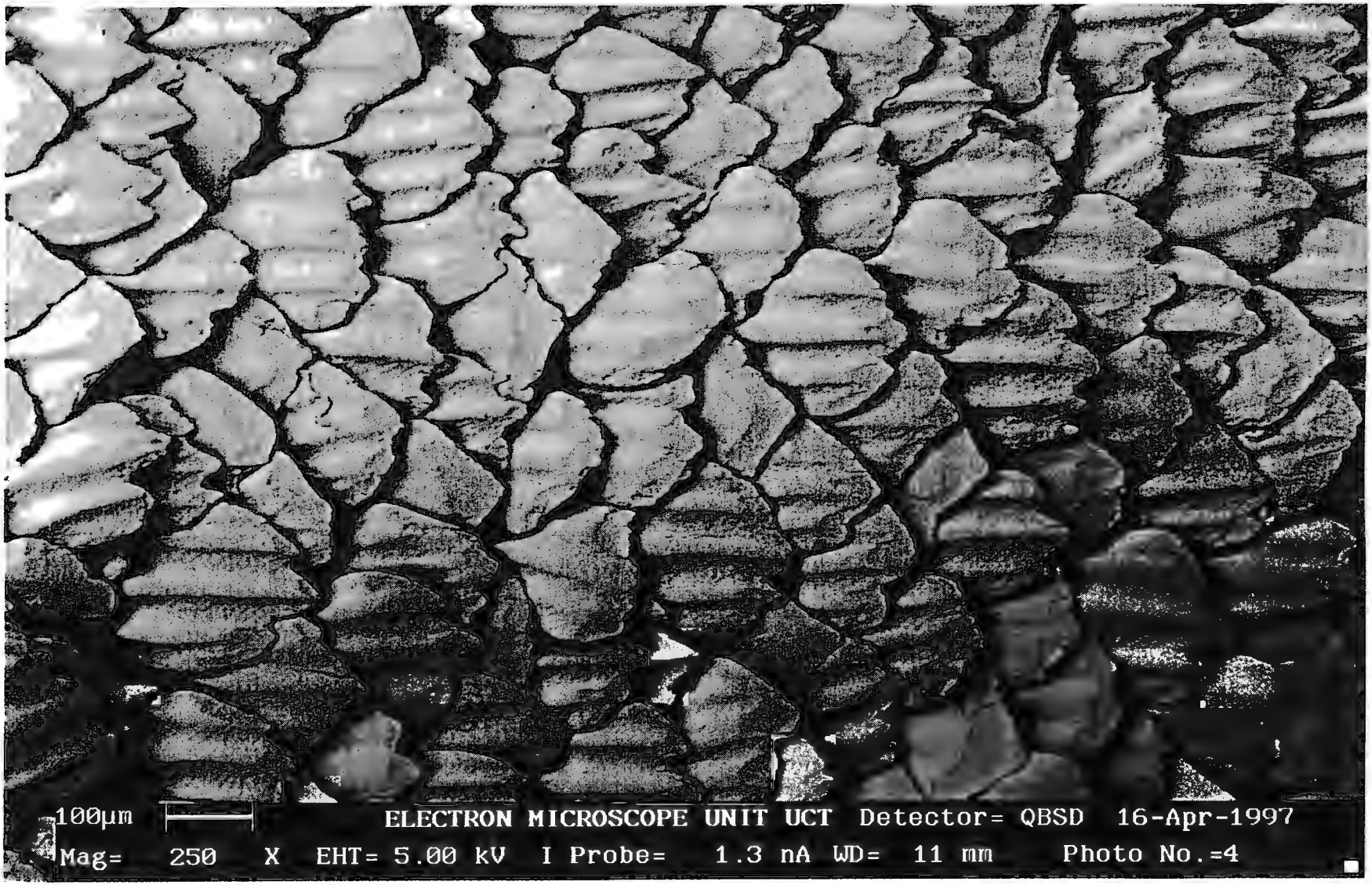
100µm
ELECTRON MICROSCOPE UNIT UCT Detector= QBSD 16-Apr-1997
Mag= 250 X EHT= 5.00 kV I Probe= 1.3 nA WD= 11 mm Photo No.=4

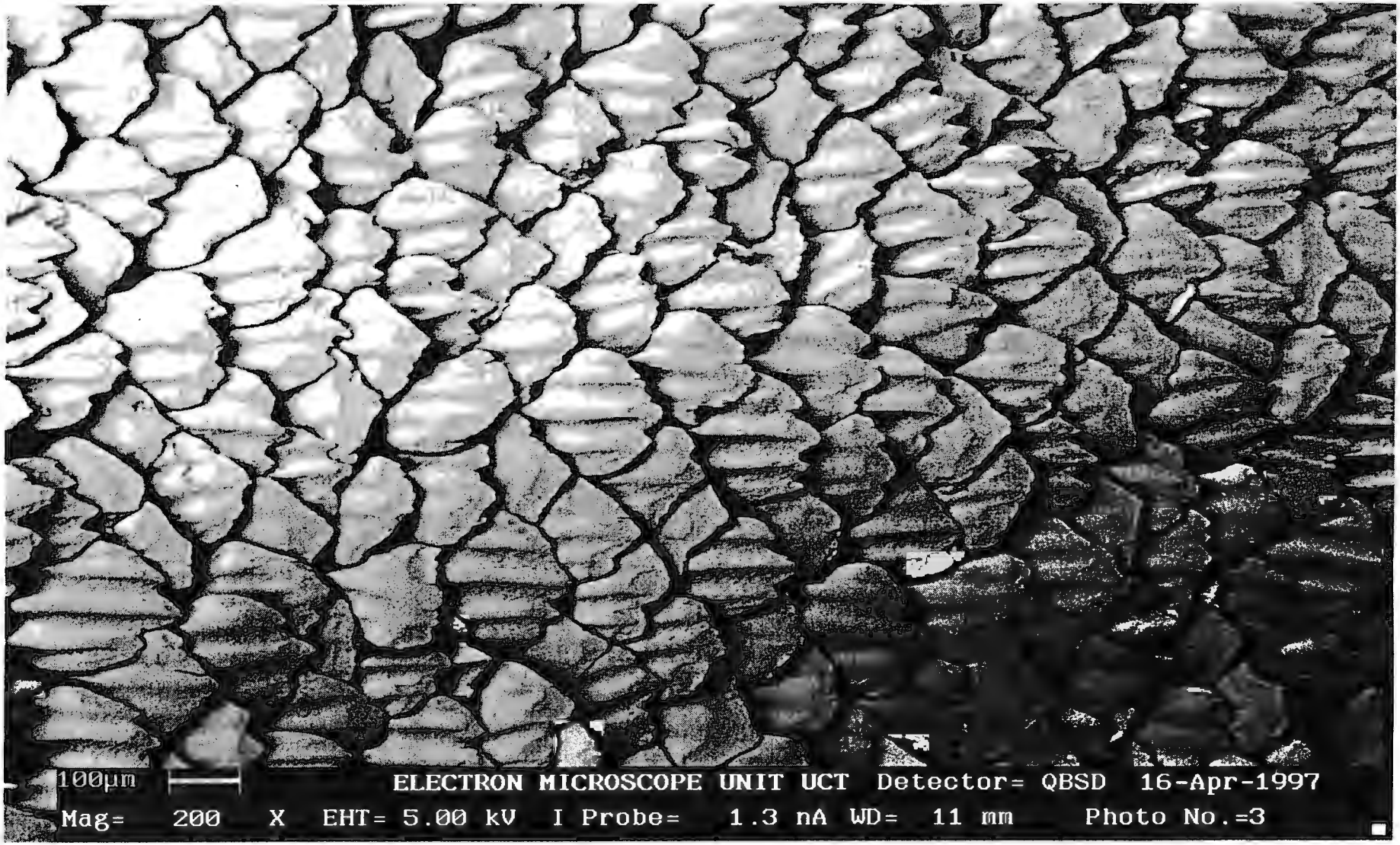
100µm
ELECTRON MICROSCOPE UNIT UCT Detector= QBSD 16-Apr-1997
Mag= 200 X EHT= 5.00 kV I Probe= 1.3 nA WD= 11 mm Photo No.=3